**SYNTHESIS OF DESIGNED Al- AND Ga- DOPED
ZINC OXIDE (ZnO) PARTICLES AND THEIR
APPLICATION FOR ANTISTATIC COATINGS**

**Master Thesis**

**Pınar ŞENGÜN**

**Eskişehir 2018**

# SYNTHESIS OF DESIGNED Al- AND Ga- DOPED ZINC OXIDE (ZnO) PARTICLES AND THEIR APPLICATION FOR ANTISTATIC COATINGS

Pınar ŞENGÜN

**MASTER THESIS**

**Department of Materials Science and Engineering**
**Supervisor: Prof. Dr. Ender SUVACI**

**Eskisehir**
**Eskisehir Technical University**
**Graduate School of Sciences**
**December 2018**

# FINAL APPROVAL FOR THESIS

This thesis titled "Synthesis of Designed Al- and Ga- Doped Zinc Oxide (ZnO) Particles and Their Application for Antistatic Coatings" has been prepared and submitted by Pınar ŞENGÜN in partial fullfillment of the requirements in "Eskisehir Technical University Directive on Graduate Education and Examination" for the Degree of Master of Science in Material Science and Engineering Department has been examined and approved on 27/12/2018.

| | **Committee Members** | **Signature** |
|---|---|---|
| Member (Supervisor) | : Prof. Dr. Ender SUVACI | ...................... |
| Member | : Prof. Dr. Emel ÖZEL | ...................... |
| Member | : Prof. Dr. Münevver ÇAKI | ...................... |

**Prof. Dr. Ersin YÜCEL**

**Director of Graduate School of Sciences**

# ÖZET

## TASARLANMIŞ Al- VEYA Ga- KATKILI ÇİNKO OKSİT (ZnO) TOZLARIN ÜRETİMİ VE ANTİSTATİK KAPLAMALARDA UYGULAMALARI

Pınar ŞENGÜN

Malzeme Bilimi ve Mühendisliği Anabilim Dalı

Eskişehir Teknik Üniversitesi, Fen Bilimleri Enstitüsü, Aralık 2018

Danışman: Prof. Dr. Ender SUVACI

İletken polimer kompozitler (İPK'ler) genellikle zemin kaplamaları, antistatik boyalar, Elektrostatik deşarj (ESD) koruma paketleri, ayakkabılar ve elektrostatik yüklerin dağıtılmasının istendiği kıyafetler de dahil olmak üzere birçok üründe kullanılmaktadır. Literatürde, istenilen iletkenliği elde etmek için bu polimer sistemlere karbon bazlı malzemeler veya metal nano parçacıklar eklendiği görülmüştür. Bununla birlikte, bu dolgu malzemeleri kontrolsüz aglomerasyon, estetik olarak koyu renk ve toksisite gibi bazı dezavantajlar sergilemektedir. Bu problemlerin çözümü için araştırma grubumuz tarafından solvotermal yöntemle sentezlenen hegzagonal plaka morfolojisine sahip Al ve Ga katkılı ZnO partikülleri geliştirilmiştir. Bu tezde Al ve Ga katkılı MicNo (Micron + naNo) olarak adlandırılan mikron boyutlu hegzagonal plaka şeklinde tasarlanmış bu tozlar, kontrollü bir şekilde aglomere edilmiş birincil küresel nanopartiküllerden oluşur. Bu çalışmanın araştırma hedefleri, Al ve/veya Ga katkısının Al ve Ga-katkılı MicNo-ZnO partiküllerinin yapısal ve fizikokimyasal özellikleri üzerinde rolünü belirlemek ve daha sonra elde edilen bu özelliklerin polimer malzemeler içerisinde kullanıldığında antistatik performansını nasıl etkilediğini değerlendirmek olmuştur. Sonuçlar, Al ve Ga katkılı MicNo'nun düşük direnç değerleri ile görünür aralıkta saydam özellik sergilediklerini ve polimer matris içerisinde dağıtılarak antistatik özellik sahip oldukları görülmüştür.

**Anahtar Kelimeler:** Elektrostatik deşarj (ESD), ESD kontrol prosedürleri, ZnO, Al katkılı ZnO, Ga katkılı ZnO, İletken polimer kompozitler

# ABSTRACT

SYNTHESIS OF DESIGNED Al- AND Ga- DOPED ZINC OXIDE (ZnO)
PARTICLES AND THEIR APPLICATION FOR ANTISTATIC COATINGS

Pınar ŞENGÜN

Department of Materials Science and Engineering

Eskisehir Technical University, Graduate School of Sciences, December 2018

Supervisor: Prof. Dr. Ender SUVACI

Conductive polymer composites (CPCs) are generally used in products including floor coatings, antistatic-paints, ESD protecting packages, shoes and clothes where dissipation of electrostatic charges are desired. There are several polymeric materials and conductive fillers used in CPCs. In the literature, carbon-based materials or metal nano particles are added to these systems for obtaining desired conductivity. However, these filler materials exhibit some disadvantages such as uncontrolled agglomeration, aesthetically dark color and toxicity. The solution to these problems, developed by our research group, is utilization of Al and Ga doped ZnO particles with designed hexagonal platelet morphology synthesized by a modified solvothermal method. Such designed particles, denoted as Al and Ga doped MicNo (Micron + naNo) throughout the thesis, are composed of primary spherical nanoparticles agglomerated in a controlled manner to form micron sized hexagonal platelets. Accordingly, the research objectives of this study were to determine the role of Al and/or Ga doping on the structural and physicochemical properties of Al- and Ga-doped MicNo-ZnO particles and then to evaluate how the resulting properties affect the performance of antistatic resin in which such particles are used as fillers. The results showed that Al and Ga doped MicNo exhibit highly transparent characteristics in the visible range with low bulk resistivity values and they provide antistatic properties to polymer composites.

**Keywords:** Electrostatic discharge (ESD), ESD control procedure, ZnO, Al doped ZnO, Ga doped ZnO, Conductive polymer composites

# ACKNOWLEDGEMENTS

**STATEMENT OF COMPLIANCE WITH ETHICAL PRINCIPLES AND RULES**

I hereby truthfully declare that this thesis is an original work prepared by me; that I have behaved in accordance with the scientific ethical principles and rules throughout the stages of preparation, data collection, analysis and presentation of my work; that I have cited the sources of all the data and information that could be obtained within the scope of this study, and included these sources in the references section; and that this study has been scanned for plagiarism with "scientific plagiarism detection program" used by Anadolu University, and that "it does not have any plagiarism" whatsoever. I also declare that, if a case contrary to my declaration is detected in my work at any time, I hereby express my consent to all the ethical and legal consequences that are involved.

Pınar ŞENGÜN

# TABLE OF CONTENTS

# TABLE OF CHARTS

# TABLE OF FIGURES

# 1. INTRODUCTION

Nowadays, economical investments provide technological improvements. One of the most important components of technology are electric/electronic devices and large manufacturing areas. Electricity is essential for manufacturing areas and daily lives. Although electricity brings lots of advantages, its major disadvantage is economical and vital risks such as accidents due to electiricity. One of the most important examples of this static charges and electrostatic discharge (ESD) events. ESD events are occured by static charge formation. Firing, explosions, arc formation, breakdown of electronic circuits and devices can be occured by ESD events. Moreover, electrical shocks may even end human lives. For these reasons, preventing ESD events and their catastrophic end results are very critical.

Recently, antistatic products that dissipate electrostatic charges are being used to prevent ESD events. There are many examples for antistatic products, such as floor coatings, dyes, packages, shoes and clothes. A promising approach for such applications is using conductive polymer composites (CPCs) which consist of conductive filler materials embedded in insulative polymer matrices. Conductive pathways are formed thanks to conductive fillers which carry and ground of electrical charges. Polymers are generally insulator materials with resistivity values greater than $\approx10^{11}$ $\Omega$/sq, whereas antistatic materials have resistivities ranging from $\approx10^6$ to $10^{11}$ $\Omega$/sq. Moderate resistivity of antistatic materials is usually sufficient to provide slow decay of the static charges. If antistatic materials have very low resistivity, they might be caused arc formation.

Different types of polymer materials used in CPCs, but mostly epoxy based resins are preferred due to their good phsical and chemical properties such as chemical resistance, durability, color etc. Generally, carbon-based materials and metal nano particles are used as conductive fillers. Carbon based fillers are much more efficient than other filler materials; however, they are aesthetically undesirable due to their dark color. On the other hand, metal nano particles exhibit uncontrolled agglomeration that prevent the formation of effective conductive channels and therefore undesirable in CPC applications.

CPCs electrical performance is determined by the amount and physicochemical properties of conductive fillers. There is a critical filler concentration which is defined as percolation threshold ($p_t$). $p_t$ is the critical concentration leading to effective formation of conductive channels within polymer matrix. $p_t$ is the point above which resistivity decreases significantly. Percolation treshold is influenced by the type, morphology, size and its distribution of filler particles. High aspect ratio particles can easily create conductive networks. Nanoparticles have high surface area, but they can easily agglomerate and hinder formation of effective pathways pushing $p_t$ to higher values. It is crucial to obtain conductive pathways in polymer matrices by using less amount of filler material (i.e. low $p_t$). Fiber materials are more effective than nanoparticles and mostly carbon-based fibers are used. However, such materials have some disadvantages such as aesthetically dark color of carbon-based fillers, difficulties in production processes and toxicity. Consequently, there is a need for new materials that exhibit high electrical conductivity, high aspect ratio and if possible, transparent characteristics in the visible region.

## 1.1. The Research Objectives

To overcome the above mentioned problems, our group have developed a novel particle technology, denoted as MicNo particle technology, MicNo particles are micron sized, nanometer thick hexagonal platelets that are formed as a result of controlled agglomeration of primary spherical nanopowders. MicNo® (MicNo=Micron+naNo) particle technology brings advantages of both nano and micron size while mitigating their disadvantages. Recently, pure ZnO particles were synthesized by this process and the resulting structural and physicochemical properties of powders were investigated in detail. These particles can provide conductive networks in CPCs without exhibiting uncontrolled agglomeration due to their unique platelet morphology. Additionally, MicNo particles have transparent characteristic in the visible range, thus CPCs prepared using such particlesis also expected to be transparent which is crucial for aesthetic appearance of the end product. Doping of semiconductors to generate extra carriers is typically utilized to enhance electrical conductivity. Depending on the type of dopant (the charge value with respect to host atom), free holes or electrons are generated provided that host atoms are substitutionally replaced by the dopant in the crystal structure. Here, Al- and Ga- doped ZnO particles were synthesized by a modified solvothermal process

and the effect of doping on chemical, physical, electrical and optical properties of powders were investigated. These particles were also embedded in polymer matrices to assess their electrical performance as conductive fillers.

## 2. THE LITERATURE SURVEY

### 2.1. Electrostatic Discharge (ESD)

Technological applications in our daily lives brings various risks as well as some important advantages. These risks, especially in electrical applications, are mainly based on accidents due to static charge formation. Static electricity related accidents can cause firing, explosions, arc formation, breakdown of electronic circuits and devices which may even end human lives. According to a study conducted in Ireland, it is stated that there are 67 fire accidents due to electricity between 1996 and 2015 [1]. Routinely occurring electrostatic discharge events (ESD) in our daily lives are given in Table 2.1. Electrostatic discharge at 50-volts and above pose a great risk for human life. For this reason, electrostatic control/confinement procedures have been established to prevent electrostatic discharge events. What is important for the creation of electrostatic control procedures is to determine how static electricity and electrostatic discharge occurs and how to provide the necessary conditions for prevention. These are mentioned in the the following sections.

**Table 2.1.** *Examples of Static Generation [2]*

| Means of Generation | Voltage (V) | |
|---|---|---|
| | 10-25 % Relative Humidity | 65-90 % Relative Humidity |
| Walking across carpet | 35,000 | 1,500 |
| Walking across vinyl tile | 12,000 | 250 |
| Worker at bench | 6,000 | 100 |
| Poly bag picked up from bench | 20,000 | 1,200 |
| Chair with urethane foam | 18,000 | 1,500 |

### 2.1.1. Static electric, electrostatic charges and ESD

To explain ESD events and take necessary precautions, we need to understand the formation of static electricity. All the materials in our environment are composed of atoms. Atoms consist of protons (positive charged particles, +), neutrons (uncharged particles) and electrons (negative charged particles, -) as shown in Figure 2.1. The force of the protons and electron charges is equal, so if the number of protons is equal to the number of electrons, the atom is neutral. If the number of protons is more than electrons,

the atom is positively charged. The higher number of electrons indicates that the atom is negatively charged.
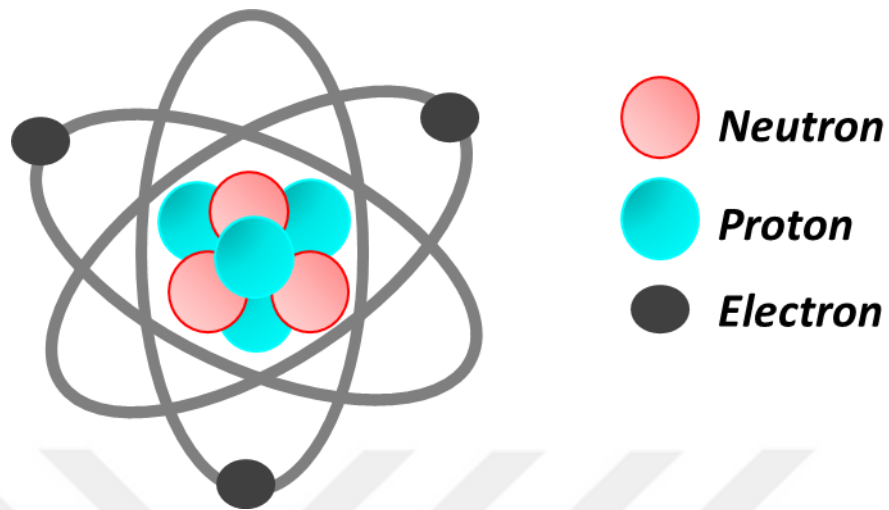


**Figure 2.1.** *Configuration of an atom*

When the interactions of charged objects are examined the objects with the same charge repel each other and the opposing charged bodies attract each other. This behavior is shown in Figure 2.2. There is also an interaction between a neutral object and a charged object. When a charged object comes into contact with a neutral object, it can cause the charging of the surface of the neutral object by sharing its charges (Figure 2.2). Static electricity means stationary electricity. The formation of static electricity occurs when the bodies share the surface electrons because of their interaction with each other. When they are separated, object is charged with excess electrons (Figure 2.3).

**Opposite charges attract**

(a)

**Like charges repel**

(b)

**Neutral and charged materials attraction**

(c)
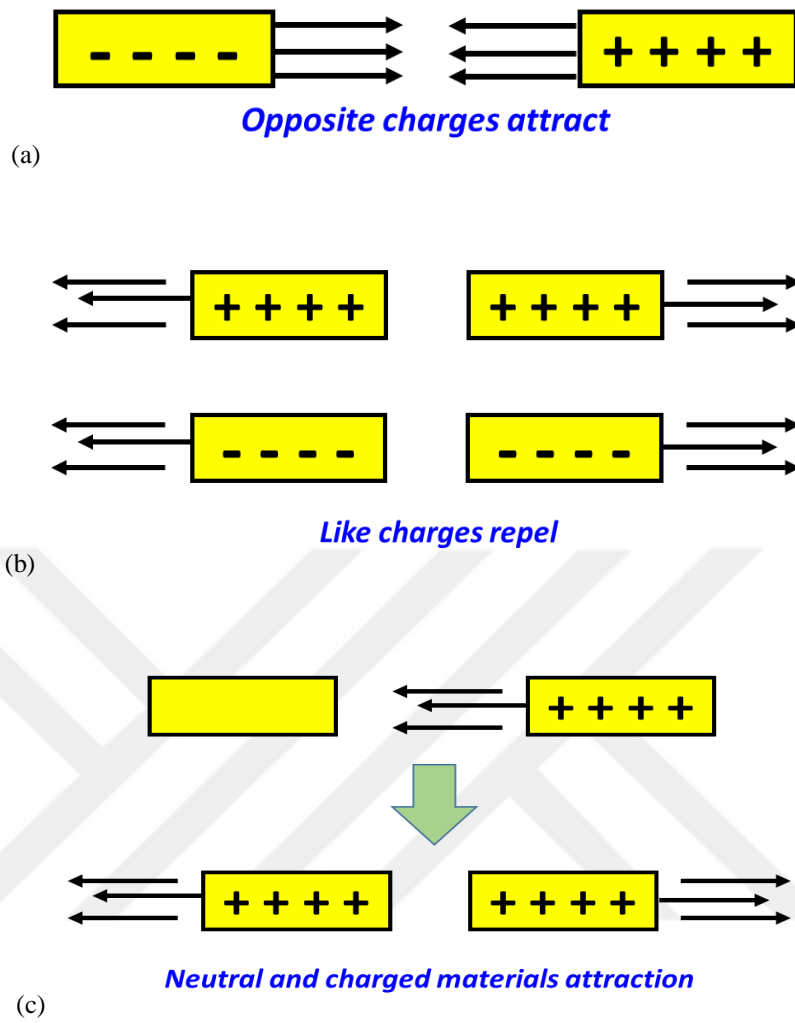
**Figure 2.2.** *Attraction between (a) opposite charged, (b) same charged and (c) neutral materials*



*Material contact*

*Material seperate*

Excess electrons
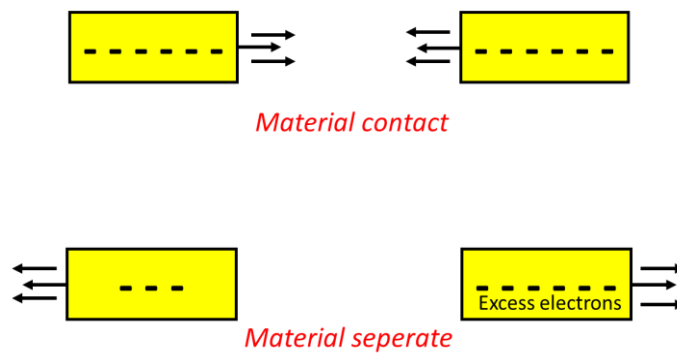
**Figure 2.3.** *Formation of static charges*

6

Static electricity is also formed when the amount of opposing electrical charges are not equal in the interior or on the surface of an object. If these charges can not find a path to flow, they will be accumulated on the surface of object resulting in build up of static charges. After a period of time, when a conductive path is formed, these charges freely move from the surface causing formation of an arc. Such events are also called ESD. ESD is caused by sudden and rapid charge flow. The most common electrostatic discharge event we often encounter in our daily lives when we touch someone after rubbing ourselves on carpet or a charged floor. In this case, our body is charged due to friction and the charges flow in an unstable manner exposing the person in contact to short-term electric shock.

We can classify the materials in 4 group depending on their behaviour under electric field;

- Insulator
- Anti-static
- Static dissipative
- Conductive

Insulating materials are materials that limit or prevent the flow of electricity. Such materials have high electrical resistance ($>10^{11}$ Ω), whereas conductive materials have low electrical resistance ($<10^4$ Ω). On the other hand, antistatic materials provide static charges formation at a minimum level. The electrical resistance of the anti-static and static-dissipative materials is between that of conductive and insulating materials ($10^4 <\rho<10^{11}$ Ω).

According to the ESD control procedures to prevent electrostatic discharges, static dissipative materials should be used to help static charges move away from the system. The charge formation on the static dissipative material surface occurs triboelectrically. Static dissipative materials provide flow and grounding of static charges on the material surface. Additionally, antistatic materials also have a slower charge flow than conductive materials. This especially important since the sudden removal of static charges from a highly conductive surface can lead to arc formation, electric shocks and various accidents. In order to prevent this, static charges must be grounded slowly from the material. Antistatic materials allow the flow of static charges, but this electrical flow is under the

control of the bulk or surface resistance. Thus, charge flow takes longer time compared to flow observed in conductive materials. Therefore, electrostatic discharge is not carried out suddenly [3]. Materials, which are used in ESD applicatons, should have electrical resistivity in the range of $10^6 - 10^9 \, \Omega$/sq [4]. A recent promising advance, to avoid harmful effects of ESD events, is using conductive polymer composites (CPCs) [5-8].

## 2.2. Composite Materials

Composite materials are obtained by combining more than one material at a macro level without dissolution behavior. The most important feature of the composite materials is that the materials have superior performance than the stand alone properties [9].

In general, composites are fomed by two main components which are matrix phase and reinforcements. These materials are classified according to the matrix phase and reinforcement type. Figure 2.4 shows the classification of composites based on reinforcement types. Furthermore, classification of the composites according to the matrix phase is shown in Figure 2.5.
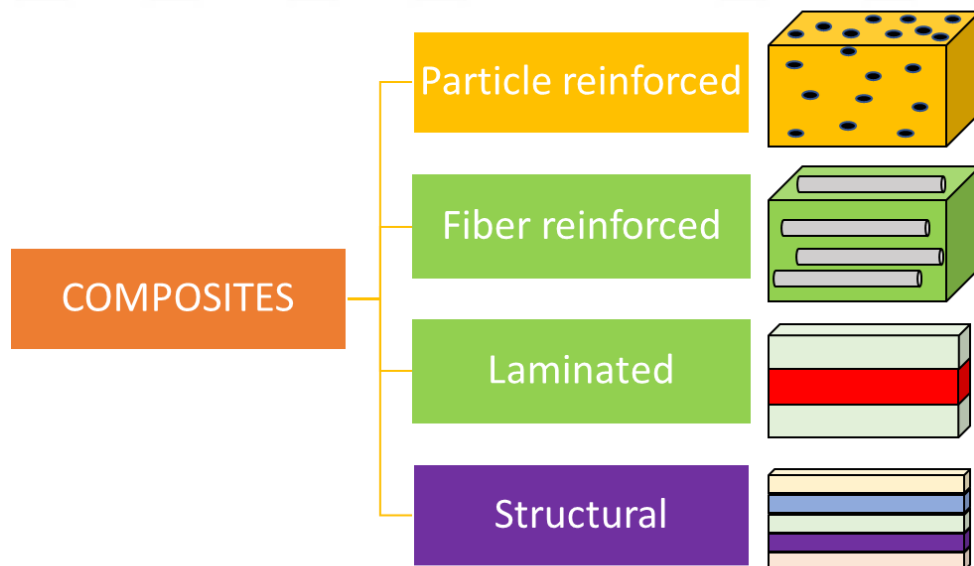


**Figure 2.4.** *Classification of composites according to the reinforcement types*
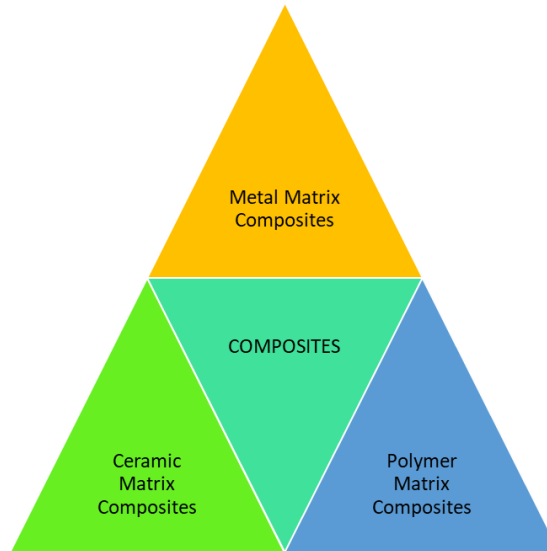
**Figure 2.5.** *Classification of composites according to the matrix phase*

In our study we used polymer matrix to obtain CPCs parts. Therefore, Part 2.2.1 explain polymer matrix composites briefly.

### 2.2.1. Polymer matrix composites (PMCs)

Polymer matrix composites (PMCs) are composite materials obtained by dispersing the reinforcing element in the polymer matrix. PMCs are advantageous due to their flexibility and lightness, apart from chemical and mechanical resistance.

Polymer matrix composites are classified into 2 main group and they are given in Table 2.:

- Thermoplastic composites
- Thermoset composites

**Table 2.2.** *Commonly used matrix phases used in thermoplastic and thermoset polymers [10]*

|  | **Matrix Phase** |
| --- | --- |
| **Thermoplastic Composites** | Polyamide |
|  | Polypropylene |
|  | Polyphnylene sulfate |
| **Thermoset Composites** | Epoxy |
|  | Polyester |

9

PMCs have many uses such as aviation, automotive, construction, electrical and medical applications, Table 3. In addition to these conductive polymer composites (CPCs) are one of the most important applications and they are significant for anti-static applications.

**Table 2.3.** *Common application areas of polymer matrix composites [11]*

| Application areas | Examples |
|---|---|
| **Aviation** | Airspace structures, satellite antennas, rocket engine enclosures, high pressure fuel tanks, fairings, wings, helicopter propellers |
| **Chemical** | Pipes, tanks, pressure tanks, valves |
| **Construction** | Bridges and walkways, handrails, cables, frames, grates |
| **Domestic** | Internal and external panels, chairs, tables, bathrooms |
| **Electrical** | Panels, housings, switchgear, insulators, connectors |
| **Sport** | Tennis rackets, ski poles, skis, protective helmets, fishing tackle, playground equipment, bicycle frames |
| **Medical** | Prostheses, wheelchairs, orthoses, medical equipment |
| **Marine** | Body, deck, mast, engine shrouds, inner panels |
| **Transportation** | Body panels, dashboards, frames, cabinets, bumpers |

## 2.3. Conductive Polymer Composites (CPCs)

Conductive polymer composites (CPCs) are obtained by mixing the insulating polymer matrix and the conductive filler materials [12]. They are preffered for antistatic applications due to their light weigths, corrosion resistance, ease production and processablity [4]. There are different types of polymers and fillers using in CPCs. Polypropylene, epoxy, phenolformaldehyde, nylon 6.6, polyvinyl alcohol, polycarbonate are commonly used in such applications [12]. With a few exceptions polymers are generally insulative materials.

Epoxy resins are mostly used resin type for the antistatic applications. They are in the thermoset resin group. Epoxy materials are used in many different application areas with the selection of curing agents, modifying elements and the use of reinforcing materials. Epoxy materials are prefered due to the high strength, high chemical stability, low production cost and low toxic properties [13]. Simple chemical structure of epoxy group is shown in Figure 2.6.
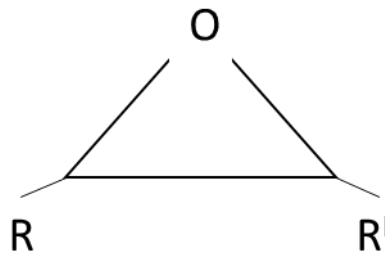


**Figure 2.6.** *Simple chemical structure of epoxy group*

In this study we used Bisphenol-A based epoxy resin which are mostly preferred in antistatic applications. Fıgure 2.7 shows the chemical structure of Bisphenol-A based epoxy resin. Epoxy resins are polymerized by the addition of a curing agent and complete the curing process in this way. Resin type and hardening agent are factors affecting the reaction rate [10].
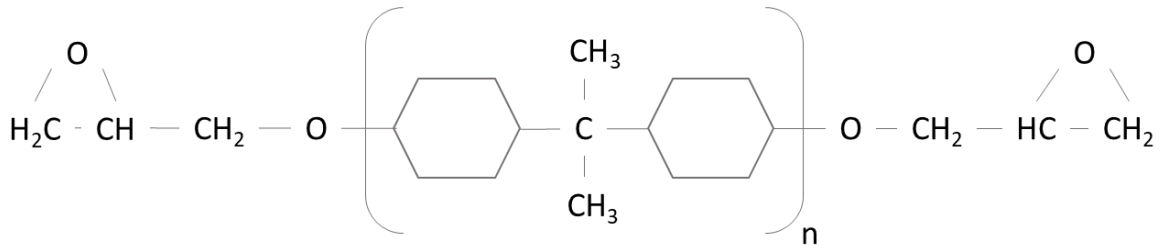
**Figure 2.7.** *Chemical structure of Bisphenol A based epoxy resin*

The transition of the polymer composite material from the electrically insulating to the conducting class is directly achieved by the filler materials and is related to the critical filler amount. This critical filler amount can be defined as the electrical percolation or percolation threshold ($\rho_t$) [14]. Additionally, percolation threshold can be defined as formation of a conductive pathway into a polymer matrix [4]. Increasing the concentration of conductive filler material contribute to increase the electrical conductivity while affecting the mechanical properties negatively. Therefore, using of conductive filler at the limit of $\rho_t$ provide advantages.

For conductive polymer composite materials to be electrically conductive, the conductive phase (filler materials) concentration must be higher than the $\rho_t$. Percolation theory can be categorized into two groups; percolation limit below and above. If the filler amount is below the $\rho_t$, the conductivity directly related to the polymer matrix. With the increase of the conducting phase, the conductive network begins to form, and the conductivity will be increased to a critical concentration.

There are also some important parameters for CPCs conductivity. These are conductive filler material properties and network structure in the polymer matrix. In the polymer matrix non-isolated fillers are formed contact which are provide conductive path. It is determined that the dominant conduction mechanism is formation of conductive network. Figure 2.8 illustrates the distribution of fiber particles in the form of isolated and percolation [4]. Filler materials show different distribution behavior due to particle shapes such as spherical or rod-shape. The increase in the aspect ratio will result in a reduction in percolation threshold and a smaller amount of filler material will be used in the use of rod materials than in the case of spherical particles.
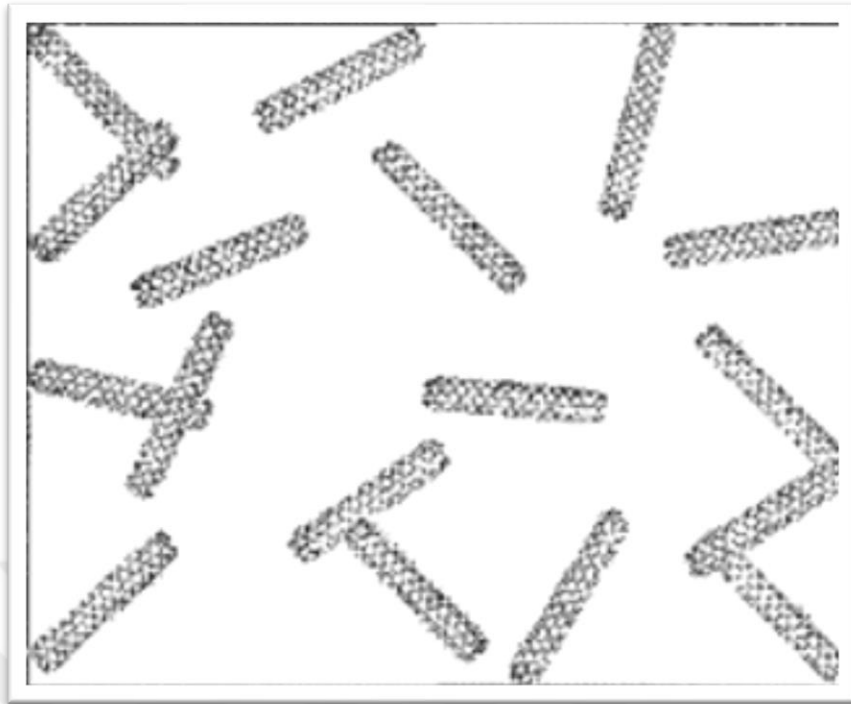
(a)
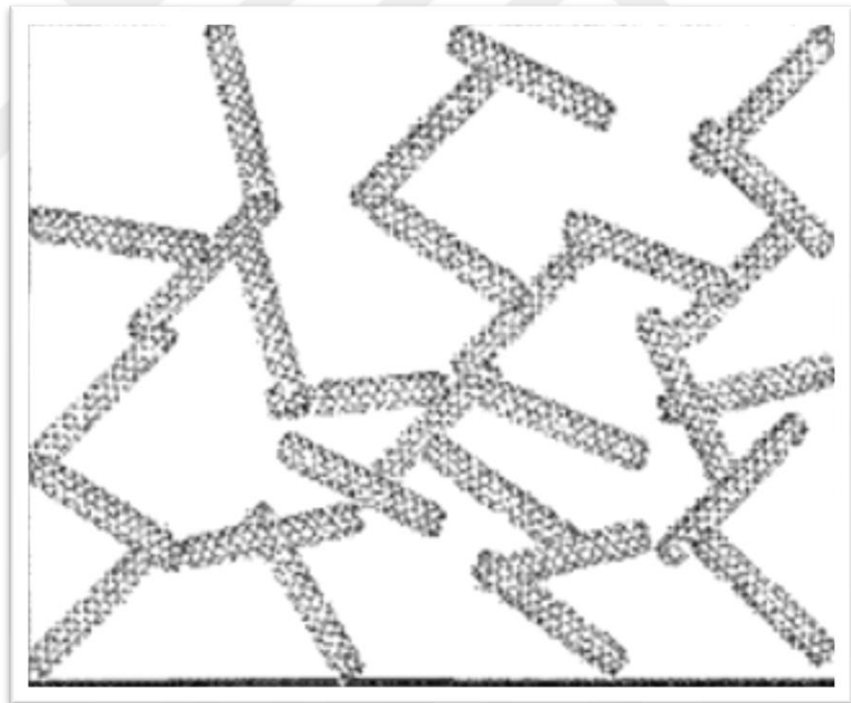


(b)

**Figure 2.8.** *Schematic description of conductive polymer composite matrix and filler material distribution (a) isolate conductive filler, (b) percolated conductive fillers*

As described above there are various parameters that may affect the electrical conductivity of the CPCs. These are the distribution of the conductive filler material, the shape and size of the particles, the conductivity of the filler material and its interaction between the matrix, the polymer matrix structure, the wettability of the conductive filler material, surface energies and production processes.

There are various types of conductive filler materials such as inorganic salts, metal nano particles and carbon-based materials [15-17]. In the Table 2.4, advantages and disadvantages of these materials are given. Examples of conductive fillers are carbon black (CB), carbon fibers (CF) carbon nano tubes (CNTs) and metal nano particles such as silver, copper and nickel particles [12].

Carbon black (CB) is an amorphous form of carbon and it is commercially obtained by thermal or oxidative degradation of hydrocarbons. Its electrical resistivity is given as $10^{-2}$ $\Omega$.cm [18,19]. The availability, chemical stability and low cost of carbon black provided the most widely used filler material for ESD protection. However, it has disadvantages and limitations in practice. The use of high rates of CB improves electrical properties but leading to reduced mechanical properties and increased costs. In addition, their dark color is aesthetically disadvantageous [4,17].

On the other hand, metal nano particles such as Ag, Cu and Ni have good electrical performance. However, they have low oxidation resistance and high surface resistivity. This is basically related to the electromigration of metallic fillers. Because of these, some of the metal nanoparticles should modified with surface modification processes [17].

There is a study in the literature by Shang et al., where $BaTiO_3$ particles were modified by rear earth elements (La, Ce, Pr, Nd, Sm and Gd) then dispersed into epoxy polymer matrix and electrical properties were analyzed. It shows that modified $BaTiO_3$ particles were added into polymer, they have lower surface electrical resistivity which is $1.18x10^{10}$ $\Omega$ [15,17]. These results clearly show that conductive filler properties directly affect the conductivity of composite materials.

Shui and Chang were studied on nickel coated carbon filament/PES composites. They observed that metal coated particles improve electrical resistivity and these particles were also enhance the composite materials' electrical conductivities [20].

**Table 2.4.** *Advantages and disadvantages of usually used conductive filler materials*

| | Conductive Fillers | | | |
| --- | --- | --- | --- | --- |
| | **Carbon Based** | **Metal Nano Particles** | | |
| | | *Silver* | *Copper* | *Nickel* |
| **Advantages** | ▪ Chemical stability<br>▪ Electrical conductivity | ▪ Electrical conductivity | ▪ Electrical conductivity | ▪ Electrical conductivity<br>▪ Production cost<br>▪ High oxidation resistance |
| **Disadvantages** | ▪ Production cost<br>▪ Dark color | ▪ Production cost<br>▪ High surface electrical resistance | ▪ Low oxidation resistance | ▪ Surface modification requirements |

In addition to these filler materials, conductive oxides are used as conductive filller materials in the polymer matrix. Due to the recent development of technological and more aesthetic products, transparent and conductive oxides are used as conductive filler in antistatic coatings and conductive inks [21]. Conductive oxides (COs) have wide band gap and high electrical conductivity. Additionally, they are also prominent in applications where transparency and electrical conductivity are needed. Commonly used conductive oxides can be given as $In_2O_3$, $SnO_2$, $CdO$, $Ga_2O_3$ and $ZnO$ [22].

COs are widely used in liquid-crystal display (LCD) panels and in various electronic circuits. Indium tin oxide (ITO) is genarally used in such applications. Nevertheless, scarcity of indium sources and environmental problems of indium materials, there is a need for alternative materials. Zinc oxide (ZnO) and doped ZnO materials are alternative materials due to their advantages such as chemical properties, electrical properties, ease production and less toxicity [23]. Moreover, ZnO based materials are alternatively used in antistatic products as conductive filler.

## 2.4. Zinc Oxide (ZnO) and Doped ZnO Materials

In recent years, the pure ZnO and ZnO based materials have been named as the materials of the future because of their unique properties. ZnO is the oxide form of metallic Zn in the IIA group. This material is used for many different applications because of its piezoelectric, semiconductor and optical properties. Table 2.5 shows that the general properties of ZnO material [24]. Additionally, ZnO materials are the semiconductor compound in the group of II-IV and it has 3 different crystal forms. Figure 2.9

demonstrates that the different types of ZnO crystal structures. ZnO is stable in the hexagonal wurtzite phase under ambient conditions and the lattice parameters are a = 0.32495 nm and c = 0.52069 nm.

**Table 2.5.** *Physical properties of Zinc Oxide (ZnO)*

| Properties | |
|---|---|
| **Lattice Constant (T = 300k)** | |
| $A_o$ | 0,32469 nm |
| $B_o$ | 0,52069 nm |
| **Density** | 5,606 g/cm$^3$ |
| **Melting Point** | 2248 K |
| **Dielectric Constant** | 8,66 |
| **Band Gap** | 3,37 eV |
| **Carrier Concentration** | $<10^6$ cm$^{-3}$ |
| **Activation Energy** | 60 meV |
| **Electron Mass** | 0,24 |
| **Electron Mobility (T = 300k)** | 200 cm$^2$/V. s |
| **Electron Gap Mass** | 0,59 |
| **Space Mobility (T = 300k)** | 5 – 50 cm$^2$/V. s |
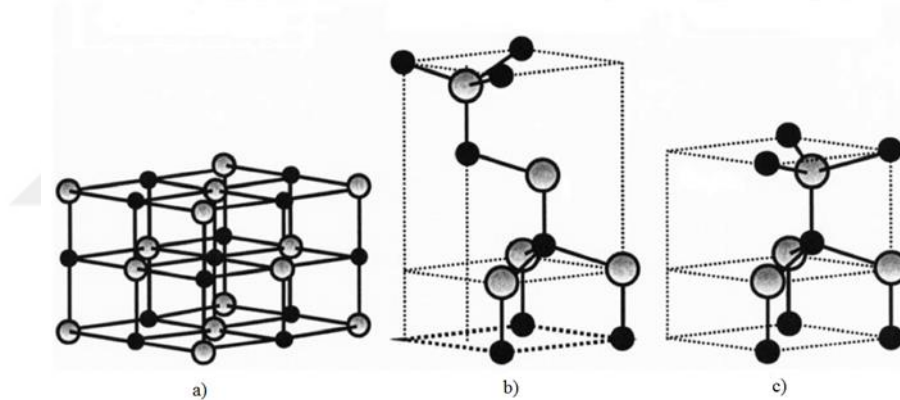
**Figure 2.9.** *Zinc oxide (ZnO) crystal structures (a) cubic rock-salt, (b) cubic zinc sülfite and (c) hexagonal wurtzite (gray spheres are Zn and black spheres are identified O atoms)[25]*

ZnO materials have wide direct band gap values that 3.37 eV. This value provides absorption of ultraviolet (UV) rays. According to these properties ZnO particles can be used in cosmetics products [26].

ZnO has the mineral zincite form and hexagonal wurtzite (P63mc) structure in the nature. In wurtzite type ZnO structure, Zn interstitial atoms and electrons are produced by oxygen vacancies and crystal defects [27-32]. In other words, defects in ZnO crystal structure lead to intrinsic n-type conductivity characteristics [33]. The electrical conductivity of zinc oxide is directly related to the charge carrier concentration and stoichiometry in the structure. While pure ZnO crystals have $10^{15}$ cm$^{-3}$ carrier

concentrations, this value can be $10^{20}\,cm^{-3}$ in doped ZnO crystals [23]. Pure bulk ZnO has relatively high electrical resistivity; however, there are different methods for improving the electrical resistivity of ZnO materials such as doping process. Electrical, optical, thermal and magnetic properties of ZnO materials are improved by adding dopant elements.

There are many studies in the literature, where to increase electrical conductivity of ZnO materials doping method was used to increase charge carrier concentration. Al, Ga, B, In, Y, Sc, F, V, Si, Ge, Ti, Zr, Hf, Mg, As and H elements are used to n-type doping of ZnO crystal structure [21,22]. The selection of the dopant elements is important for obtaining stable crystal structure. In ZnO crystal structure $Zn^{2+}$ and $O^{2-}$ ions are tetrahedrally coordinated. Thus, it is expected that dopant element should be placed in the crystal structure and must be stable in that position. For dopant ion to be stable there it should have similar ionic radius with $Zn^{2+}$ ion which is 0.074 nm. Two of the most possible dopant elements for ZnO system are Al (0.053 nm) and Ga (0.060 nm) [35,36]. Additionally, Al and Ga doped nanoparticles have transparent characteristics. There are several studies on Al and / or Ga doped ZnO systems from past to present. In the literature, there are studies which are synthesize doped ZnO particle with different Al and Ga dopant ratios by mol or weight percentage. Hartner et al. were studied on synthesis of Al doped ZnO by solid phase mixing method and solubility limit of Al is found that 37.6 wt % [37]. According to studies in recent years, there are critical dopant concentration for Al and Ga doping. Electrical resistivity decreases up to critical dopant limit value. When the critical value is exceeded, it is observed that the electrical resistivity is increased [36,37].

The electrical resistivity of the particles may change by additional heat treatment processes, except of the doping amount effect. In the study conducted by Zhang et al., the electrical resistivity of the 6 mol% Al doped ZnO particles, which are synthesized by sol gel method, have 1.2 Ω.cm resistivity at 1173 K and the electrical resisitivity decreased as a result of the heat treatment process [38]. In addition to this, Izumi et al. were reported that 1 wt% Al doped ZnO particles have $10^4$ Ω.cm electrical resistivity and 3 wt% Ga doped ZnO particles have 30 Ω.cm [38]. These electrical resistivity values show that Al and / or Ga doped ZnO powders can be used in antistatic applications. There are commercial Al and Ga doped ZnO products, which belongs to Hakusui Tech., are used

17

in antistatic applications. The specific characteristics of these products are given in Table 2.6.

**Table 2.6.** *Properties of commercial Al and Ga doped ZnO particles [38]*

| Sample & Properties | 23 – K | Pazet Ck | Pazet Gk – 40 |
|---|---|---|---|
| Composition | *Al doped ZnO* | *Al doped ZnO* | *Ga doped ZnO* |
| Bulk Resistivity (Ohm.cm) | 100 – 500 | $5 \times 10^3 – 2 \times 10^4$ | 20 – 100 |
| Specific Surface Area ($m^2$/gr) | 4 – 10 | 30 – 50 | 30 – 50 |
| Primary Particle Size (nm) | 120 – 150 | 20 – 40 | 20 – 40 |
| Average Particle Size ($\mu$m) | 4 – 7 | 2 – 5 | 2 – 5 |

## 2.5. Statement of The Problem and Proposed Solution

Nanoparticle application areas are broadened by development of technology and these particles are taked part in antistatic products. Nano size materials have unique properties due to their high specific surface areas. However, high specific surface area is caused the uncontrolled agglomeration. This led to different performances of products and also in production processes.

Nanoparticles are used as conductive filler materials in conductive polymer composites, so they provide advantageous to interaction between the filler material and the polymer material due to their high surface areas. However, they are caused uncontrolled aglomeration because of their high surface energy. Therefore, need to some modification process for nanoparticles used in polymer matrix [39]. At the same time, considering the current environmental conditions, the toxicity effects of nano-sized materials are also important. There are many studies on the use and application of nano particles as well as the harmful effects of these powders on people exposed to nanoparticles during production [40,41]. Therefore, it is necessary to develop products that minimize the negative effects of nano particles on human health and environment. There is a need for new materials that will not affect the application performance, also have unique properties of nano particles, and prevent the disadvantages such as uncontrolled aglomeration and toxicity. At this point, previously pure haxagonal platelet shape ZnO particles, which are consisted of primary particles, were produced by using

modified solvothermal method [42]. Scanning electron micrographs of this particles are given in Figure 2.10. According to these graphs these particles are 5-10 micron sized particles that consist of 25-35 nm primary particles. To the best of our knowledge, there is no study on the production of designed shaped Al and Ga doped ZnO particles.
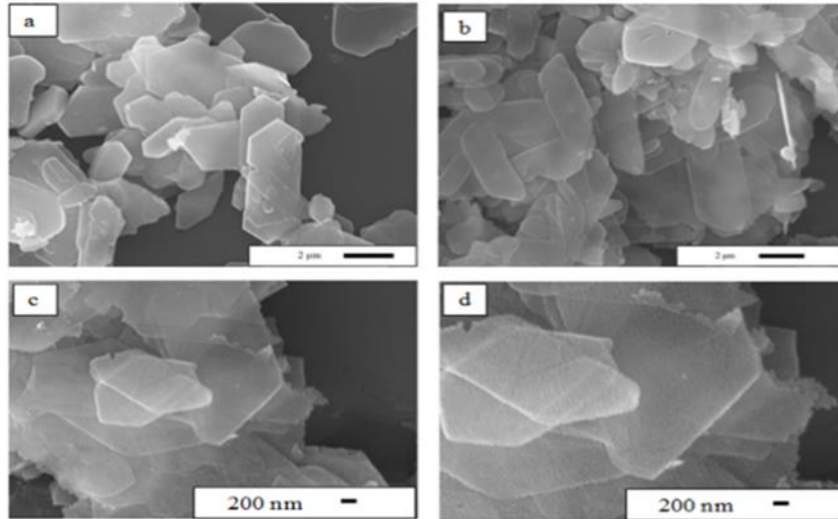


**Figure 2.10.** *Scanning electron micrographs of designed shape platelets consisting of nano sized ZnO particles [42]*

When examined many of the studies in the literature, we can say that the conductivity of CPCs is directly related to the amount of percolation threshold, the electrical properties and the shape of filler materials. In this project, designed shape Al and Ga doped ZnO particles were dispersed in the epoxy polymer matrix. It is expected that the platelet particles have better percolation behavior than spherical particles, thus optimum electrical resistivities for antistatic products may achieved by lower conductive filler concentrations. Figure 2.11 demonstrates that possible percolation network by using platelet morphology particles, then the amount of filler in the polymer increases from the first to the third picture. It is expected that the desired resistivity values is achieved by the addition of lower amounts of designed shape Al and / or Ga doped ZnO particles than the nano size and spherical shape conductive fillers. Expected performance of this study is hypothetically drawn on Figure 2.12.
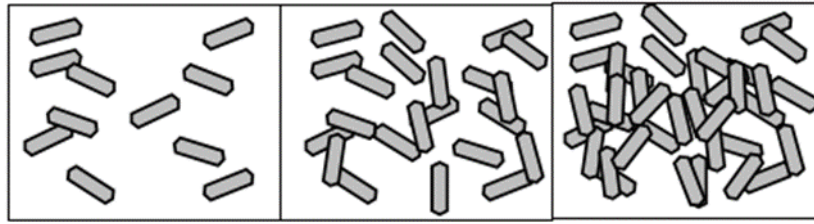
**Figure 2.11.** *Expected conductive network structure of Al and / or Ga doped ZnO powders in polymer matrix*
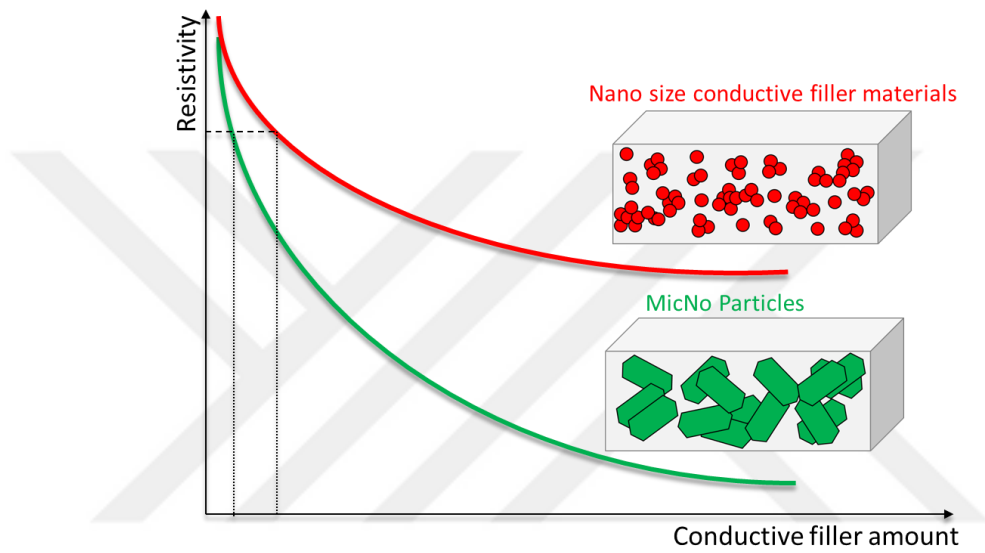


**Figure 2.12.** *Hypothetically drawing of expected performance impact*

## 3. EXPERIMENTAL PROCEDURE

In this study we synthesized undoped and doped MicNo-ZnO particles and characterized their structural, morphological, electrical and optical properties. Then, we determined the effect of doped MicNo-ZnO particles in antistatic coatings, epoxy polymer matrix composites were prepared. Therefore, experiments can be divided into three parts;

- Undoped and doped MicNo-ZnO particles synthesis
- Structural, morphological, optical and electrical characterizations of undoped and doped MicNo-ZnO particles
- Preparation and electrical characterization of conductive polymer composites (CPCs)

## 3.1. Undoped and Doped MicNo-ZnO Particles Synthesis

In this project, Al and Ga doped ZnO particles were synthesized by MicNo process. Previously, this process investigated by our group and pure ZnO particles were synthesized by MicNo process [42]. MicNo processes flow chart were shown in Figure 3.1. The synthesis of doped ZnO particles were carried out by adding the doping source material in the synthesis process. Figure 3.2 shows that general experimental flow chart.
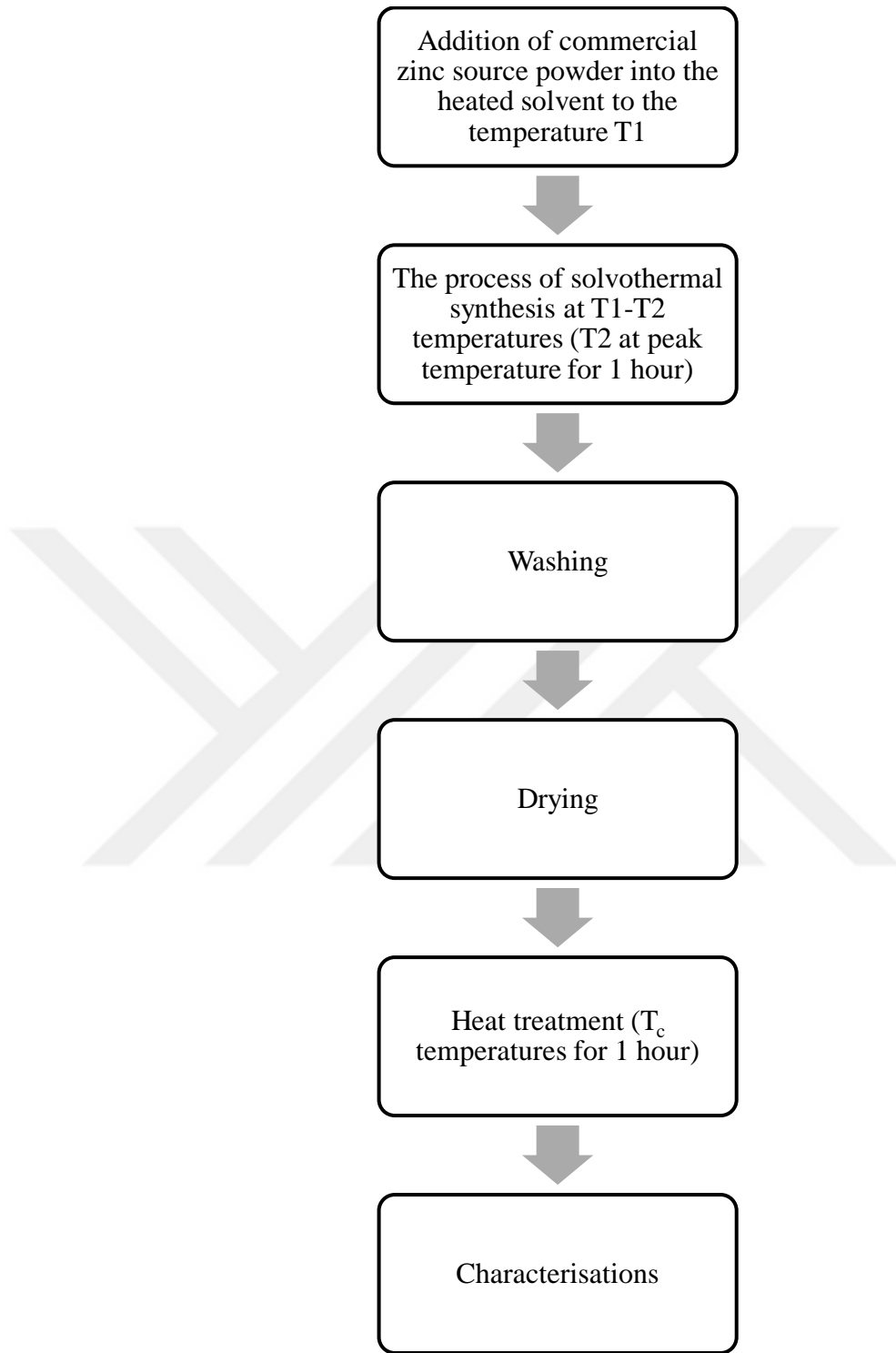
**Figure 3.1.** *MicNo process flow chart*
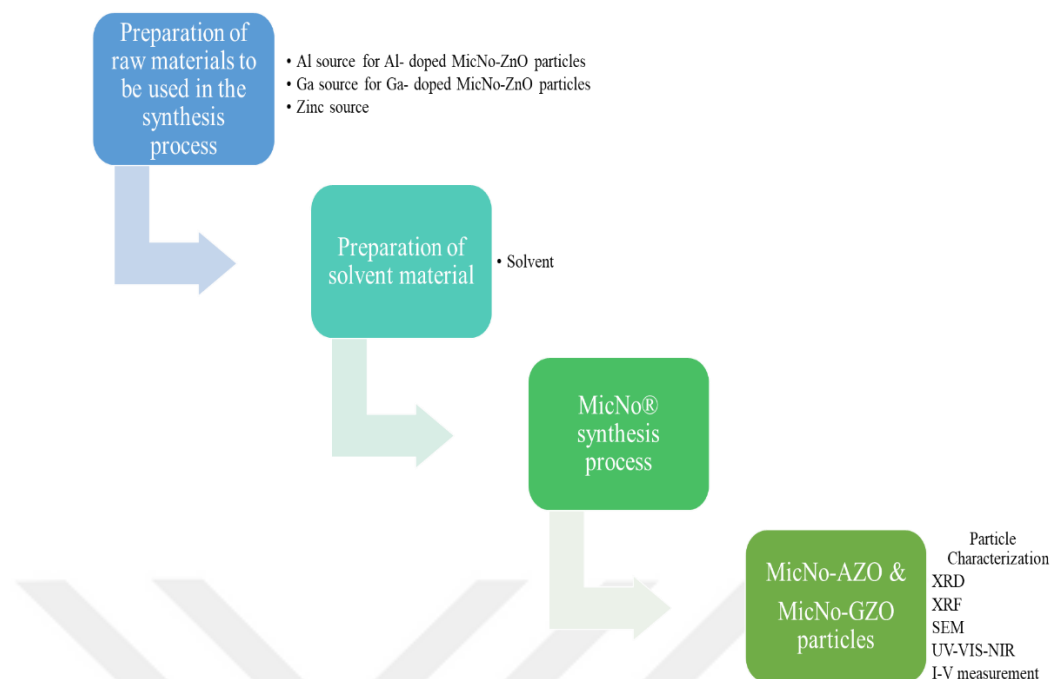
**Figure 3.2.** *General experimental flow chart*

## 3.1.1. Al doped MicNo-ZnO particle synthesis

### 3.1.1.1. *Determination of the effect of Al dopant material on MicNo-ZnO particles*

In this section of the study Al doped MicNo-ZnO particles were synthesized by MicNo process with using different Al source materials and concentrations. The Al source was denoted as Material A and Material B. Experimental studies were completed to determine the effects of Al dopant on particle properties such as phase and morphology;

> ➢ Synthesis temperature
> ➢ Effects of Al dopant concentration

*Determination of the effects of synthesis temperature*

In this part of the study, the effects of synthesis temperature, which is a synthesis parameter, were analyzed. Normally, MicNo synthesis process, there are two critical temperature; $T_1$ and $T_2$. While raw materials were added at $T_1$ temperature, the system is held at $T_2$ temperature about 1 hour.

23

To determine the effects of synthesis temperature, the system is held at $T_3$ temperature instead of $T_2$ temperature. Samples were prapered by using Material A and Material B with same doping concentration. Synthesis process were completed at $T_2$ and $T_3$ peak temperatures. According to these, the relationship between doping amount and the morphology was investigated. In Table 3.1 samples and synthesis parameters are presented.

**Table 3.1.** *Samples and synthesis parameter information*

| Samples | Synthesis Information |
|---------|-----------------------|
| I | Material A, $T_2$ synthesis temperature |
| II | Material B, $T_2$ synthesis temperature |
| III | Material A, $T_3$ synthesis temperature |
| IV | Material B, $T_3$ synthesis temperature |

### *The effect of Al dopant amount on particle morphology and physicochemical properties*

To determine the effect of Al doping concentration on particles structural, chemical properties and morphological characteristics, different amount of Al dopant concentrations was studied, and the doping amount was calculated by using the Equation 3.1.

$$\frac{x \, mol \, Al}{y \, mol \, ZnO + x \, mol \, Al} \, x \, 100 = Al \, mol \, \% \qquad (3.1)$$

Within the scope of this project, determine the particle properties with respect to Al dopant concentration. During the synthesis process dopant amounts were calculated according to the mol percentage. In Table 3.2 shows sample names and dopant amounts of the particles.

**Table 3.2.** *Sample names and dopant amounts*

| Doping Amount | Sample Name | |
| --- | --- | --- |
| | **Material A** | **Material B** |
| 0 | *MicNo - ZnO* | |
| 1 | *A-1* | *B-1* |
| 2 | *A-2* | *B-2* |
| 4 | *A-3* | *B-3* |
| 6 | *A-4* | *B-4* |
| 8 | *A-5* | *B-5* |
| 10 | *A-6* | *B-6* |
| 15 | *A-7* | *B-7* |

## 3.1.2. Ga doped MicNo-ZnO synthesis

In this section of the study Ga doped MicNo-ZnO particles were synthesized by MicNo process with different Ga dopant concentrations. The Ga source was denoted as Material C. The Equation 1 was used to calculate Ga amount. Sample names and dopant amounts of the particles were shown in Table 3.3.

**Table 3.3.** *Ga doped MicNo-ZnO particles dopant amounts and sample names*

| Doping Amount | Sample Name |
| --- | --- |
| | **Material C** |
| 0 | *MicNo - ZnO* |
| 1 | *C-1* |
| 2 | *C-2* |
| 4 | *C-3* |
| 6 | *C-4* |
| 8 | *C-5* |
| 10 | *C-6* |
| 15 | *C-7* |

## 3.2. Characterization of Undoped and Doped MicNo-ZnO Particles

Undoped and doped MicNo-ZnO particles were characterized to determine their structural, morphological, electrical and optical properties. Structural, morphological, electrical and optical properties of MicNo-ZnO were investigated with respect to Al and Ga dopant concentration. Phase analyses of the powders were performed by x-ray diffraction (D2 Phaser, Bruker) with CuKα (λ=0.154 nm) radiation and x-ray source operating voltage of 40 kV. The Scherrer equation was used to determine the crystallite size of particles from the XRD spectra. X-ray diffraction technique is qualitative and quantitative analysis method which are mostly used for phase analyses [43]. According to the XRD patterns of the powders crystallite size of particles were calculated by using the Scherrer equation as given Equation 3.2.

$$t = \frac{0.9\,\lambda}{B\,cos\theta} \qquad (3.2)$$

t: Avarage particle size

λ: Wavelength of X-Ray

B: Full width at half maximum (FWHM)

Ө: The diffraction angle

Light scattering method used for measuring particle size (Mastersizer 2000, Malvern). Powder samples were dispersed into diluted water and put into ultrasound bath for 5 min. before measurements. Additionally, specific surface area, Brunauer–Emmett–Teller (BET), analyses were performed (Autosorb-1, Quantachorome Instruments). Then, equivalent diameter of particles was calculated from BET results assuming the MicNo particles are spherical. Equation 3.3 were used for this calculation [44].

$$S.S.A = \frac{6}{\rho\ x\ d} \qquad (3.3.)$$

S.S.A: Measured specific surface area

ρ: Density of ZnO

d: Equivalent diameter of particles

Undoped MicNo-ZnO particles have hexagonal platelet morphology. To investigate the effect of Al- and Ga- doping on particle morphology scanning electron microscopy (SEM EVO 50 LP, Zeiss) analyses were operated at 15 kV.

Electronic structure of the materials might be changed by doping process. In addition to this defect structure might be changed. Raman spectrums were collected via Raman microscopes (InVia Raman Microscope, Renishaw) to characterize the differences undoped and doped particles. Measurement parameters are:

- Laser 532 nm wavelength
- Laser power is 50 LP
- Scanning range of 200-800 cm$^{-1}$

Additionally, IR vibrational modes of undoped and doped MicNo-ZnO particles were analyzed by using Fourier Transformed IR spectrophotometer (IR Tracer-100, Shimadzu) with diffuse reflectance spectroscopy (DRS-8000A) attachment. Measured samples prepared with KBr and scanning range of spectrums are 380-2000 cm$^{-1}$.

To identify transmittance and absorbance behavior of undoped and doped MicNo-ZnO particles, UV-VIS-NIR spectrophotometer (UV-3600 Plus UV-VIS-NIR, Shimadzu) were used. Spectrums are in a wavelength range of 240-800 nm. Measurement samples were prepared by an aqueous suspension that was 0.1 mg/ml.

Band gap calculations were made from reflectance measurements. Powder samples were used for these analyses and particles pressed into powder sample holder. These spectrums used for drawing Tauc plots via Kubelka Munk theory. On each samples Tauc plots draw a tangent line at linear portion to obtain band gap value at intersection point of this tangent line and x=0 position [45,46].

Once and for all particle characterizations electrical measurements were completed with pellet samples which were obtained under 20 MPa pressure. Electrical resistivities were measured by using two-point probe configuration (4200 SCS, Keithley). Figure 3.3 shows that measurement system schematically.
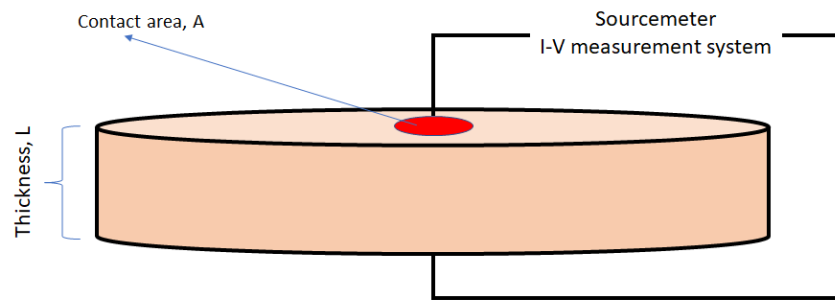
**Figure 3.3.** *Schematic configuration of electrical measurement system for undoped and doped MicNo powder compacts*

## 3.3. Preparation and Electrical Characterization of Conductive Polymer Composites (CPCs)

In this part of the study, to determine the effect of doped MicNo–ZnO particles in antistatic coatings, epoxy polymer matrix composites were prepared using a commercial antistatic coating epoxy polymer resin, which is Bisphenol A based epoxy resin, and hardener (ADS Kimya Co.). The polymer resin and hardener were used as 2:1 resin/hardener ratio. Different amounts of filler were added into the polymer matrix. Symbol f is used for filler amount in wt %. We studied f= 0, 2, 5 and 10 wt % of filler materials. CPCs were cured at room temperature for 7 hours. After the curing process, I-V measurement were completed by using two-point probe. Figure 3.4. shows the flow chart of the CPCs production process.
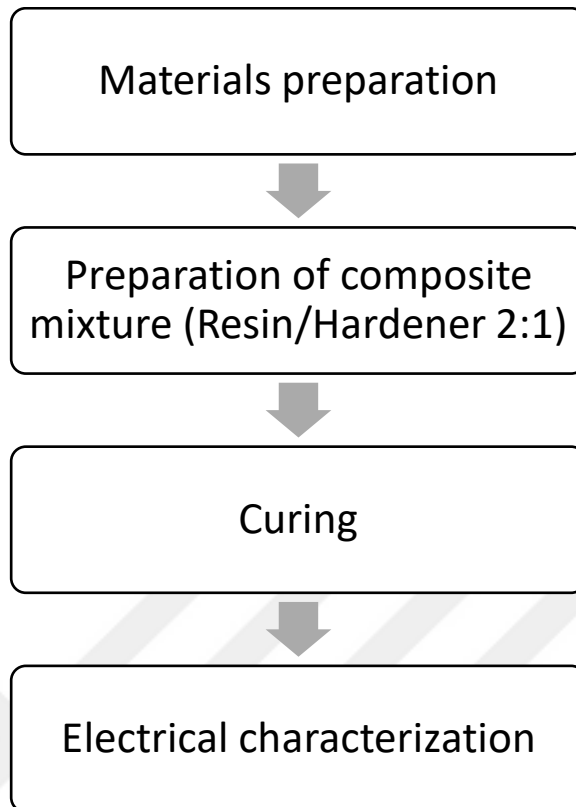
**Figure 3.4.** *CPCs production flow chart*

# 4. RESULTS

## 4.1. Undoped and Doped MicNo-ZnO Particle Synthesis

### 4.1.1. MicNo-ZnO particles

Undoped MicNo-ZnO particles were synthesized by MicNo process. Phase analysis of these particles examined by x-ray diffraction techniques as shown in Figure 4.1. This sample shows hexagonal wurtzite type ZnO crystal structure with PDF card number is 89-1397. MicNo-ZnO crystallite size was calculated from Debye Scherrer equations and it was found that ~22 nm.
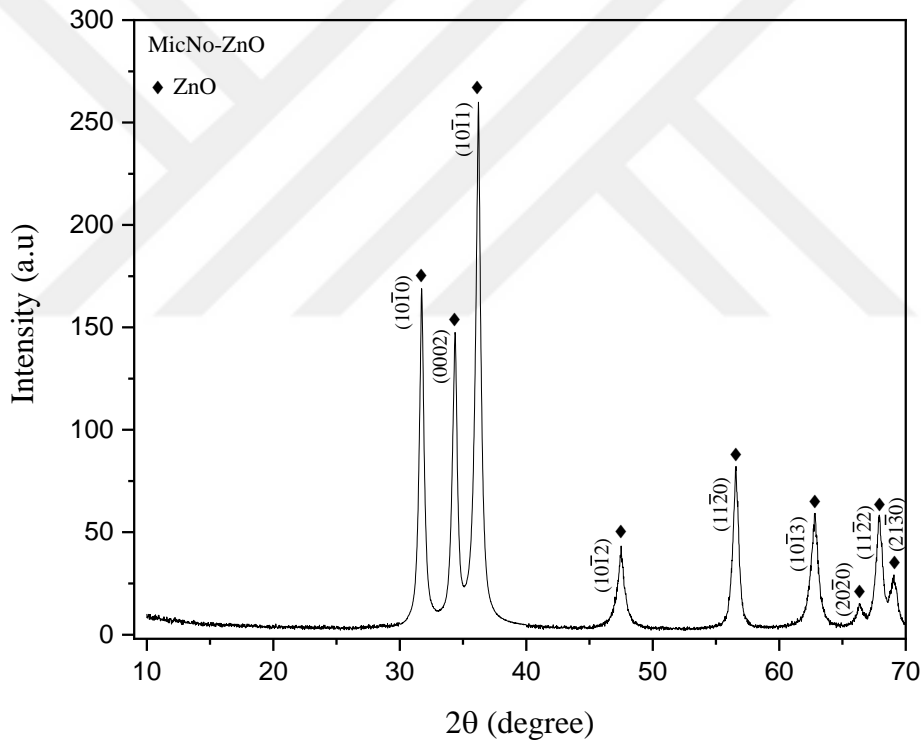


**Figure 4.1.** *XRD patern of the undoped MicNo-ZnO particles*

Figure 4.2 shows that SEM micrograph of MicNo-ZnO particles. Typically, MicNo particles have hexagonal platelet morphology and they are 5-10 μm in size with thicknesses less than 100 nm. Additionally, particle size measurements were completed and MicNo-ZnO particles are approximately 6 μm in size and have broad particle size range, Figure 4.3. Specific surface area of the MicNo-ZnO particle is ~25 g/m$^2$. According to this, equivalent spherical diameter is ~ 35 nm.
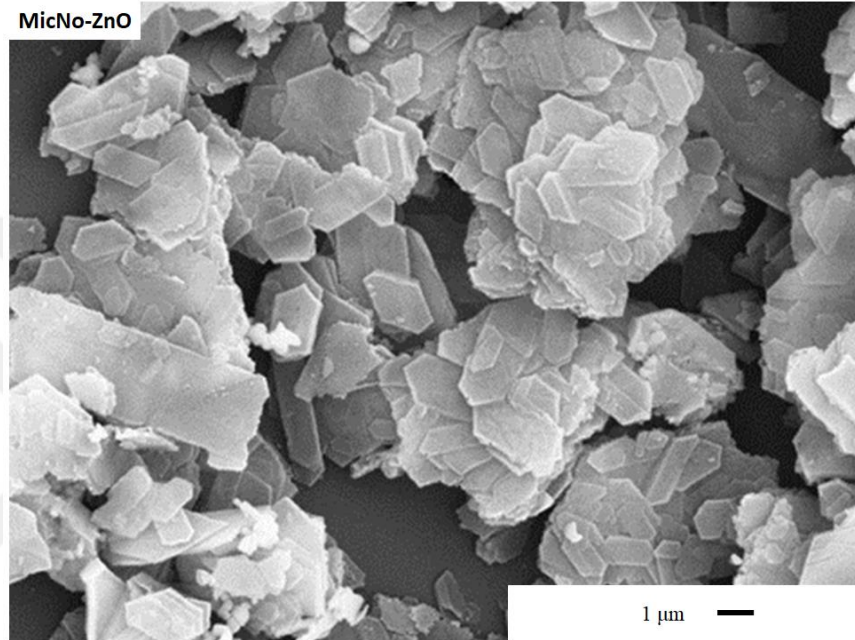


**Figure 4.2.** *SEM micrograph of undoped MicNo-ZnO particles, 15kX*



| Sample Name | Particle Size (μm) | | |
|---|---|---|---|
| | $d_{10}$ | $d_{50}$ | $d_{90}$ |
| MicNo-ZnO | 3 | 6 | 14 |
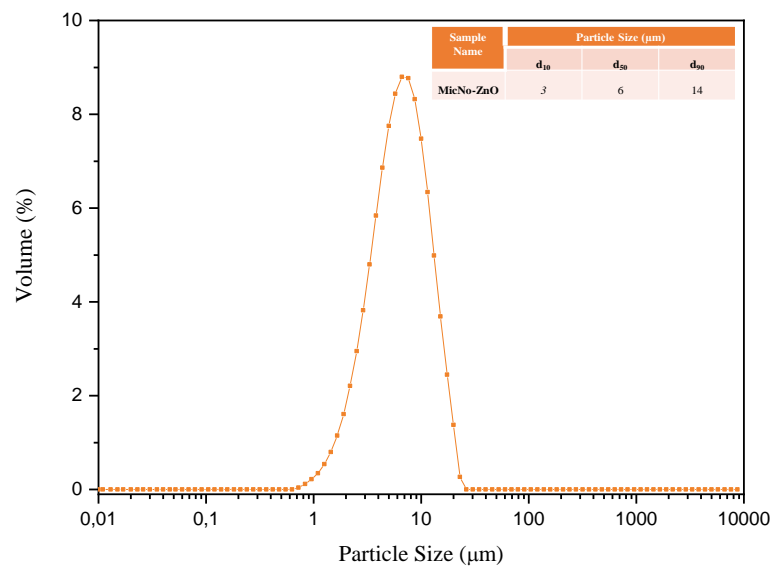
**Figure 4.3.** *Particle size distribution graph of MicNo-ZnO particles*

Optical characteristics of undoped MicNo-ZnO particles were identified by UV-VIS spectrophotometer as shown in Figure 4.4 that shows Transmittance – Wavelength spectrum of MicNo-ZnO particles. They have highly transparent characteristics in the visible range (400-700 nm). In the UV range (240-400 nm) absorption characteristic is more prevalent as also shown in Figure 4.5.
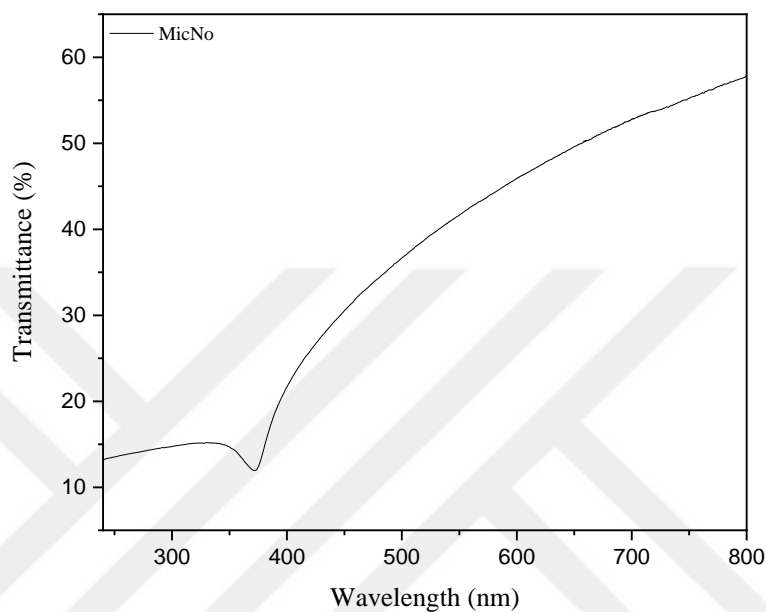


**Figure 4.4.** *Transmission graph of MicNo-ZnO particles*
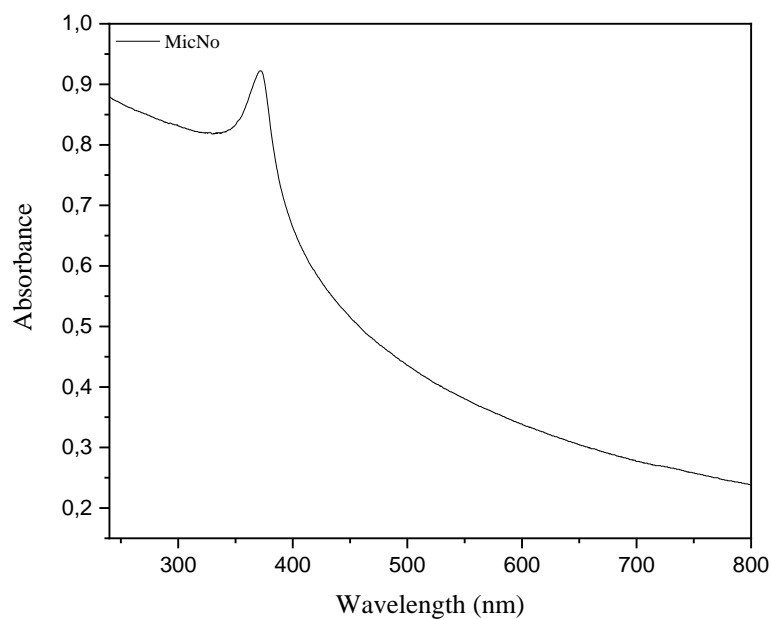


**Figure 4.5.** *Absorption graph of MicNo-ZnO particles*

### 4.1.2. Al doped MicNo-ZnO particles

#### 4.1.2.1. *Effects of synthesis temperature and dopant materials on MicNo-ZnO particles*

Normally, during the MicNo process there are two critical temperature as mentioned above (Part 3.1.1.1.) which are $T_1$ (raw materials add into system at this temperature) and $T_2$ (system holds on 1h at this temperature, $T_2 > T_1$). We synthesized Al doped MicNo-ZnO particles at $T_3$ temperature with different Al source (Material A and Material B).

Figure 4.6 shows that x-ray diffraction analysis of these particles and all the particles have hexagonal wurtzite type of ZnO structure like as undoped MicNo-ZnO particles.
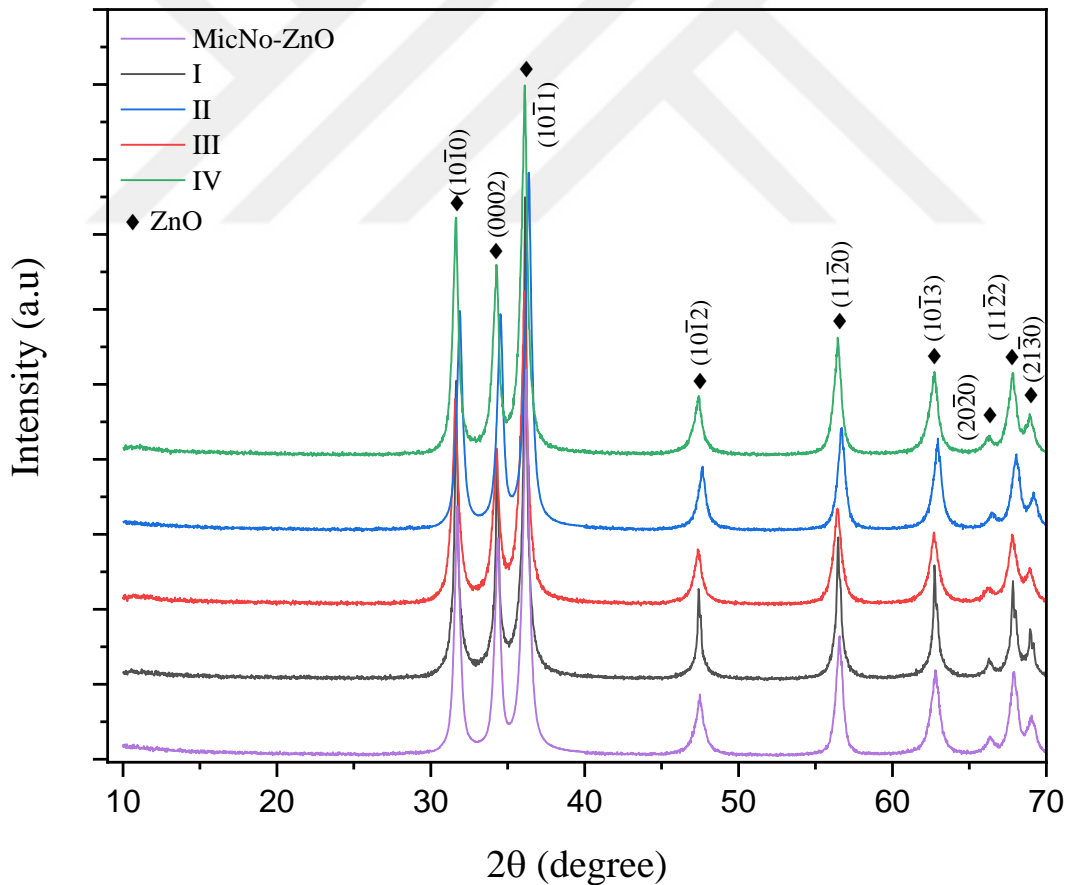


**Figure 4.6.** *X-Ray diffraction patterns of Al doped MicNo-ZnO particles synthesized at different temperatures with different Al dopant matarials*

SEM micrographs of these particles were shown in Figure 4.7. Sample I and III belong to Material A doped MicNo-AZO particles. While Sample I was synthesized at $T_2$ temperature, Sample III synthesized at $T_3$ temperature. As observed both Sample I and III were not have typical MicNo-ZnO morphology. Sample I have micron size elongated shaped particles. On the other hand, Sample III have micron size non equiaxed agglomerated particles. Besides of these, Samples II and IV which were synthesized by using Material B as Al source, have MicNo morphology. Sample II was synthesized at $T_2$ temperature, Sample IV synthesized at $T_3$ temperature and both have platelet morphology. Figure 4.8 demonstrates particle size distribution of these particles.
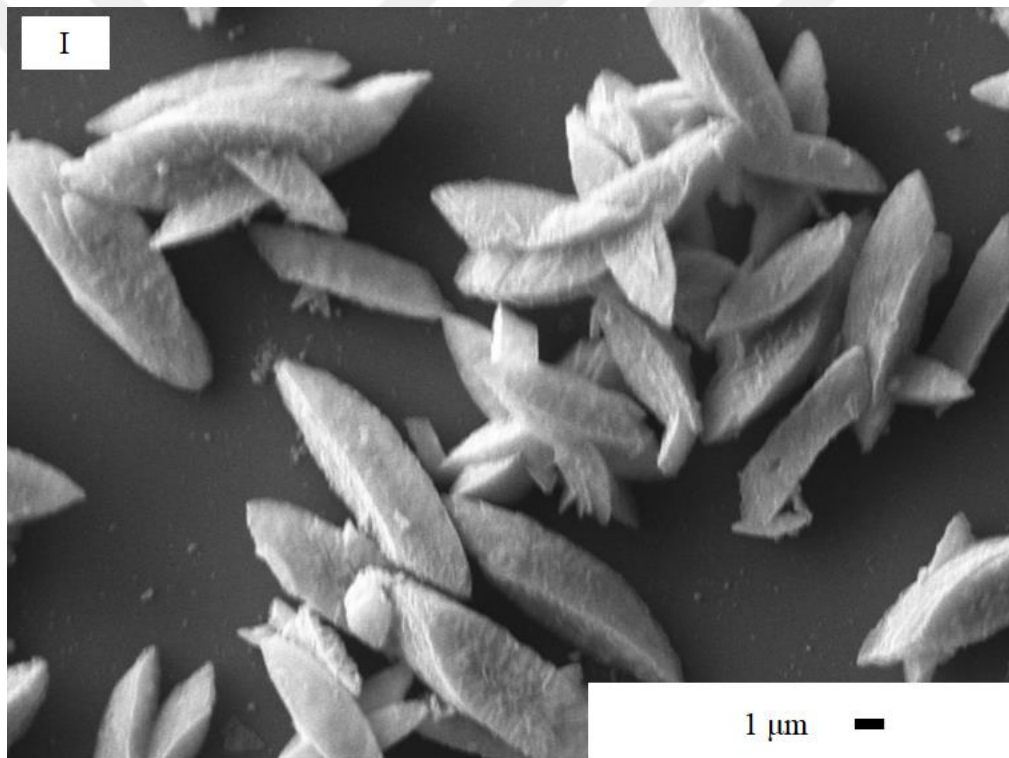


**Figure 4.7.** *SEM micrographs of MicNo-AZO particles synthesized at different temperatures with different Al source*

**Figure 4.7.** (Continued) *SEM micrographs of MicNo-AZO particles synthesized at different temperatures with different Al source*

**Figure 4.7.** (Continued) *SEM micrographs of MicNo-AZO particles synthesized at different temperatures with different Al source*



| Sample Name | Particle Size (μm) | | |
|---|---|---|---|
| | $d_{10}$ | $d_{50}$ | $d_{90}$ |
| MicNo-ZnO | 5 | 6 | 14 |
| I | 2,7 | 6,5 | 13,7 |
| II | 4,1 | 8,8 | 17,1 |
| III | 2,5 | 5,6 | 10,7 |
| IV | 2,3 | 6,2 | 13,1 |
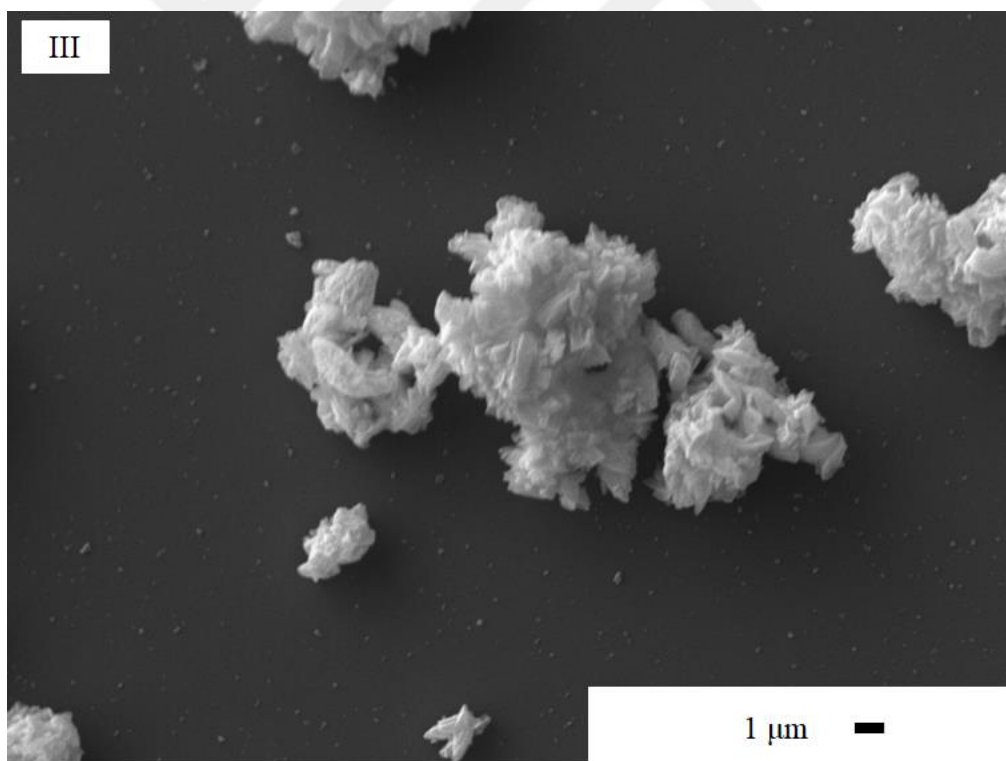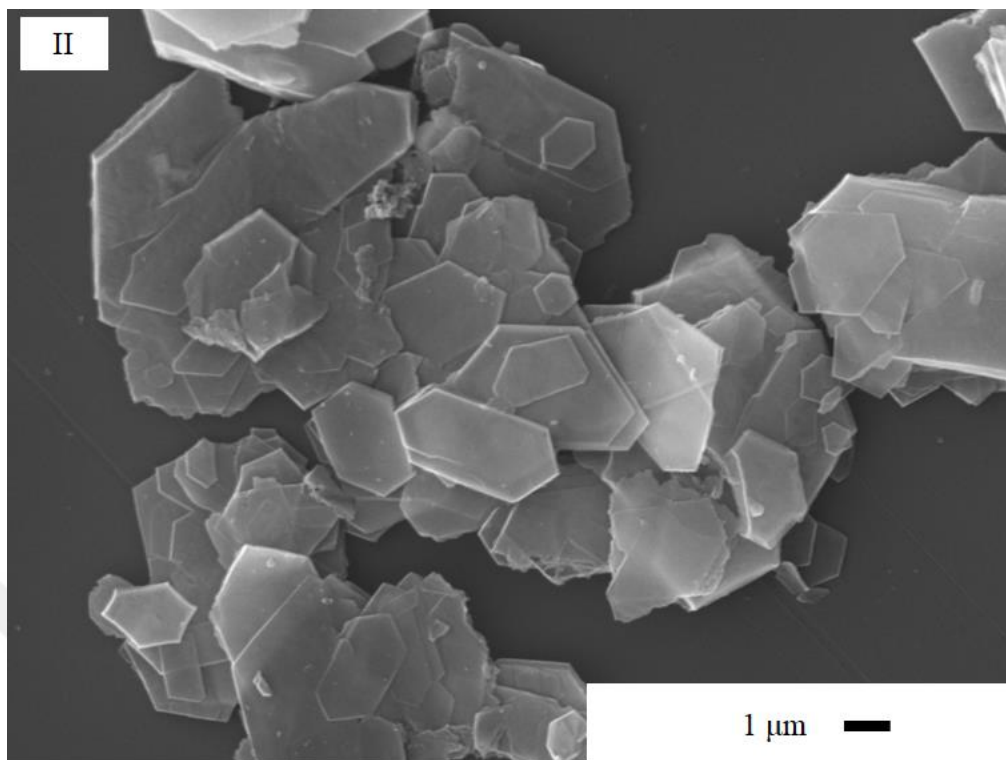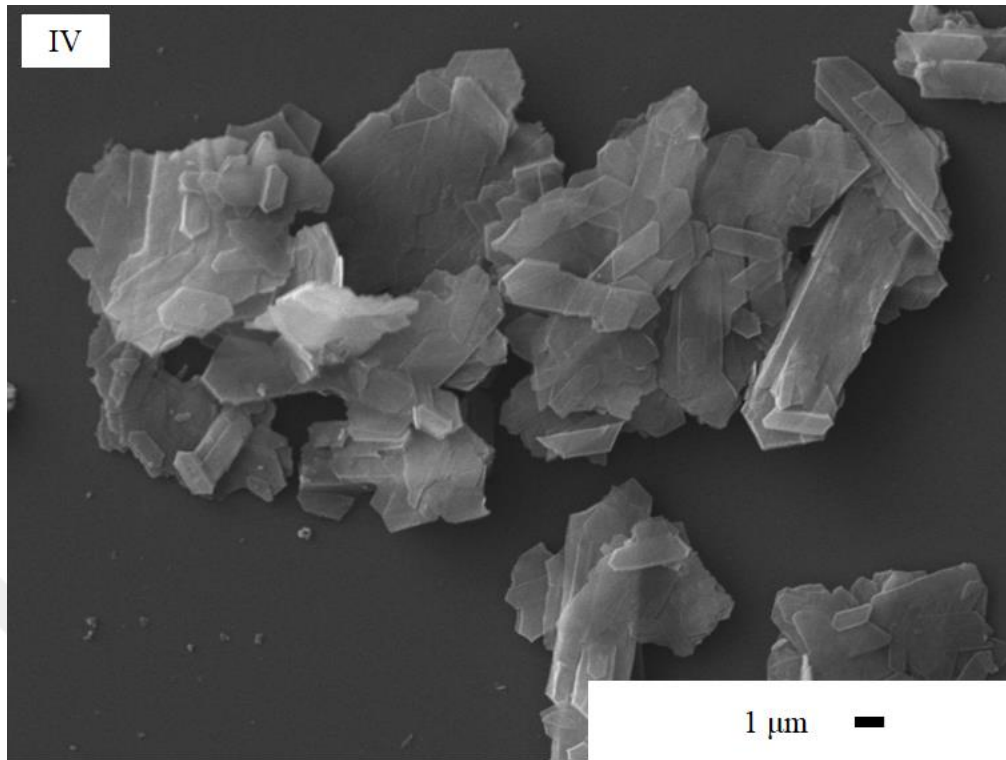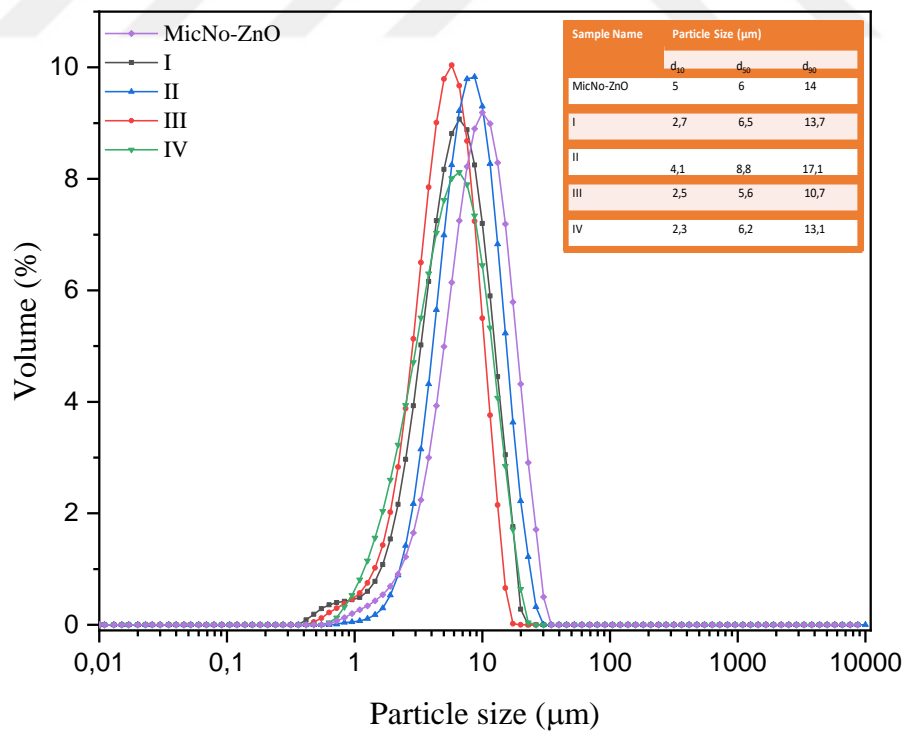
**Figure 4.8.** *Particle size distribution of MicNo-AZO particles synthesized at different temperatures with different Al dopant materials*

One of the most important properties of the MicNo-ZnO particles is optical characteristics. Figure 4.9 shows that Transmittance – Wavelength graph of these four samples. Samples I and III prominently had different transmission characteristics than MicNo-ZnO particles. Besides Samples II and IV were clearly showed that similar optical characteristic with MicNo-ZnO particles. This can be related to the particle morphology. Samples I and III do not have platelet morphology, also they are micron size particles. However, Samples II and IV have typical MicNo morphology then have same optical characteristics.
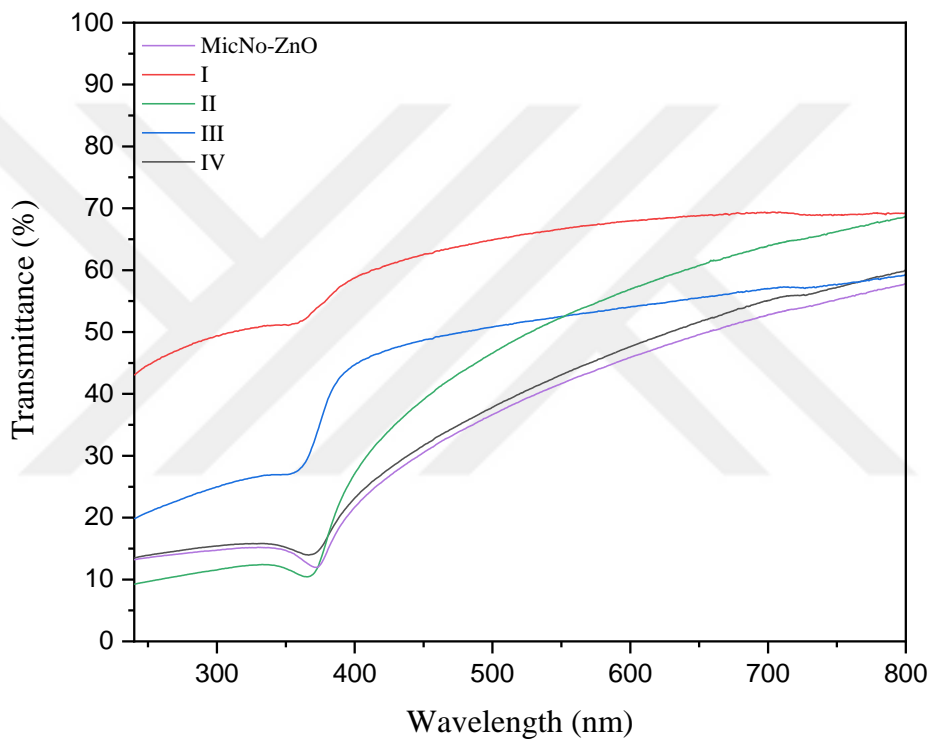


**Figure 4.9.** *Transmission graph of MicNo-AZO particles synthesized at different temperatures with different Al dopant materials*

In this part of the study we were designated that Material B and $T_2$ temperature is appropriate for Al doped MicNo-ZnO particle synthesis. Additionally, we studied on dopant concentration effect in Part 4.1.2.2.

**4.1.2.2.** *Effects of Al source and Al dopant concentration on particle morphology and the physicochemical properties*

Undoped and Al doped MicNo-ZnO particles were synthesized by MicNo processes. Firstly, these particles were evaluated by x-ray diffraction techniques to examine crystal structure and phases. Figure 4.10 a and b show XRD patterns of MicNo-ZnO and Al doped MicNo-ZnO particles by using source Material A and Material B. All particles were exhibited ZnO phase without other crystalline phases. Additionally, the high intensity peaks, which belong to $(10\bar{1}1)$ plane, shift toward to higher 2Θ values due to Al doping into ZnO.



(a)
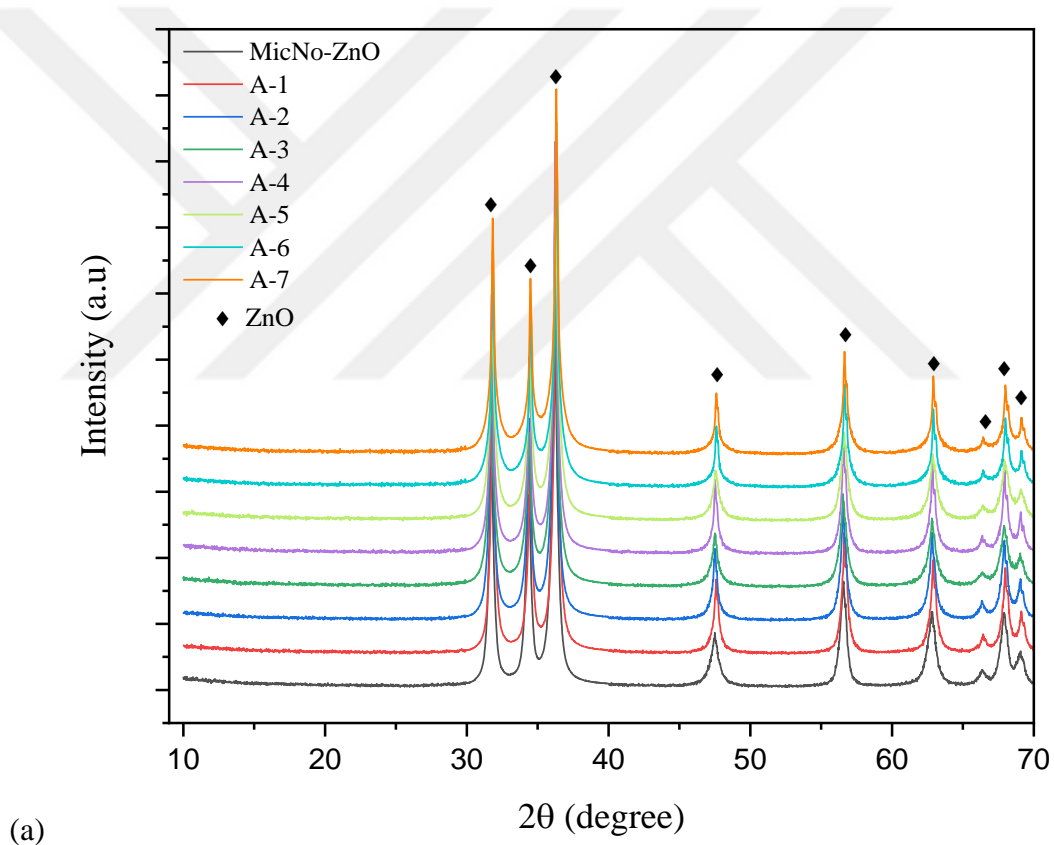
**Figure 4.10.** *X-Ray diffraction patterns of MicNo-ZnO and MicNo-AZO particles (a) doped with Material A and (b) doped with Material B*
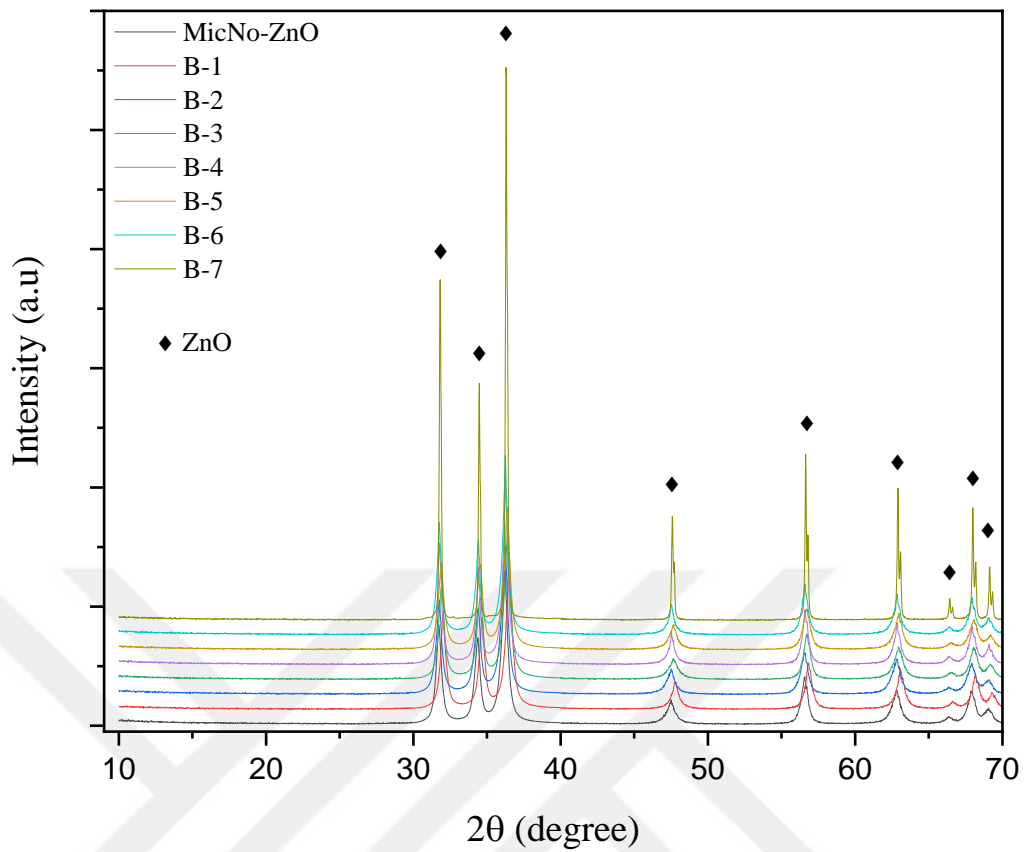
(b)

**Figure 4.10.** (Continued) *X-Ray diffraction patterns of MicNo-ZnO and MicNo-AZO particles (a) doped with Material A and (b) doped with Material B*

Peak shifts are observed on Figue 4.11 a and b. In ZnO crystal structure, $Zn^{2+}$ ions are tetrahedrally coordinated by four $O^{2-}$ ions [47]. It is anticipated that dopant ions substitute to $Zn^{2+}$ ion sites. In addition to this $Zn^{2+}$ ions have 0.074 nm ionic radius and $Al^{3+}$ ions have 0.053 nm ionic radius and both cations are coordinated tetrahedrally [48]. With doping $Al^{3+}$ ions placed into $Zn^{2+}$ ion sites and caused constriction on interplanar distances (*d*) [49,50]. This is lead to peak sihfts toward to the high 2Θ values according to the Bragg Law, Equation 4.1. Whereas the d is decreasing, Θ is increasing.

$$\lambda = 2d \sin \theta \qquad (4.1)$$

Table 4.1 shows that Rietveld analyses results, occupancy values and lattice parameters. Additionally, Rietveld analyses show that occupancy values decreasing by increasing doping amount. Lattice parameters do not change critically, especially c-axis. However minimum lattice parameter for c-axis was 5.1795 angstrom. These results were also consistent with doping amount was quite low for calculations.

39
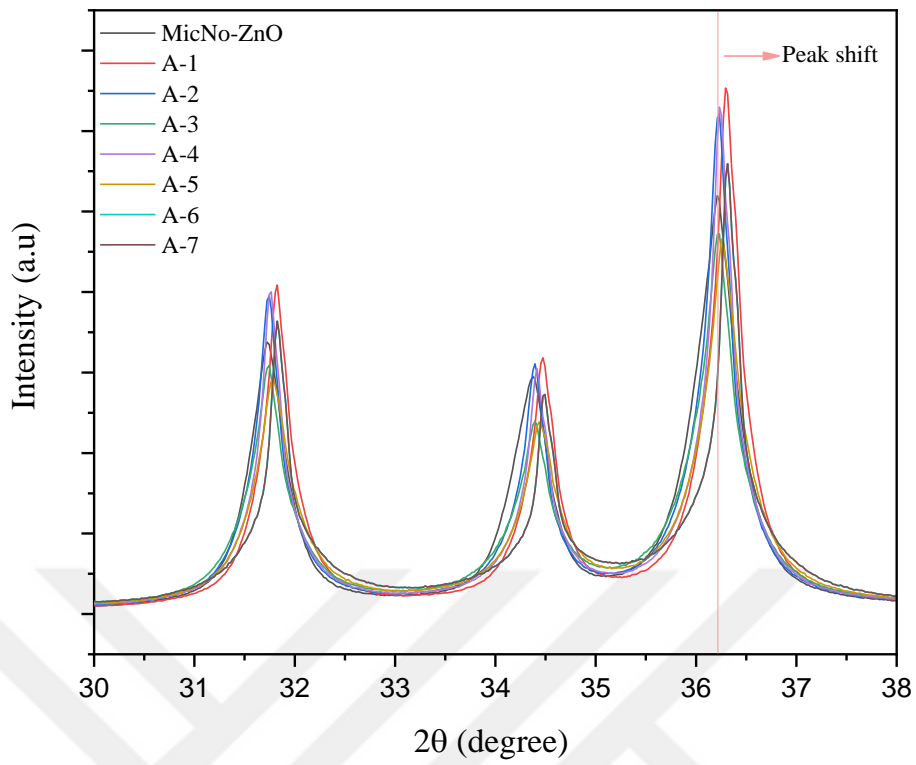
(a)
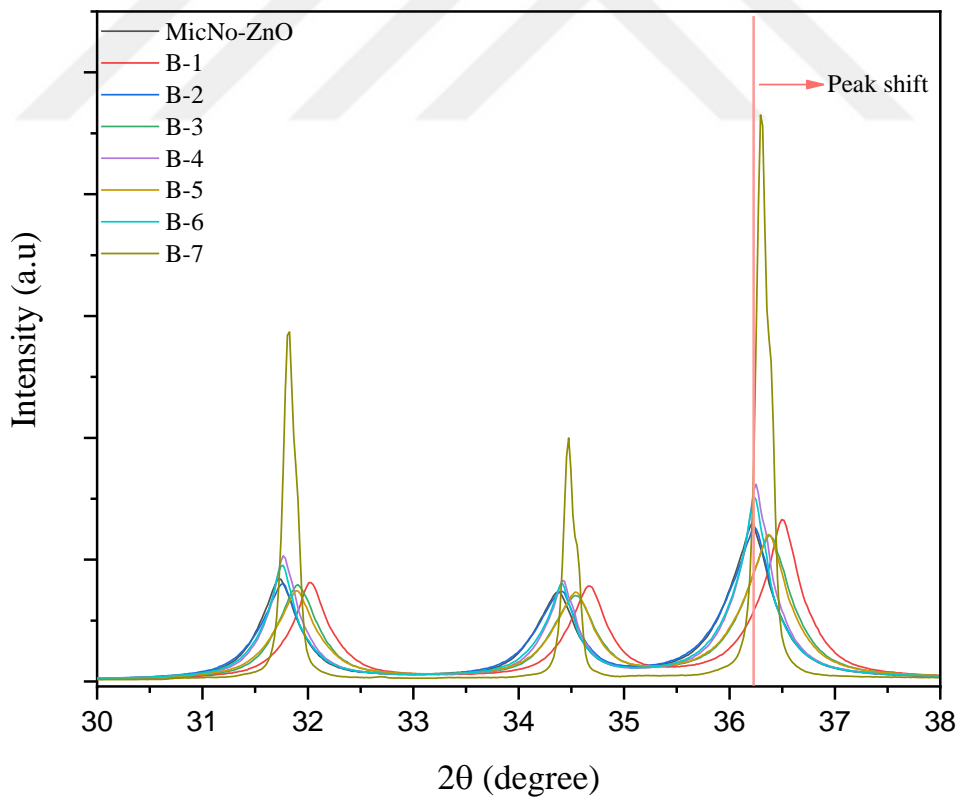


(b)

**Figure 4.11.** *X-Ray diffraction pattern peak shifts of (a) MicNo-AZO particles doped with Material A, (b) MicNo-AZO particles doped with Material B*

**Table 4.1.** *Rietveld analyses results; occupancy and lattice parameters values of source B doped MicNo-ZnO particles*

| Sample | Rexp-Rwp | GoF | Peak Position | Occupancy [Zn] % | Lattice Parameters | | c/a |
|--------|----------|-----|---------------|------------------|-------------------|--------|-----|
| | | | | | a [A] | c [A] | |
| MicNo-ZnO | 1.92-2.79 | 1.45 | 36.3131 | 100 | 3.2472 | 5.2005 | 1.60 |
| B-1 | 193-3.83 | 1.99 | 36.3999 | 98.99 | 3.2704 | 5.2359 | 1.60 |
| B-2 | 1.90-2.62 | 1.38 | 36.2780 | 98 | 3.2502 | 5.2062 | 1.60 |
| B-3 | 1.92-3.02 | 1.57 | 36.3979 | 96 | 3.2393 | 5.1824 | 1.59 |
| B-4 | 1.92-3.26 | 1.70 | 36.2307 | 96.2 | 3.2489 | 5.2037 | 1.60 |
| B-5 | 1.93-3.59 | 1.86 | 36.3624 | 93.89 | 3.2346 | 5.1795 | 1.60 |
| B-6 | 1.94-3.27 | 1.69 | 36.2089 | 91.1 | 3.2496 | 5.2049 | 1.60 |
| B-7 | 1.92-4.60 | 2.39 | 36.3277 | 97.26 | 3.2454 | 5.1980 | 1.60 |

Material A doped MicNo-AZO particles SEM micrographs are shown in Figure 4.12. These particles do not exhibit platelet morphology and have non-uniform morphology. They show different shapes with increasing doping concentration. Increasing with doping concentrations, particles have micron size thickness. Figure 4.13 showing that particle size distribution graphs of MicNo-AZO particles doped with Material A.

**Figure 4.12.** *SEM micrographs of Material A doped MicNo-ZnO particles with different Al doping amounts, 15kX*

**Figure 4.12.** (Continued) *SEM micrographs of Material A doped MicNo-ZnO particles with different Al doping amounts, 15kX*

**Figure 4.12.** (Continued) *SEM micrographs of Material A doped MicNo-ZnO particles with different Al doping amounts, 15kX*

44
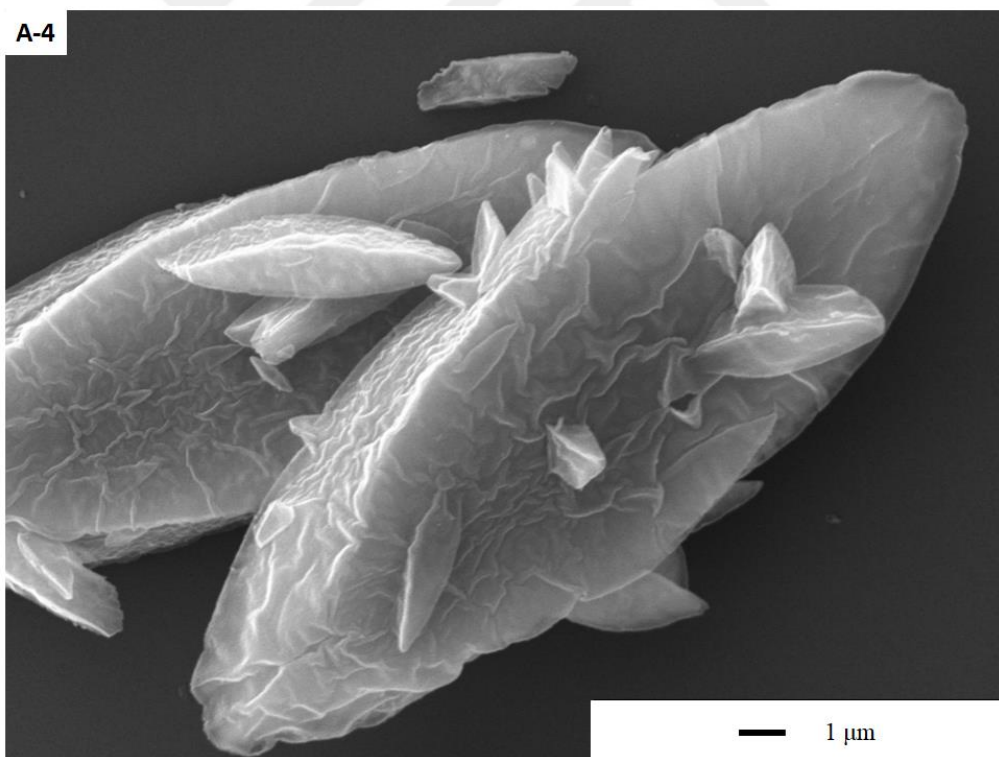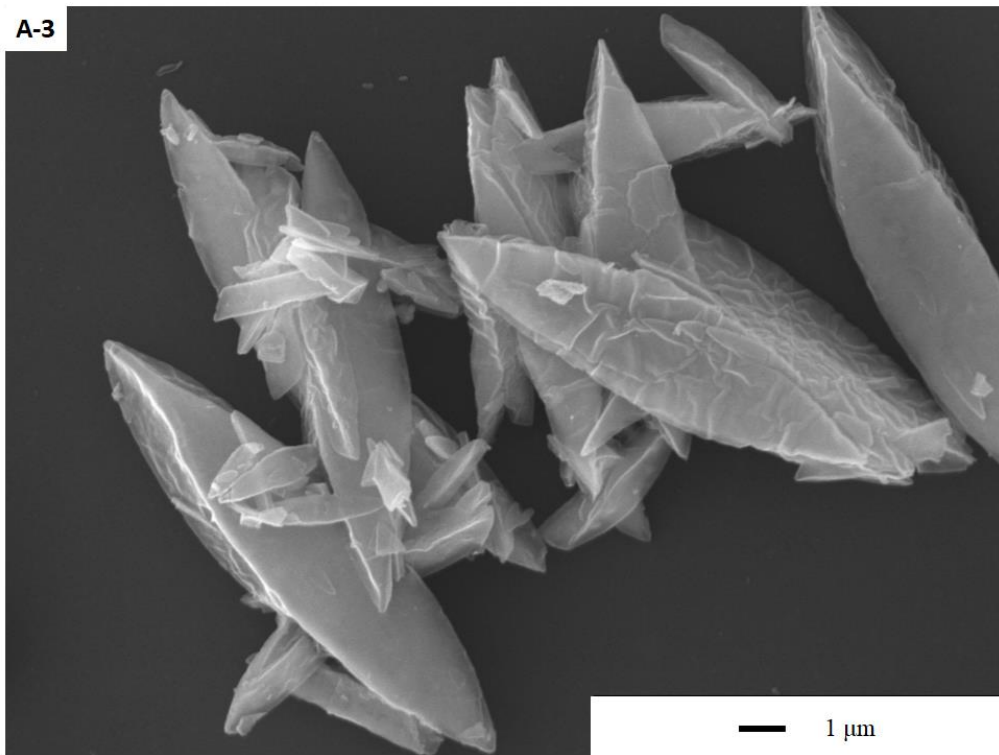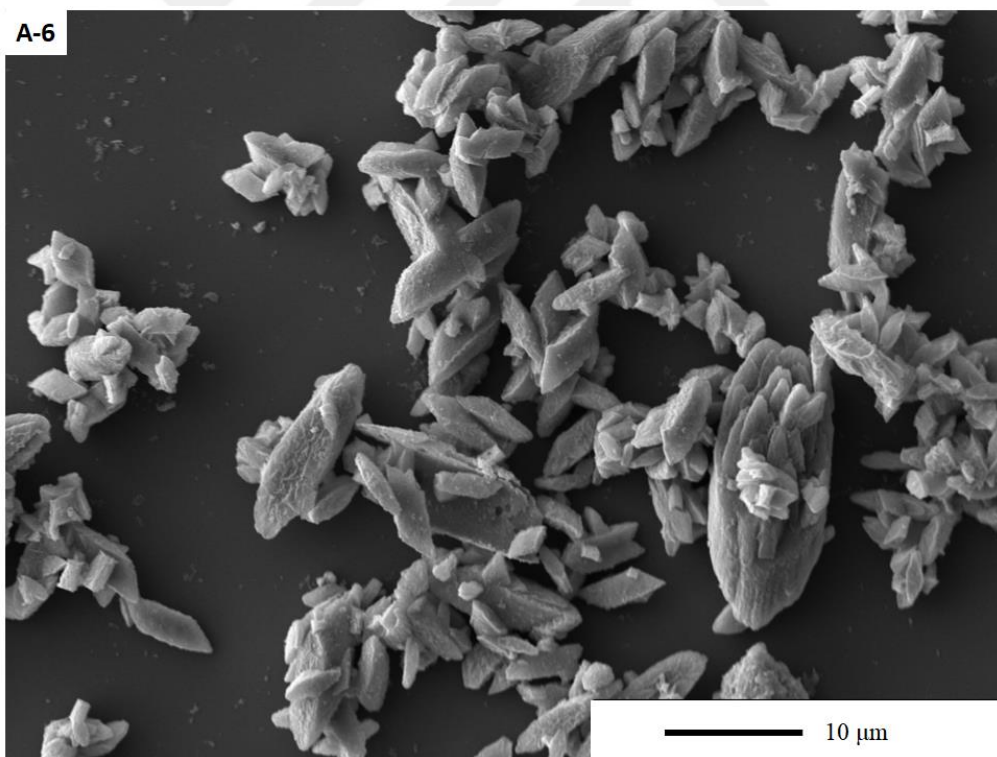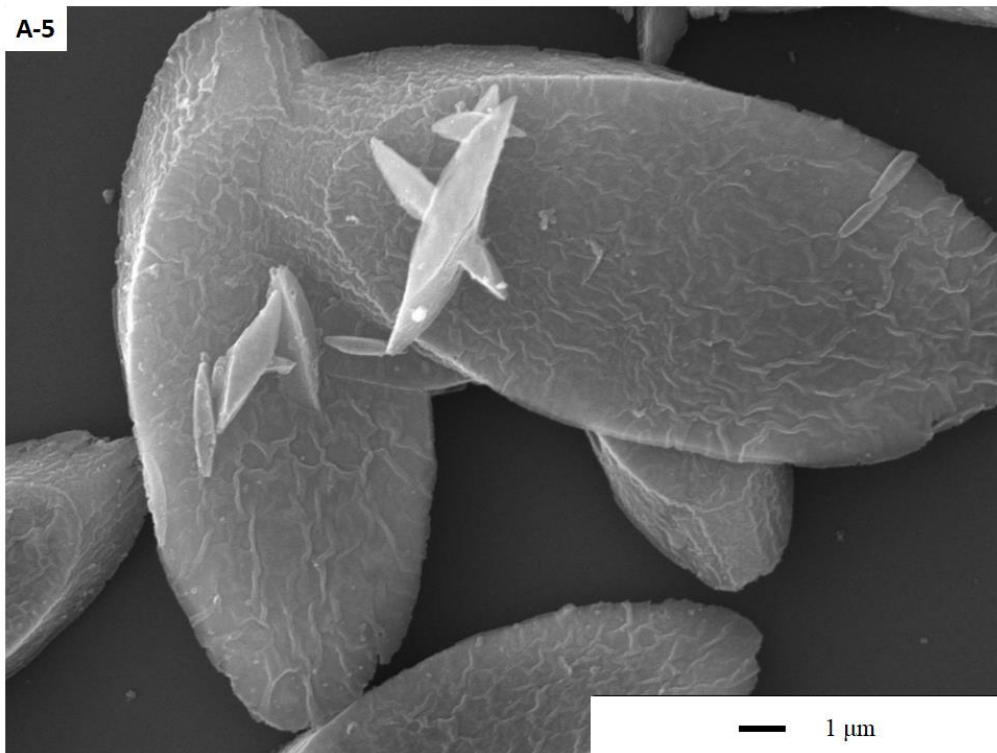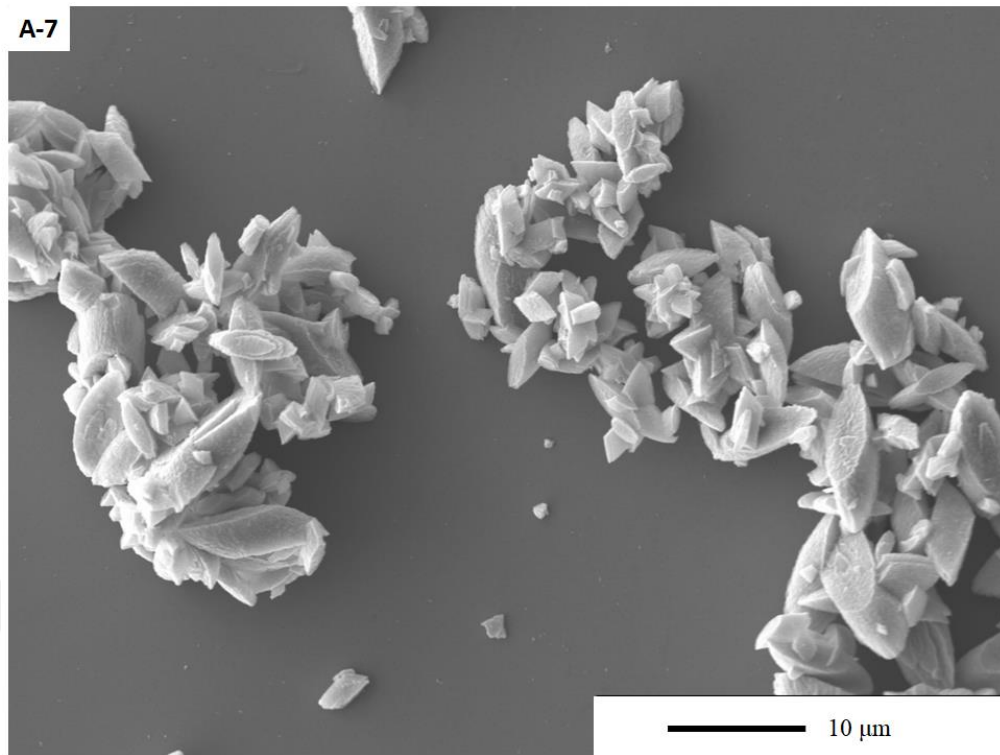
**Figure 4.12.** (Continued) *SEM micrographs of Material A doped MicNo-ZnO particles with different Al doping amounts, 15kX*
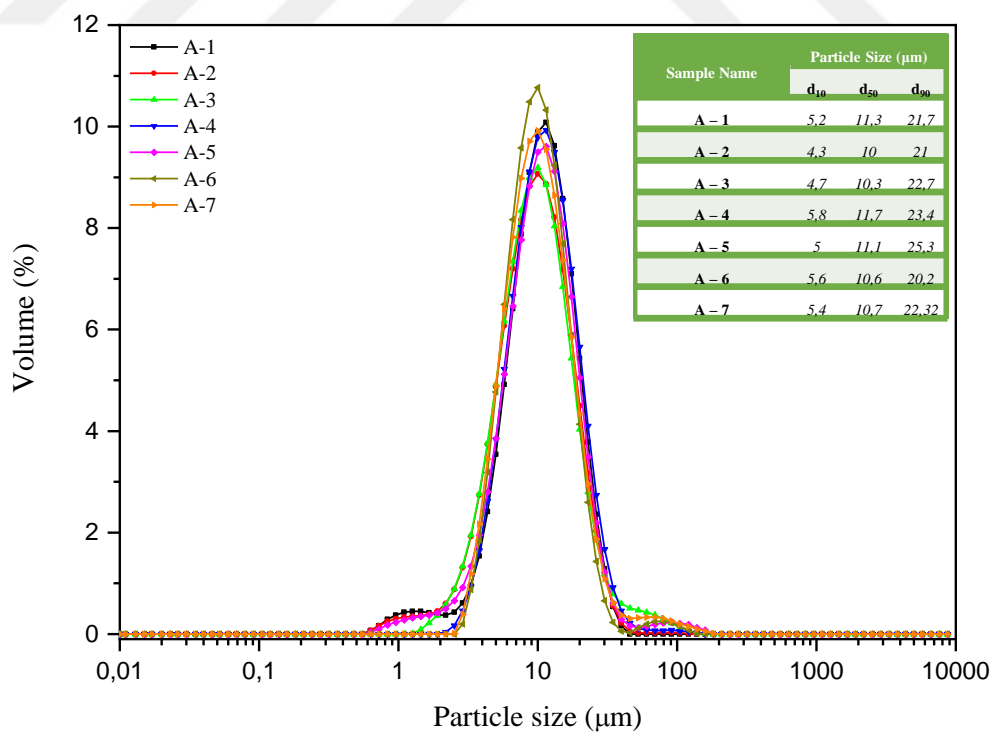


**Figure 4.13.** *Particle size distribution graph of MicNo-ZnO particles doped with Material A with different Al doping amount.*

Material B doped MicNo-AZO particles SEM micrographs are shown in Figure 4.14. These particles show platelet morphology as undoped MicNo-ZnO particles. Besides this, dopant concentration is not affect particle morphology negatively until the sample B-7 which have not platelet morphology. They are agglomerated micron sized particles. As shown above Figure 4.11 b, sample B-7 XRD pattern looks like a micron size particle. Figure 4.15 shows that particle size distribution graph of MicNo-AZO particles doped with Material B. It was observed that MicNo-AZO particles doping with Material B exhibit similar particle size distribution with undoped MicNo-ZnO particles. Additionally, crystallite sizes from XRD analyses show that MicNo-AZO particles are 22 – 30 nm size. In addition to these, the specific surface area (S.S.A) values are in the range between 25 – 35 $m^2$/g. Equivalent spherical diameter from these values are 35 – 45 nm in size.

**B-1**

1 μm

**B-2**

1 μm
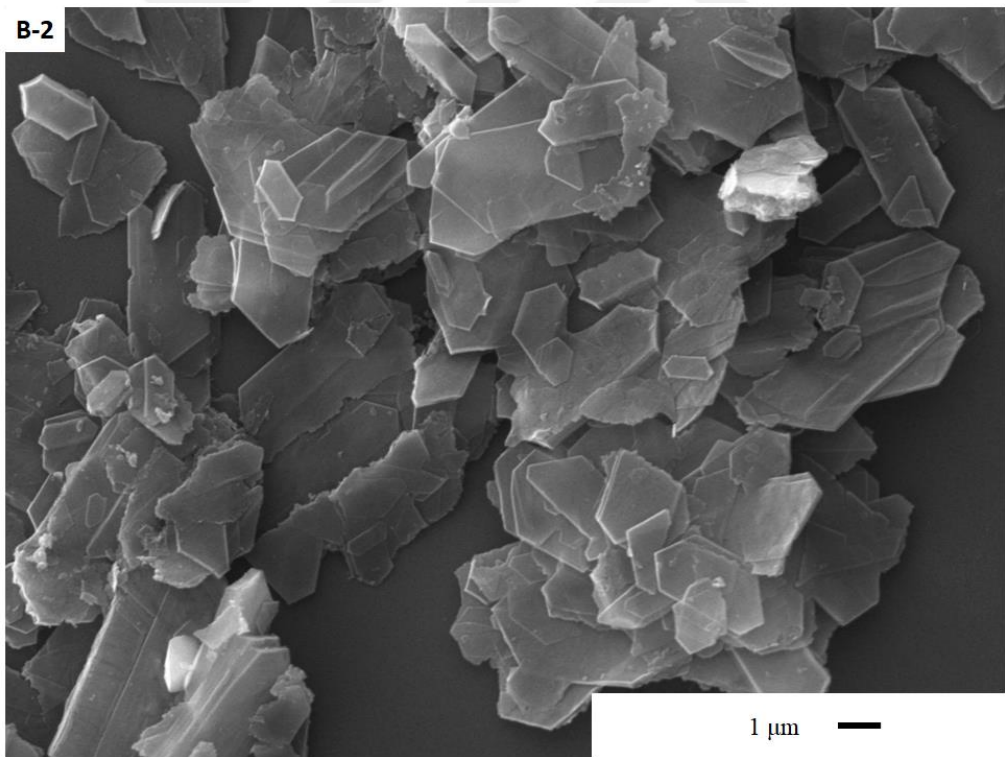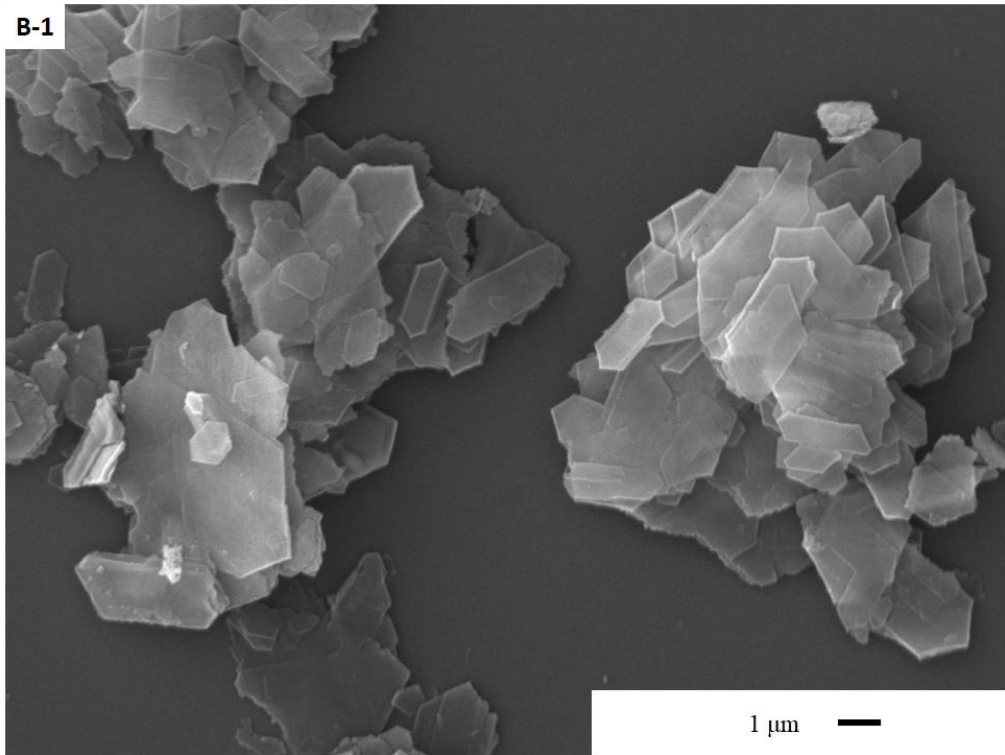
**Figure 4.14.** *SEM micrograph of Material B doped MicNo-ZnO particles with different Al doping amounts, 15kX*

**B-3**

1 μm

**B-4**

1 μm

**Figure 4.14.** (Continued) *SEM micrograph of Material B doped MicNo-ZnO particles with different Al doping amounts, 15kX*

B-5

1 μm



B-6

1 μm
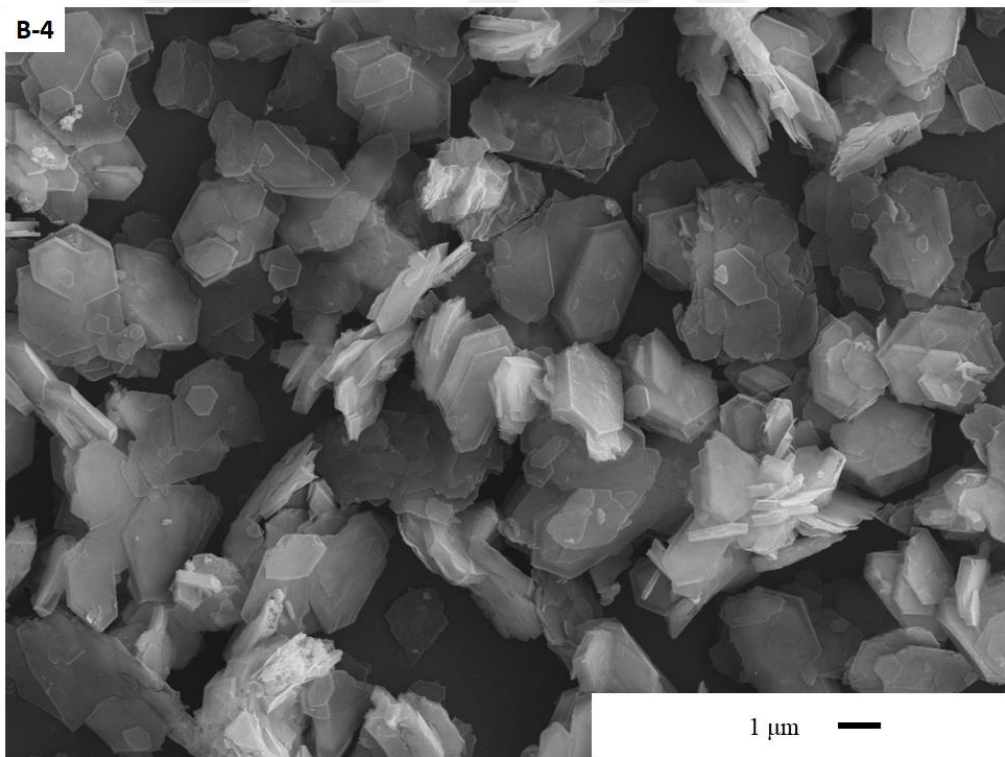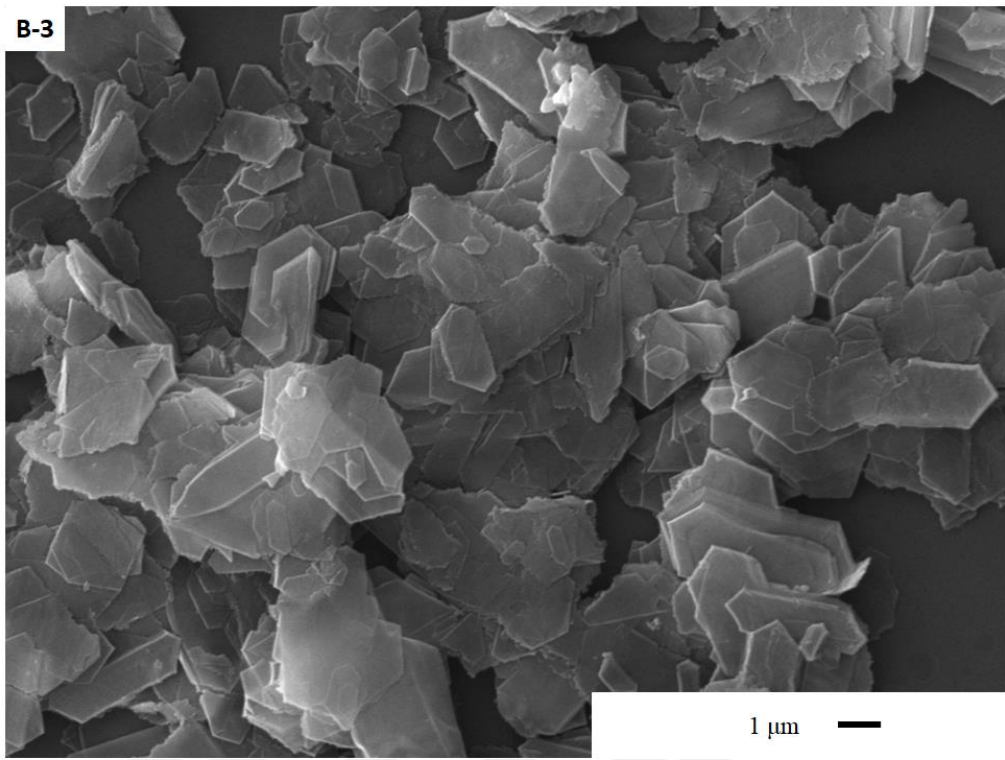
**Figure 4.14.** (Continued) *SEM micrograph of Material B doped MicNo-ZnO particles with different Al doping amounts, 15kX*
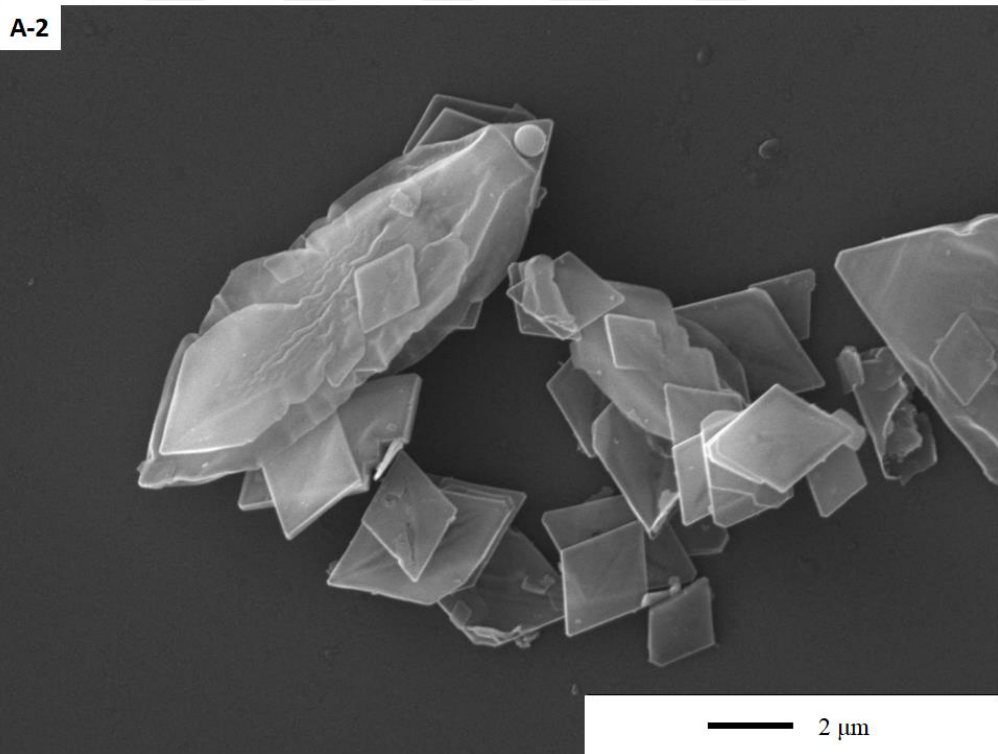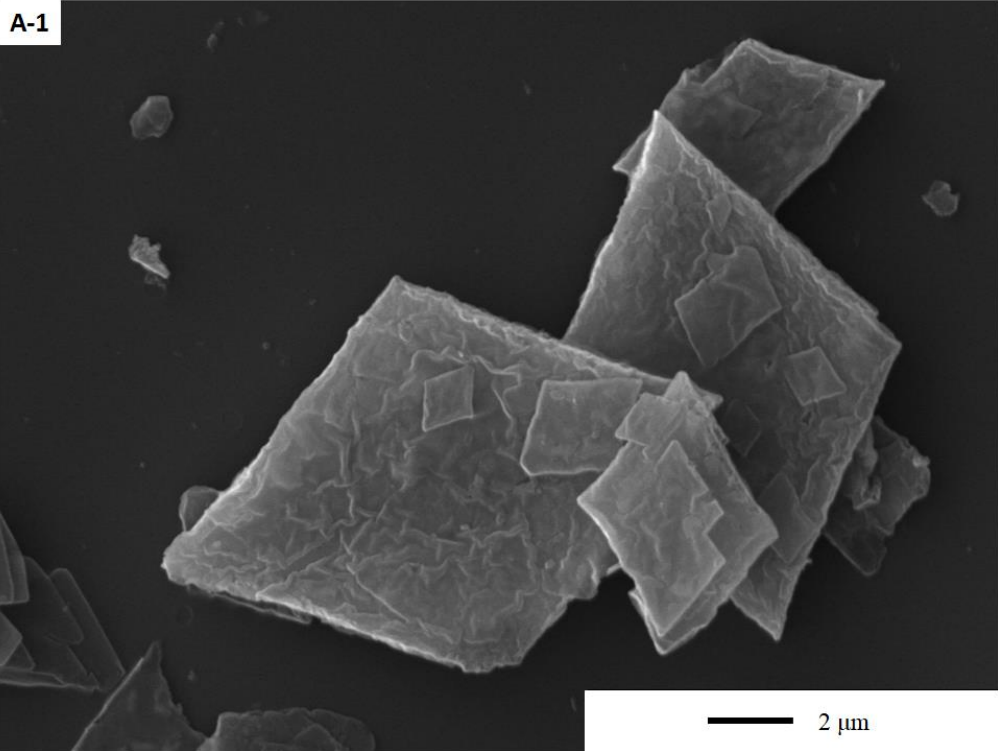
**Figure 4.14.** (Continued) *SEM micrograph of Material B doped MicNo-ZnO particles with different Al doping amounts, 15kX*



| Sample Name | Particle Size(µm) | | |
|---|---|---|---|
| | $d_{10}$ | $d_{50}$ | $d_{90}$ |
| **B – 1** | 2,4 | 6,8 | 16,1 |
| **B – 2** | 2,9 | 7,6 | 16,3 |
| **B - 3** | 3,5 | 9,3 | 20,4 |
| **B – 4** | 4 | 8,5 | 16,5 |
| **B – 5** | 4,1 | 8,8 | 17,1 |
| **B – 6** | 2,6 | 6,1 | 12,8 |
| **B-7** | 1,3 | 2,5 | 6 |
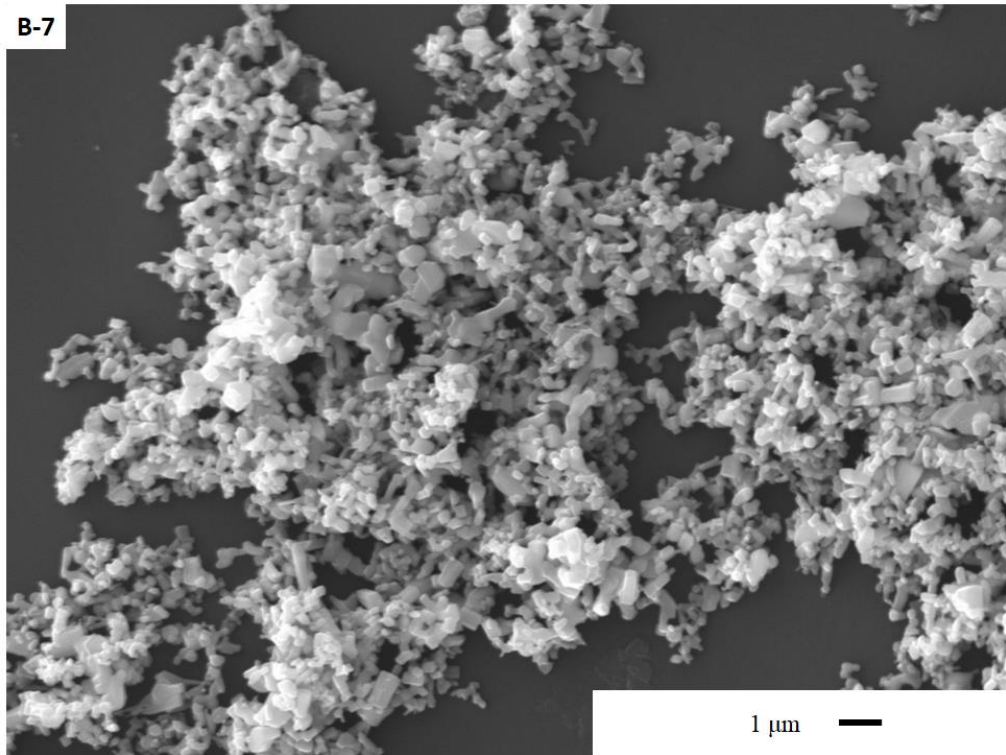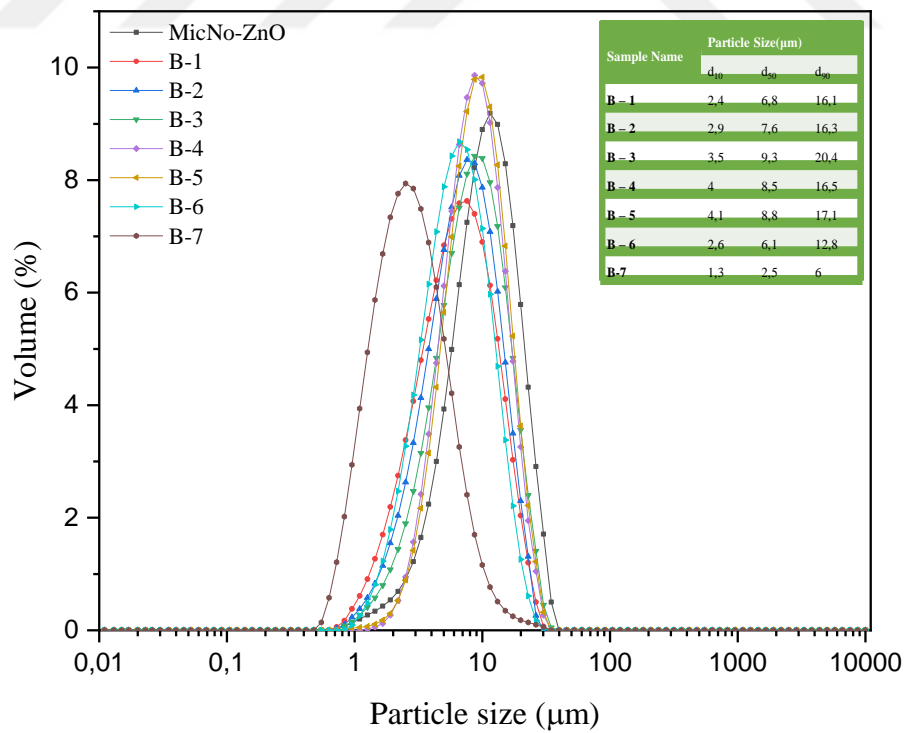
**Figure 4.15.** *Particle size distribution graph of MicNo-ZnO particles doped with Material B with different Al doping amounts.*

50

Material B doped MicNo-AZO particles were most appropriate samples for our further experimental studies because of they have specifically MicNo morphology. Therefore, we were used and characterized Material B doped MicNo-AZO particles. Additionally, ICP analyses of these particles were proved Al content in the Al doped MicNo-ZnO particles is in the range between 0-0.32 mol%.

### 4.1.2.3. *Raman and FTIR spectroscopy of MicNo–AZO particles*

Raman spectrums of MicNo-ZnO and MicNo-AZO particles are demonstrated on Figure 4.16. There are two peaks at 330 $cm^{-1}$ (2nd order peak due to the combination of $E_2$ high – $E_2$ low) and 437 $cm^{-1}$ ($E_2$ high). $E_2$ high peaks are originated by the vibration of oxygen atoms and this mode is the strongest Raman mode of wurtzite type ZnO crystal structure [51,52]. While undoped MicNo-ZnO particles have strongest and sharp $E_2$ high peaks, Al doped MicNo-ZnO particles had broad and weak $E_2$ high peaks. Y Jin. et al. studied on the effect of crystallinities of the particles on the Raman spectrums. They found that crystallinity of the particles was affected by doping and this was also led to broad and weak $E_2$ high peak formation [51].
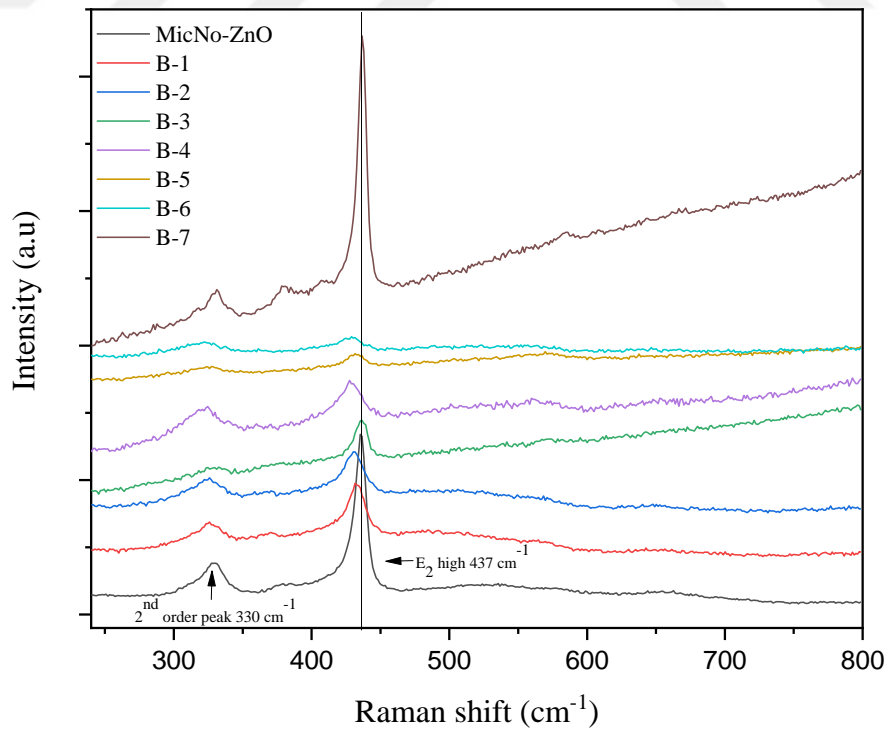


**Figure 4.16.** *Raman spectrums of MicNo-ZnO and MicNo-AZO particles with different Al doping amounts.*

Figure 4.17 shows that FTIR spectrums of MicNo-ZnO and MicNo-AZO particles. There is an absorption peak at around 380-560 cm$^{-1}$ which indicates that presence of Zn-O streching mode. All the MicNo-ZnO particles have this broad peak as shown Zn-O streching. Additionally, particles have a weak and broad peak at around 1400-1800 cm$^{-1}$ which is related to the O-H vibrations of residual water molecules. It may be attributed to the adsorbed water on the particle surface. While Al doped MicNo-ZnO particles was demonstrated small and weak peak at around 600-800 cm$^{-1}$, MicNo-ZnO particles have not this mode. Accordingly, the absence of these signals in MicNo-ZnO suggests that such vibrations can be related to Al doping.
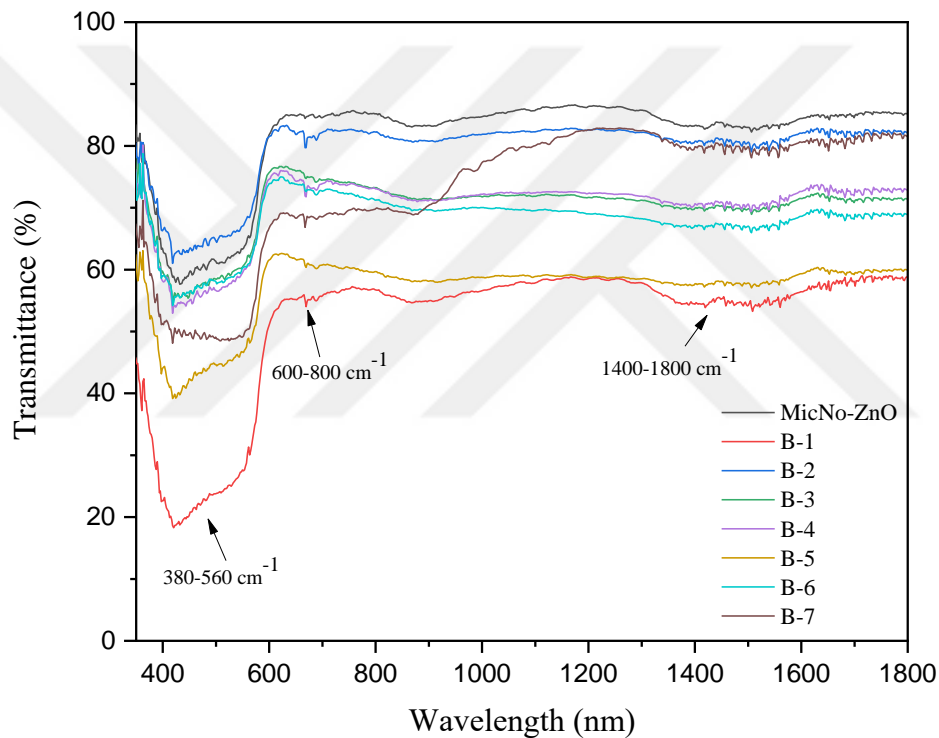


**Figure 4.17.** *FTIR spectrums of MicNo-ZnO and MicNo-AZO particles with different Al doping amounts.*

### 4.1.2.4. *Optical properties of MicNo-AZO particles*

Transmission and absorption graph of MicNo-AZO particles are shown in Figure 4.18. As explained before (Part 4.1.1.) MicNo-ZnO particles have high transparent characteristic in the visible range. In addition to this, Al doped MicNo-ZnO particles have similar characteristics with MicNo-ZnO particles except for sample B-7. This is related to the particle characteristics as mentioned above they don't have MicNo morphology.
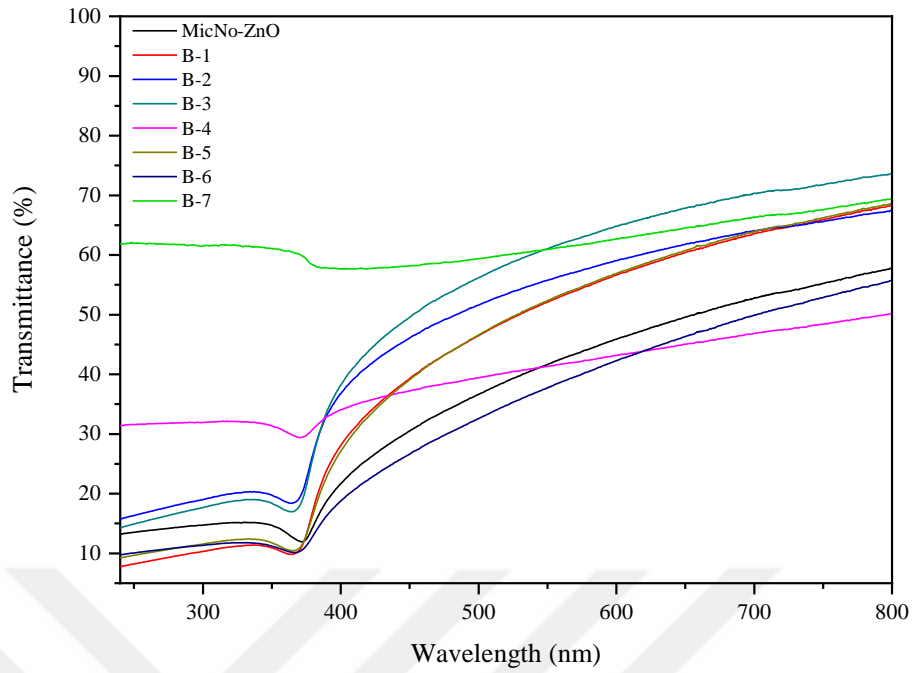
(a)
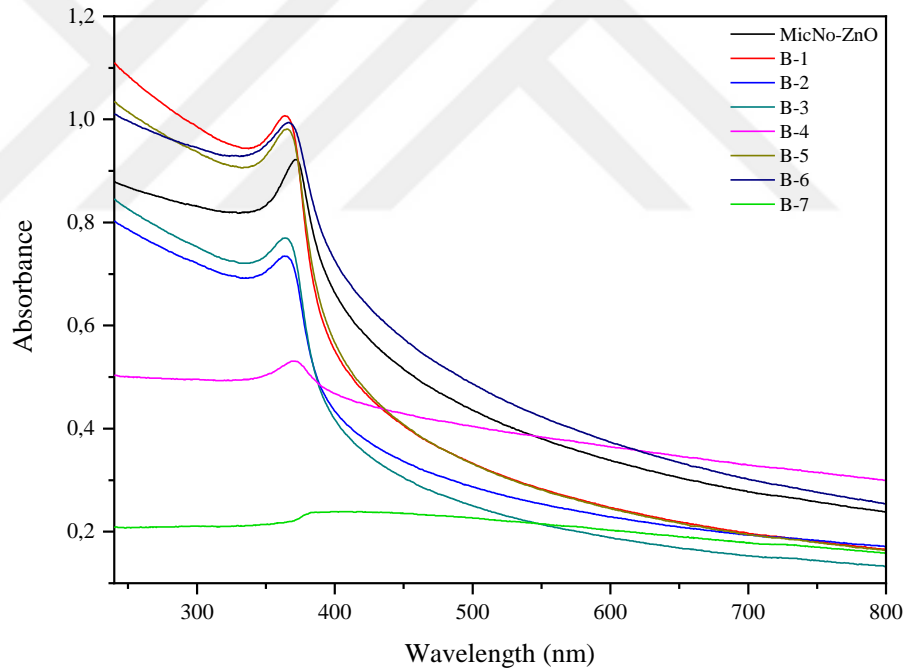


(b)

**Figure 4.18.** *(a) Transmission and (b) Absorption graphs of MicNo-AZO particles with different Al doping amounts.*

After these characterizations, reflectance measurements were completed for calculating band gap values of MicNo-AZO particles. Figure 4.19 shows $(h\alpha v)^2$ – Photon energy graphs of these particles as drawn by Kubelka-Munk theory then the band gap values of samples were determined from the Tauc plots [45,46]. A tangent line was drawn at a linear portion of the photon energy – $(hv\alpha)^2$ each sample, then band gap values were obtained from the intersection point of this tangent line and x=0 position [53]. Correspondingly, MicNo-AZO particles have band gap values between 3.05 and 3.13 eV, Table 4.2.
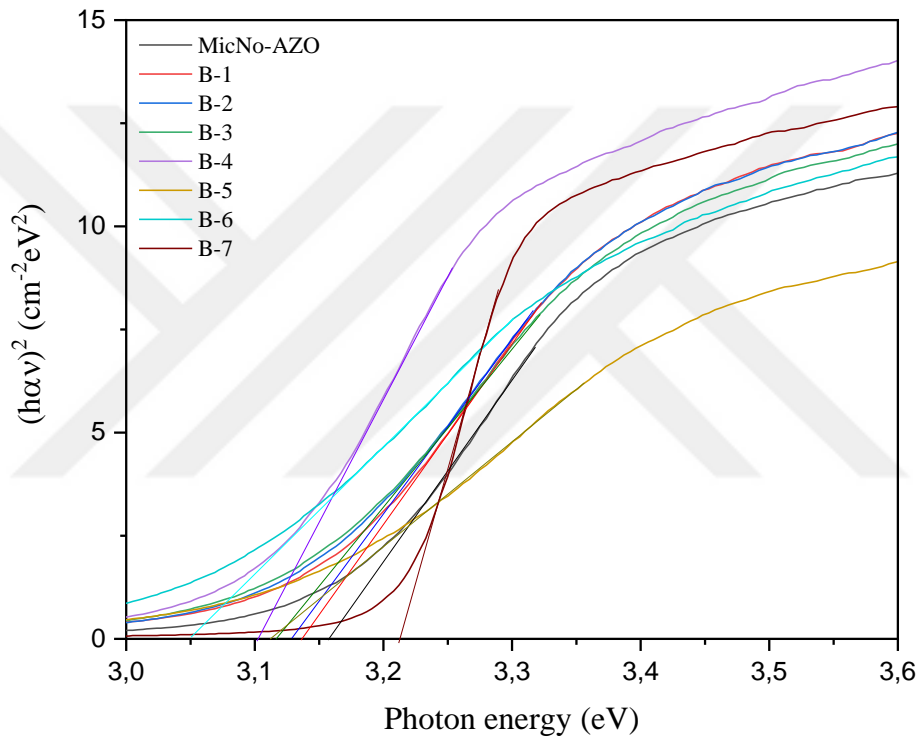


**Figure 4.19.** *Photon energy – (hαv)2 graph of MicNo-AZO particles with different Al doping amounts.*

**Table 4.2.** *Band gap values of undoped and Al doped MicNo-ZnO particles*

| Samples | Band Gap Values, eV |
|---|---|
| **MicNo-ZnO** | 3.18 |
| **B-1** | 3.12 |
| **B-2** | 3.11 |
| **B-3** | 3.1 |
| **B-4** | 3 |
| **B-5** | 3.1 |
| **B-6** | 3.05 |
| **B-7** | 3.21 |

## 4.1.3. Ga doped MicNo-ZnO particle properties

The XRD patterns of MicNo-ZnO and Ga doped MicNo-ZnO are shown in Figure 4.20. Ga doped MicNo-ZnO samples were demonstrated that ZnO crystal structure. However, increasing with Ga dopant concentration $Ga_2O_3$ phase formation was observed such as sample C-4, C-5, C-6, C-7. Additionally, Rietveld analyses show that occupancy values decreasing by increasing doping amount. Table 4.3 shows that Rietveld analyses results, occupancy values and lattice parameters. Lattice parameters do not change critically, especially c-axis. However minimum lattice parameter for c-axis was 5.1870 angstrom. ICP analyses of these particles proved Ga content in the Ga doped MicNo-ZnO particles is in the range between 0-2.3 mol% as shown in Table 4.4. According to the ICP analyses and XRD results critical doping concentration for Ga doped MicNo-ZnO particle is 0.4 mol% Ga. These results are consistent with the studies in literature which are reported maximum solubility of the Ga in the GZO ceramics is 0.5 mol% [54,55]. Additionally, we know that ZnO have $Zn^{2+}$ ions are tetrahedrally coordinated by four $O^{2-}$ ions and expected that $Ga^{3+}$ ions are replacing to $Zn^{2+}$ ion sites. Accordingly, ionic radius of the ions should lead to peak shifts toward to high 2Θ values like as Al doped ZnO particles. On the contrary, Ga doped MicNo-ZnO particles do not have peak shifts at a critical degree, Figure 4.21. To sum up, Ga atoms may not substitute to $Zn^{2+}$ ion sites.
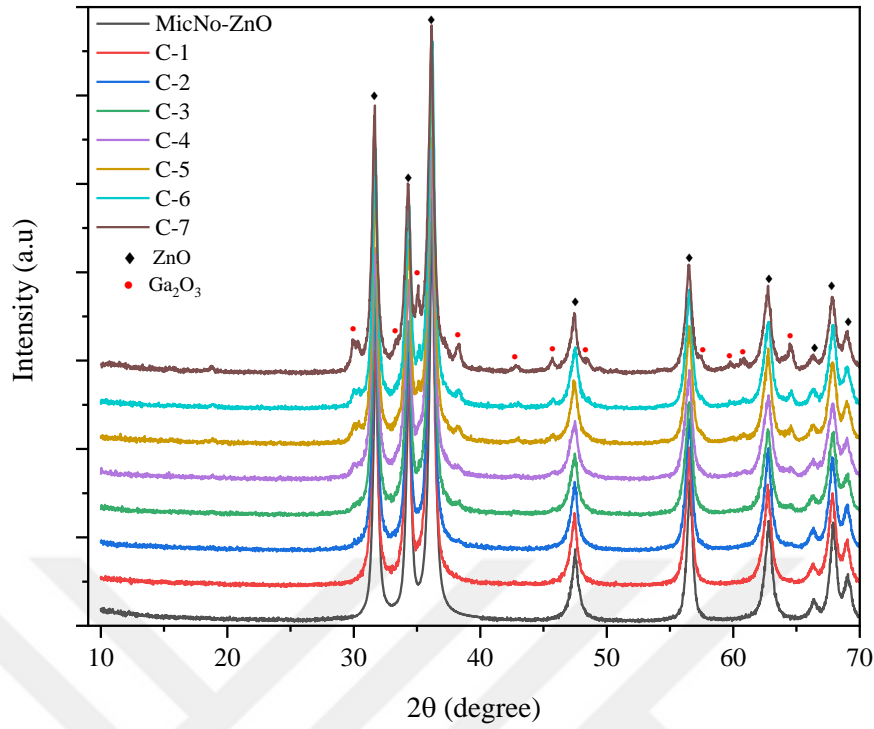
**Figure 4.20.** *X-Ray diffraction patterns of MicNo-ZnO and MicNo-GZO particles with different Ga doping amount*

**Table 4.3.** *Rietveld analyses results; occupancy and lattice parameters values of source C doped MicNo-ZnO particles*

| Sample | Rexp-Rwp | GoF | Peak Position | Occupancy [Zn] % | Lattice Parameters | | c/a |
|--------|----------|-----|---------------|------------------|--------------------|--|-----|
| | | | | | a [A] | c [A] | |
| MicNo-ZnO | 1.92-2.79 | 1.45 | 36.3131 | 100 | 3.2472 | 5.2005 | 1.60 |
| C-1 | 1.92-3.59 | 1.87 | 36.3265 | 99 | 3.2390 | 5.1870 | 1.60 |
| C-2 | 1.95-3.32 | 1.70 | 36.2712 | 98.25 | 3.2495 | 5.2047 | 1.60 |
| C-3 | 1.93-3.74 | 1.94 | 36.1993 | 98.99 | 3.2482 | 5.2039 | 1.60 |
| C-4 | 1.92-4.53 | 2.36 | 36.1980 | 99 | 3.2485 | 5.2060 | 1.60 |
| C-5 | 1.93-4.19 | 2.17 | 35.2114 | 97.25 | 3.2470 | 5.1998 | 1.60 |
| C-6 | 1.93-3.86 | 2.00 | 36.1557 | 97.67 | 3.2513 | 5.2101 | 1.60 |
| C-7 | 0.49-4.01 | 8.14 | 36.2214 | 85 | 3.2170 | 5.2027 | 1.62 |
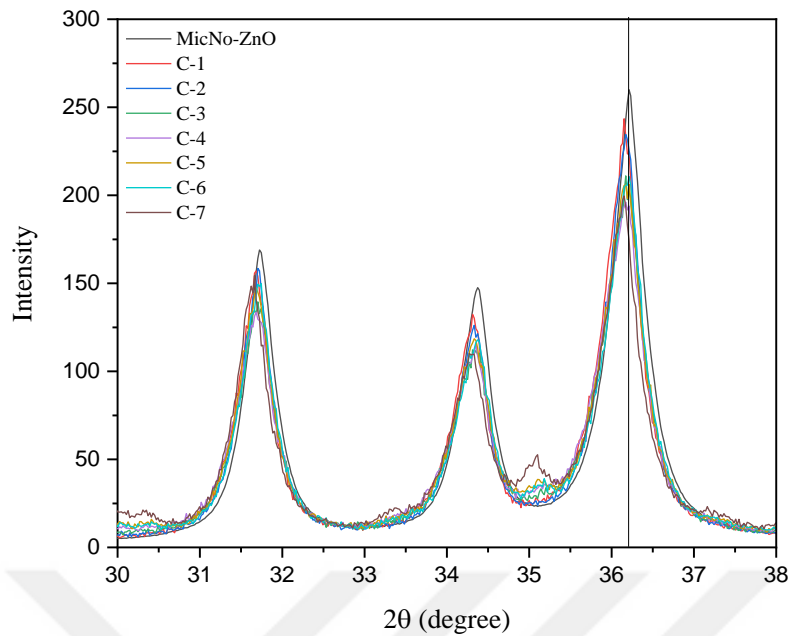
**Figure 4.21.** *X-Ray diffraction pattern peak shifts of MicNo-GZO particles with different Ga doping amount*

**Table 4.4.** *MicNo-GZO particles Ga mol% were obtained from ICP analyses*

| Sample Name | Ga Mol % From Icp |
|---|---|
| MicNo-ZnO | *0* |
| C-1 | *0* |
| C-2 | *0* |
| C-3 | *0,4* |
| C-4 | *0,8* |
| C-5 | *1,2* |
| C-6 | *1,2* |
| C-7 | *2,3* |

Morphological analyses of these particles were performed by SEM as shown in Figure 4.22. Ga doped MicNo-ZnO particles have typical MicNo morphology which have platelet shape and 5-10 µm size with nano meter thickness. Already crystallite size of Ga doped MicNo-ZnO particles were calculated from XRD paterns by Schrerr equation and they found that have approximately 20 nm crystallite size. Moreover, particle size distribution graphs are shown in Figure 4.23. MicNo-GZO particles have similar distribution with MicNo-ZnO particles with 6 µm size. In addition to this, BET measurements give the specific surface area (S.S.A) values are in the range between 25 – 35 $m^2$/g. Equivalent spherical diameter from these values are 35 – 45 nm in size. These results are compossible with MicNo-ZnO particles.
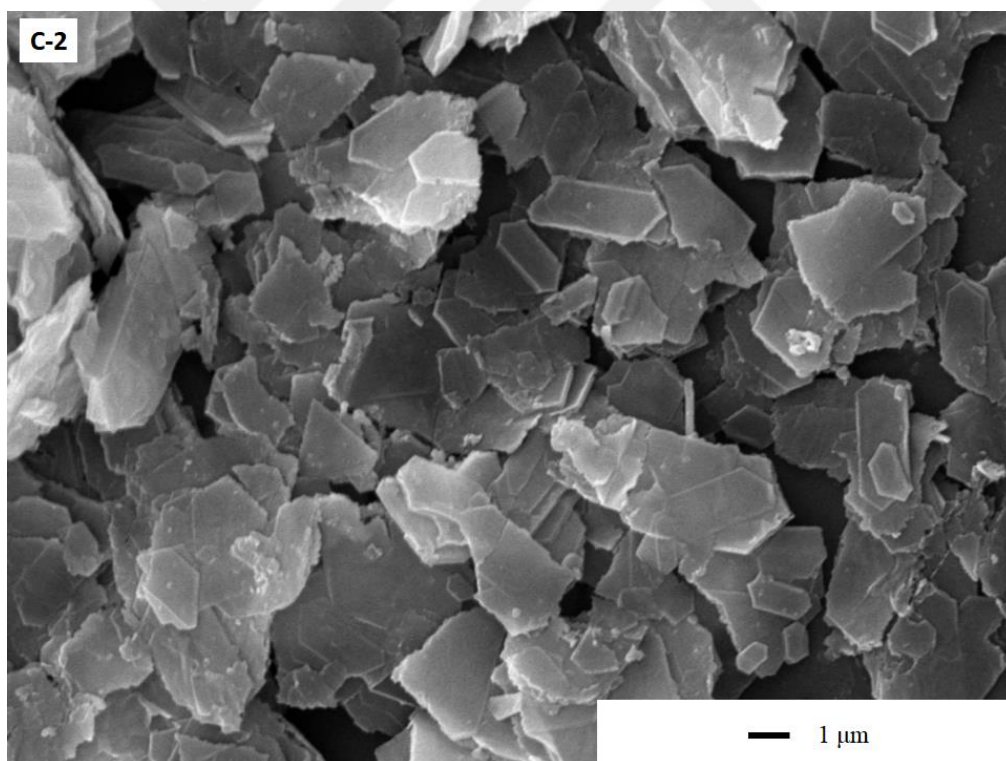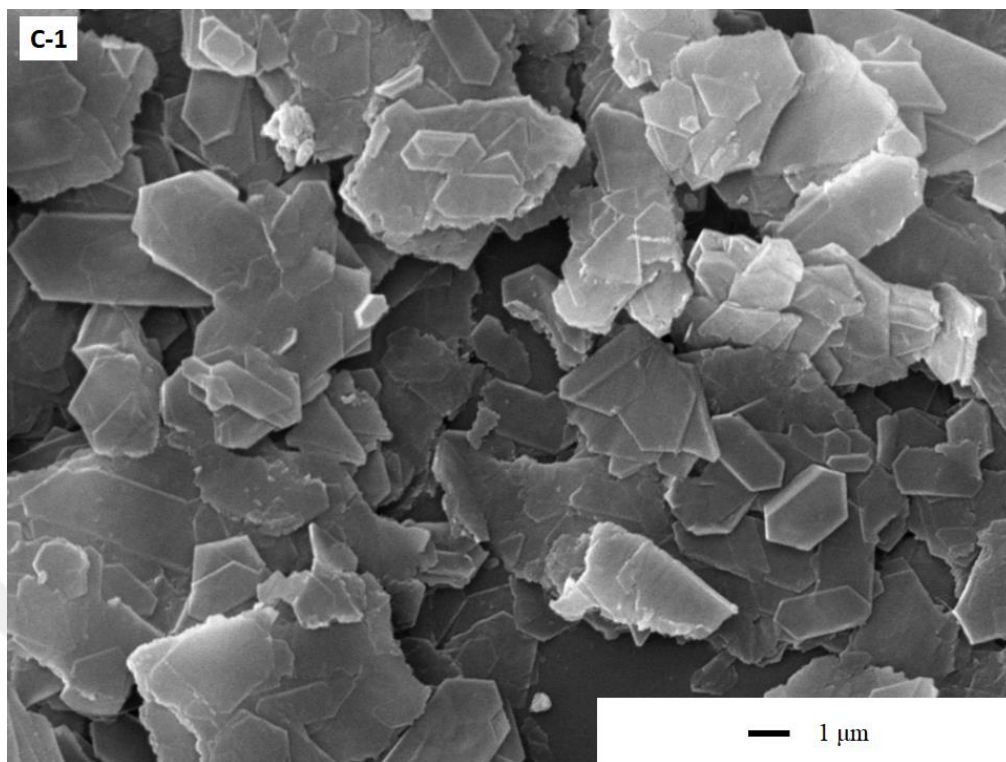
**Figure 4.22.** *SEM micrographs of MicNo-GZO particles with different Ga doping amount*
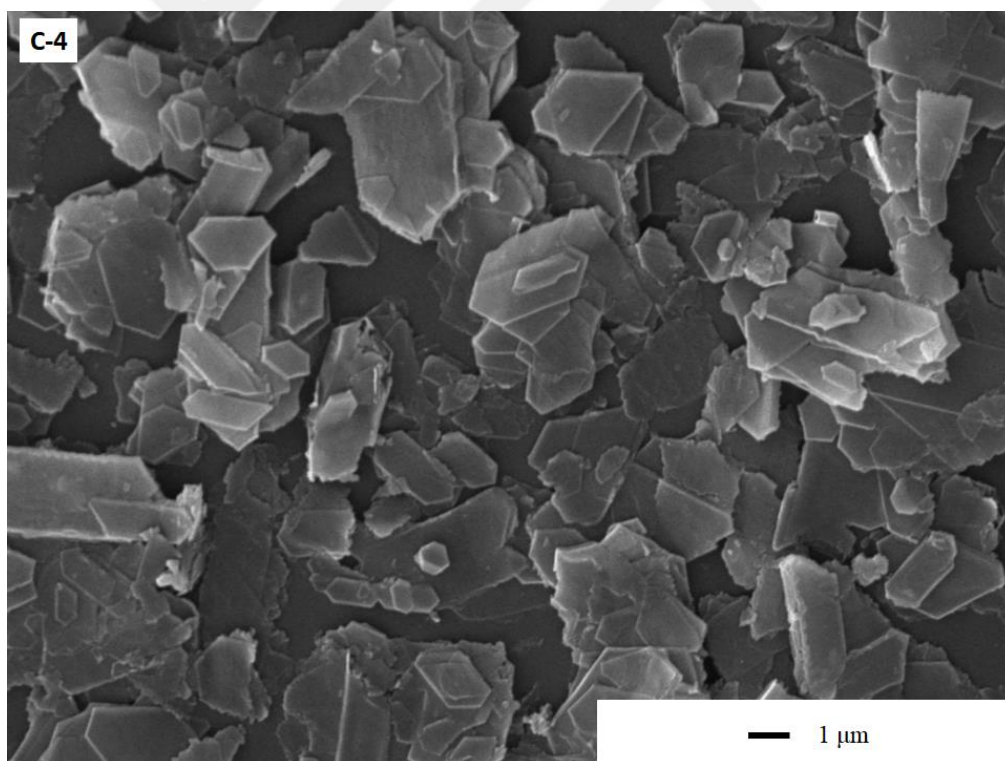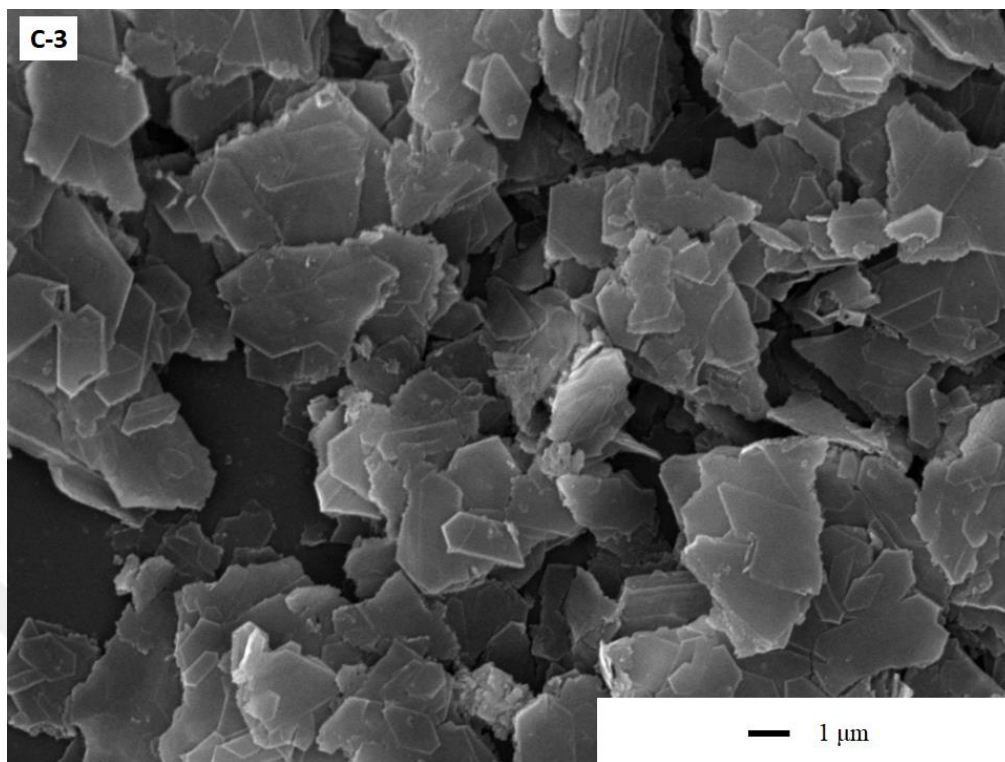
**Figure 4.22**. (Continued) *SEM micrographs of MicNo-GZO particles with different Ga doping amount*

**Figure 4.22**. (Continued) *SEM micrographs of MicNo-GZO particles with different Ga doping amount*

**Figure 4.22**. (Continued) *SEM micrographs of MicNo-GZO particles with different Ga doping amount*



| Sample Name | Particle Size (μm) | | |
|---|---|---|---|
| | $d_{10}$ | $d_{50}$ | $d_{90}$ |
| **C – 1** | 2,6 | 6,5 | 14,2 |
| **C – 2** | 2,6 | 6,7 | 14,5 |
| **C – 3** | 2,7 | 6,7 | 14,5 |
| **C – 4** | 2,5 | 5,7 | 12 |
| **C – 5** | 2,6 | 6,2 | 12,8 |
| **C – 6** | 2,5 | 6 | 12,5 |
| **C – 7** | 2,4 | 5,8 | 12,2 |
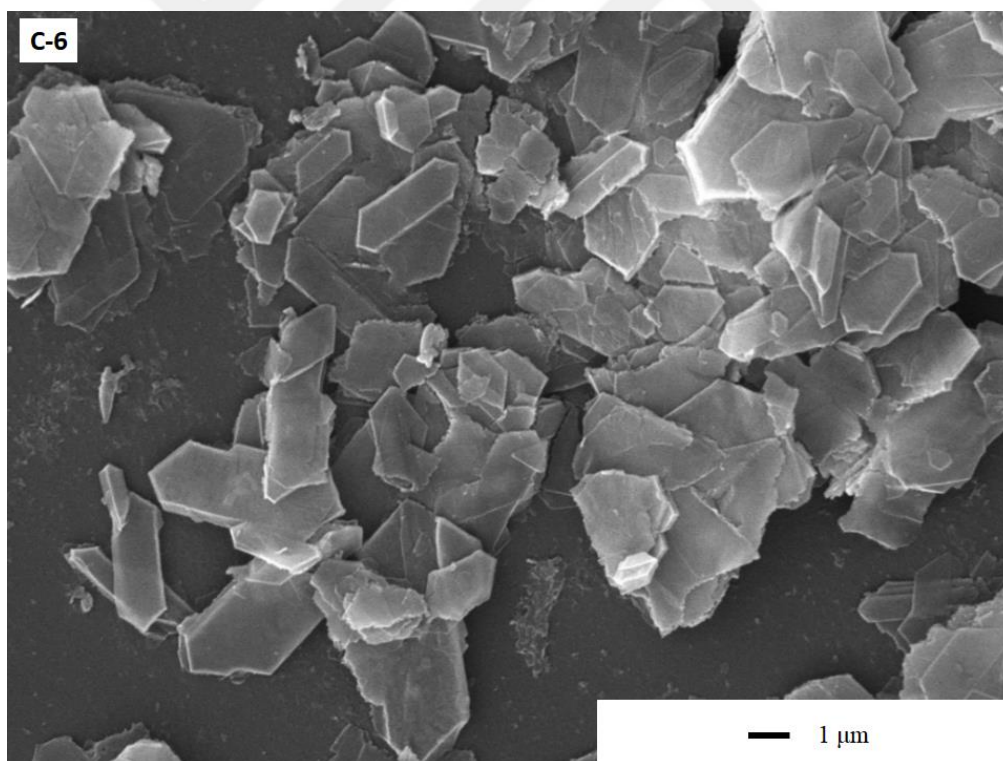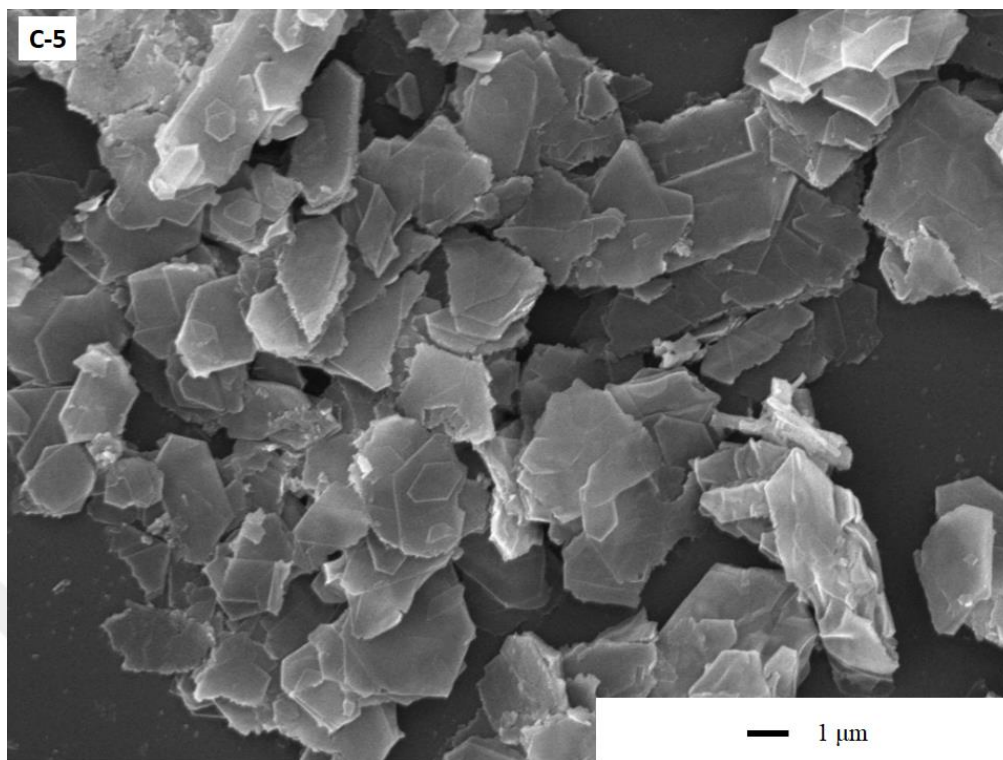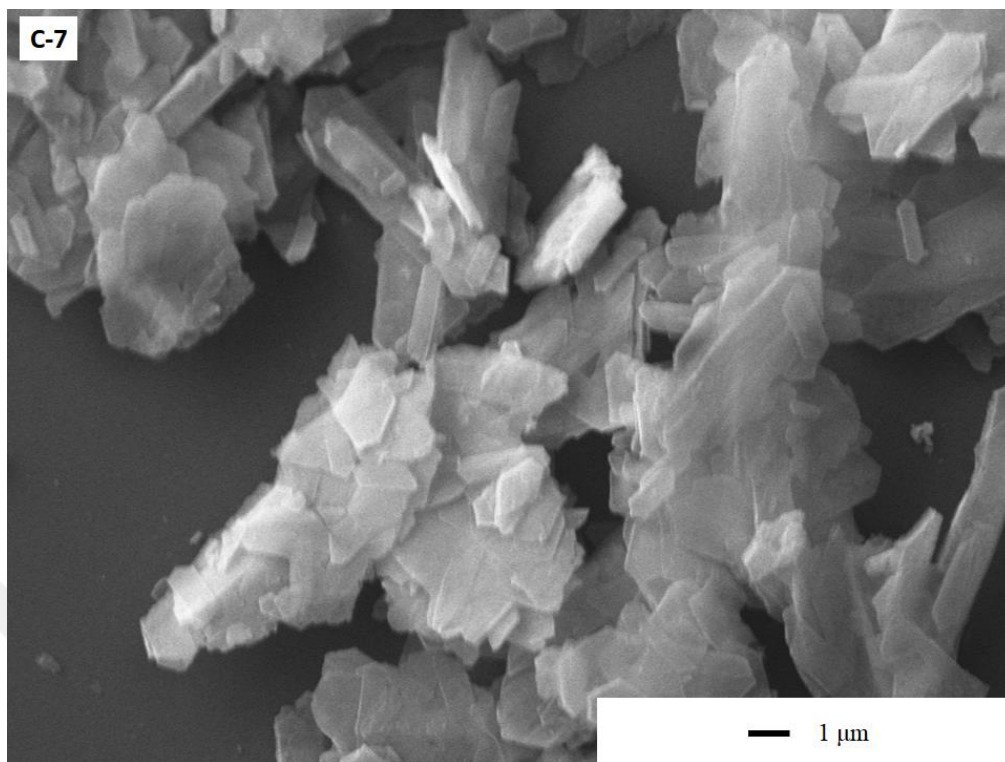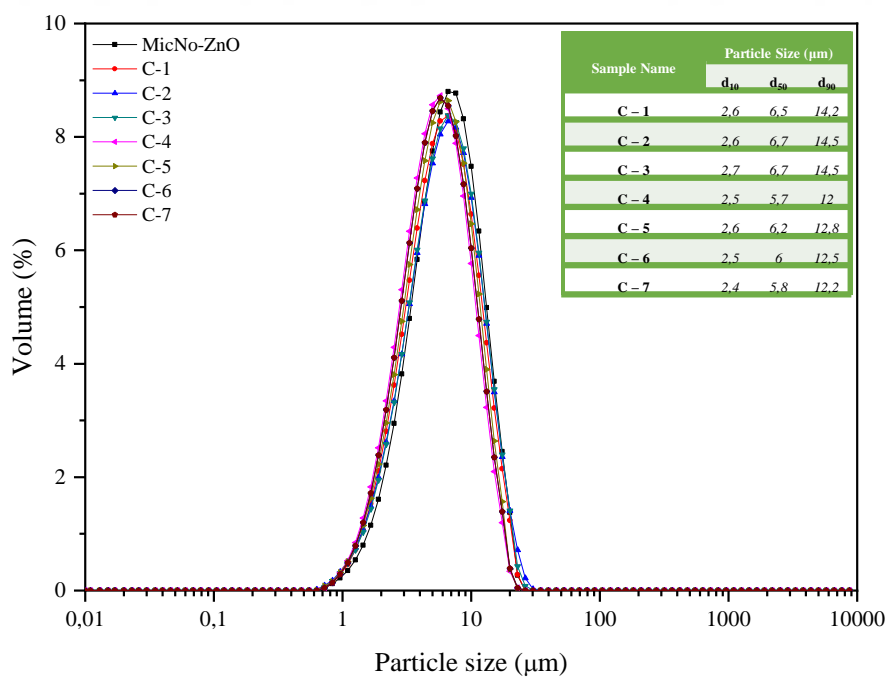
**Figure 4.23.** *Particle size distribution graph of MicNo-GZO particles with different Ga doping amount*

### 4.1.3.1. *Raman and FTIR spectroscopy of MicNo-GZO particles*

Raman spectrums of MicNo-ZnO and MicNo-GZO particles are given in Figure 4.24. At Part 4.1.2.3. mentioned about ZnO Raman active modes and spectrum. Ga doped MicNo-ZnO particles show characteristic $2^{nd}$ order peak at 330 cm$^{-1}$ and $E_2$ high mode at 437 cm$^{-1}$. Otherwise there are some additional Raman peaks at 346, 415, 472, 630, 654 and 765 cm$^{-1}$. These Raman peaks might be related to Ga doping because of peaks at 625 – 650 cm$^{-1}$ are $GaO_4$ tetrahedra related optical modes and peaks at 346 – 415 – 472 cm$^{-1}$ $Ga_2O_6$ octahedra related optical modes [56,57]. Increasing with Ga dopant concentration, these peak intensities are decreasing. In general, redsihft on the Raman spectrums may observe due to defects or impurities origins from doping process [56]. This type of peak shifts was not observed on MicNo-GZO Raman spectrum. The reason is that Ga doping level concentrations are quite low.
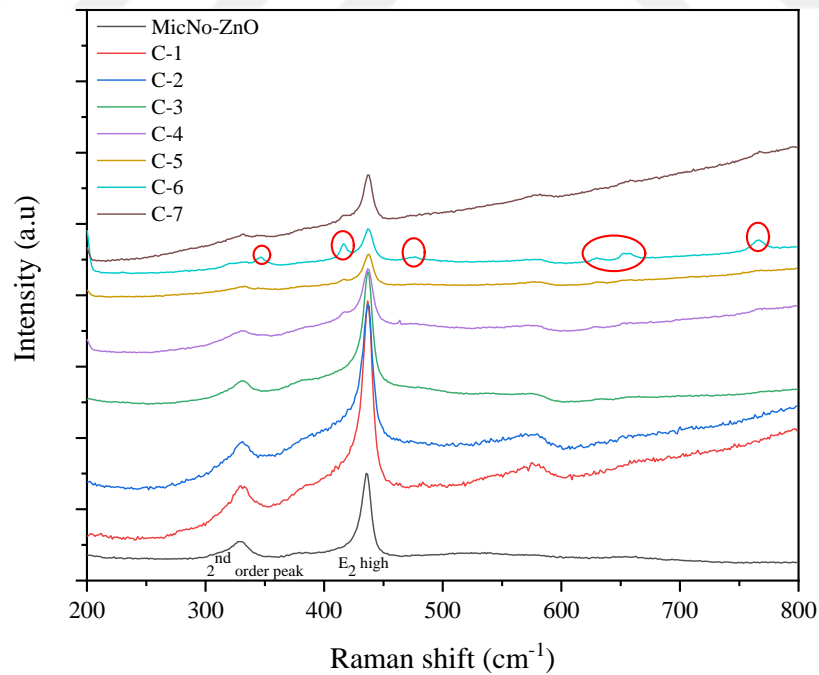


**Figure 4.24.** *Raman spectrums of MicNo-ZnO and MicNo-GZO particles with different Ga doping amount*

Figure 4.25 shows that FTIR spectrums of MicNo-GZO particles. Undoped MicNo-ZnO particles have absorption peak at around 380–560 cm$^{-1}$. This broad peak indicates the presence of Zn–O stretching modes. There are two different peaks from MicNo-ZnO particles which are at about 800 cm$^{-1}$ and 1500 cm$^{-1}$. These peaks are observed on Ga$_2$O$_3$ particles as shown on Figure 4.26. The absence of these signals in undoped MicNo-ZnO suggests that such vibrations can be related to Ga doping.
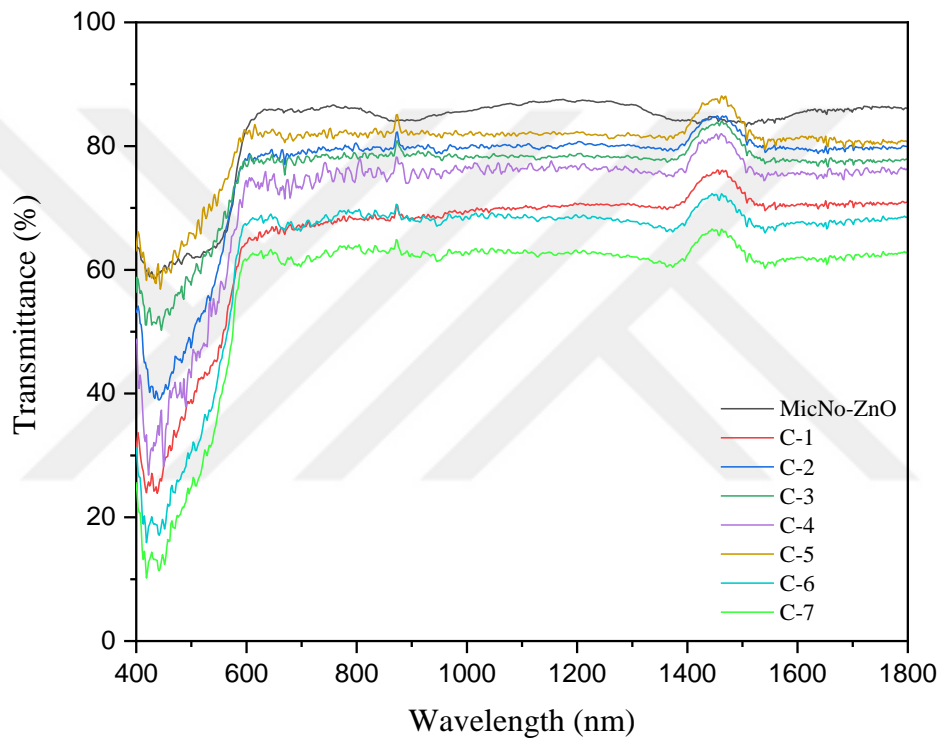


**Figure 4.25.** *FTIR spectrums of MicNo-ZnO and MicNo-GZO particles with different Ga doping amount*
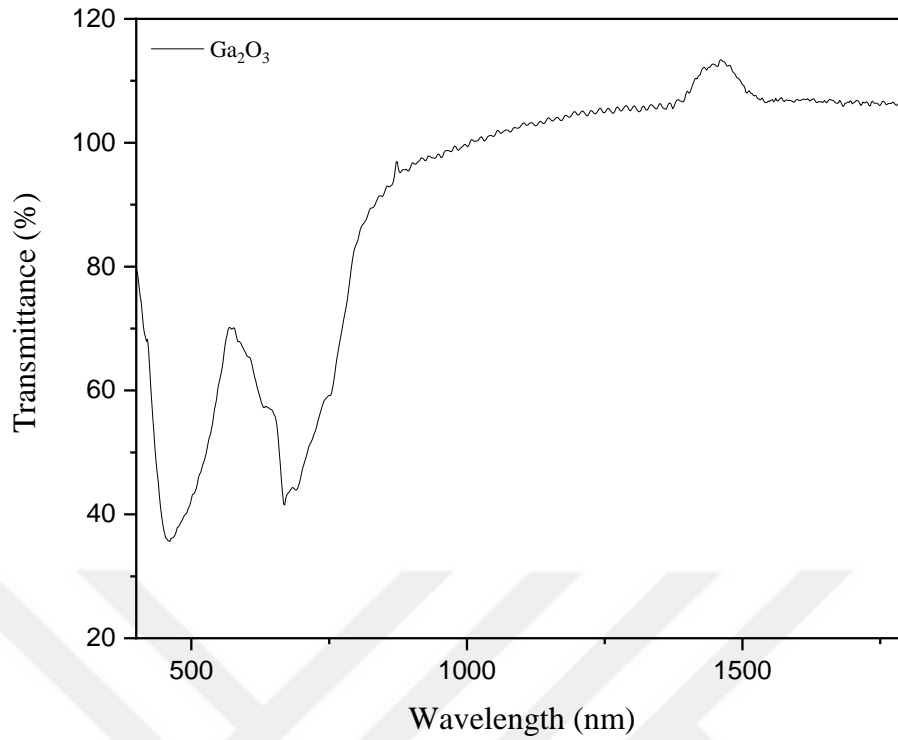
**Figure 4.26.** *FTIR spectrum of Ga₂O₃ particles*

### 4.1.3.2. *Optical properties of MicNo-GZO particles*

Figure 4.27 shows that transmission and absorption graphs of MicNo-GZO particles. They have similar optical characteristics with MicNo-ZnO particles. Additionally, band gap energies of these particles determined as explained techniques on Part 4.1.2.4. On Figure 4.28 photon energy – $(h\nu\alpha)^2$ graph is shown then band gap values were obtained between 3.1 - 3.2 eV (Table 4.5).
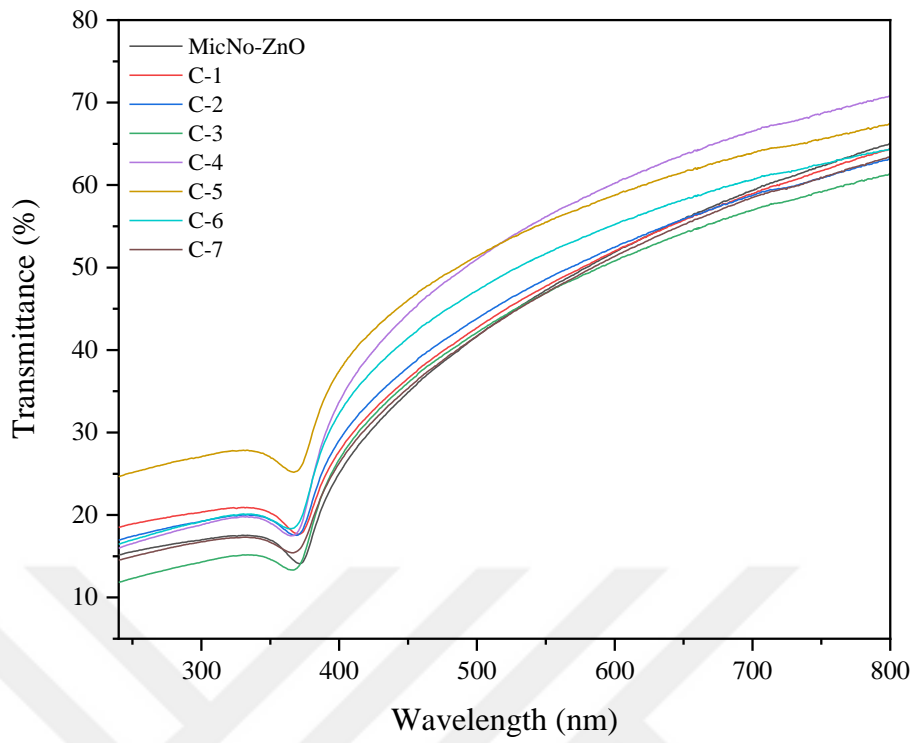
(a)
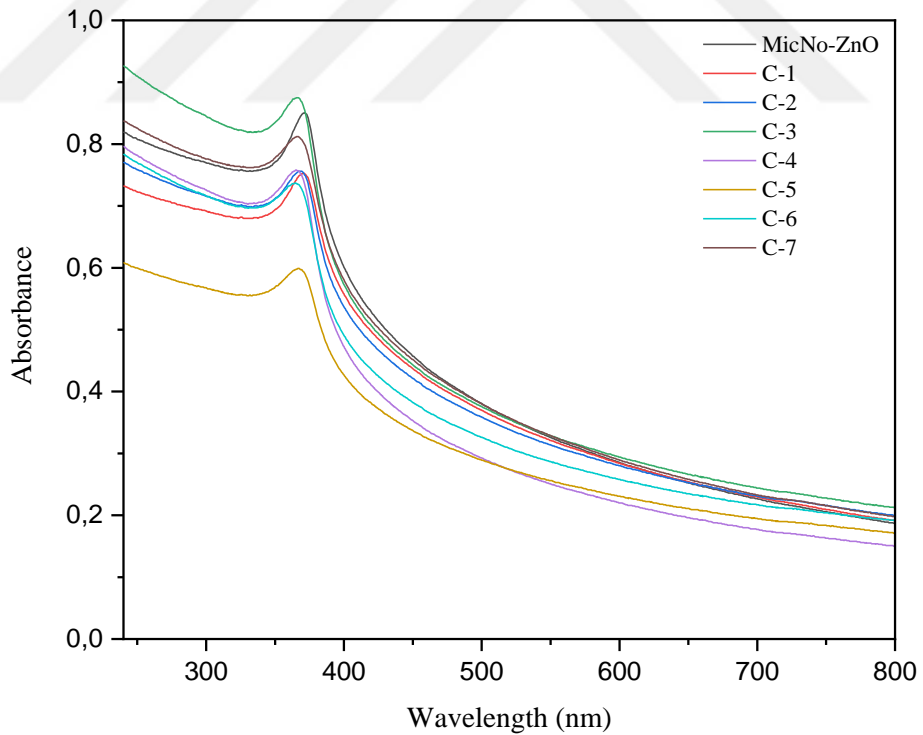


(b)

**Figure 4.27.** *(a) Transmission and (b) Absorption graphs of MicNo-GZO particles with different Ga doping amounts.*

**Figure 4.28.** *Photon energy – (hαν)2 graph of MicNo-GZO particles with different Ga doping amount*

**Table 4.5.** *Band gap values of undoped and Ga doped MicNo-ZnO particles*

| Samples | Band Gap Values, eV |
|---------|---------------------|
| MicNo-ZnO | 3.18 |
| C-1 | 3.14 |
| C-2 | 3.16 |
| C-3 | 3.16 |
| C-4 | 3.18 |
| C-5 | 3.15 |
| C-6 | 3.14 |
| C-7 | 3.15 |

## 4.2. Electrical Properties of Al and Ga Doped MicNo-ZnO Particles

In this study, our objective was to characterize electrical properties and improvement of Al and Ga doped MicNo-ZnO particles. Undoped MicNo-ZnO particles have electrical resistivity ~2500 KΩ.cm. Figure 4.29 shows that Al doped MicNo-ZnO particles' electrical resistivities. As increasing Al dopant concentration electrical resistivity is decreasing. Measurements were not achieved successfully on the sample B-7 because of these particles could not pressed successfully. Therefore, to observe inflection point on electirical resistivities sample B-8, which has Al doping concentraion value is in the range between B-6 and B-7, were prepared. These particles have ~ 250 KΩ.cm electrical resistivity and particle phase and morphology analyses were consisted with other Al doped MicNo-ZnO particles, Figure 4.29. b the minimum electrical resistivity was observed on the sample B-6 that 40 KΩ.cm. In addition to these Ga doped MicNo-ZnO particles electrical resistivities are shown in Figure 4.30 Unsurprisingly electrical resistivities are decreasing with increasing Ga doping concentration but the sample C-7 electrical resistivity was increased. Therefore C-6 concentration is critical concentration for obtaining optimum electrical resistivities. The sample C-6 has ~300 KΩ.cm electrical resistivity. Ga doped MicNo-ZnO particles have higher electrical resistivities than Al doped MicNo-ZnO particles.

(a)



(b)
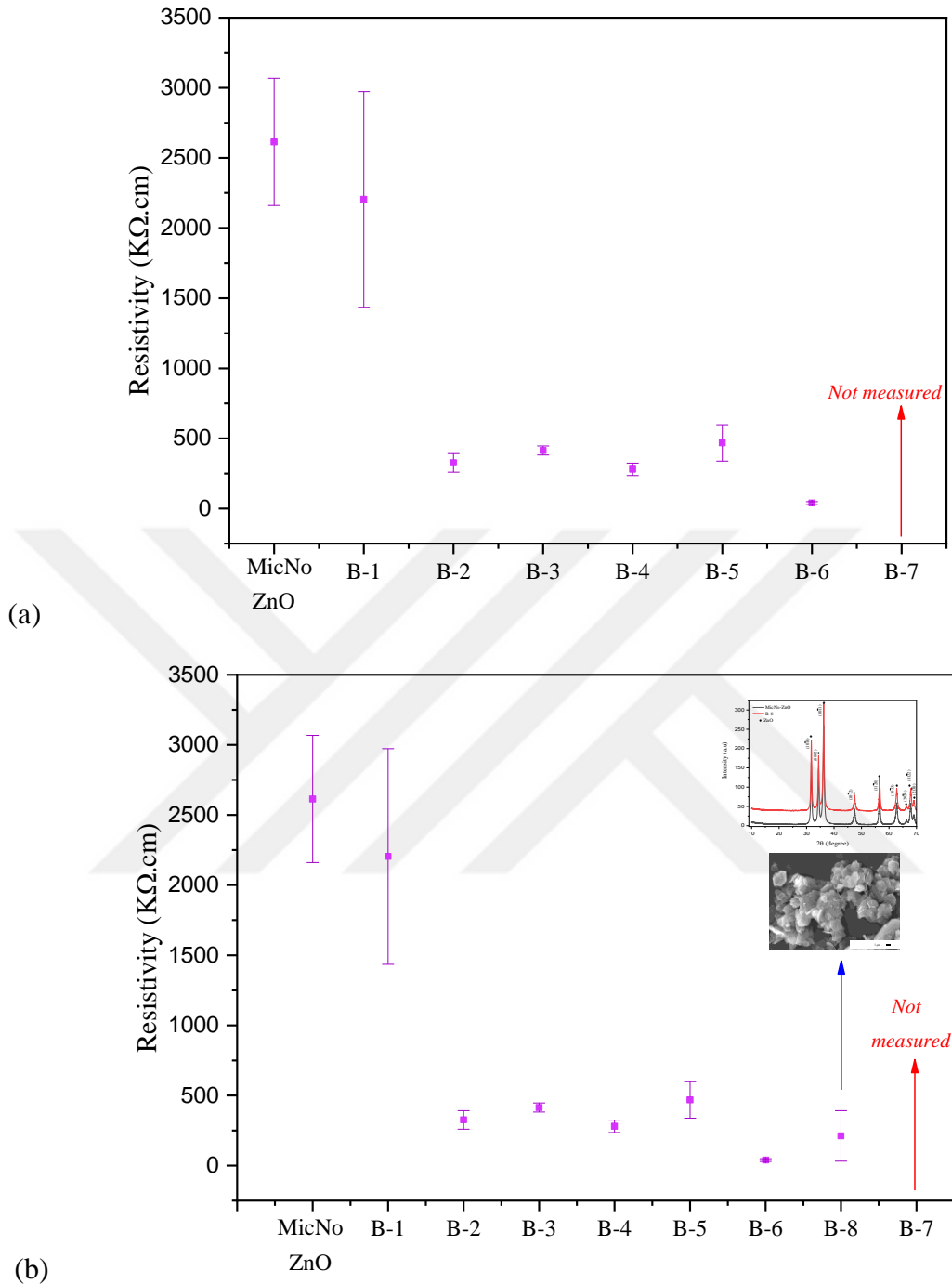
**Figure 4.29.** *(a) Electrical resistivities of MicNo-ZnO and MicNo-AZO particles with different Al doping amount, (b) adding comparision sample B-8*
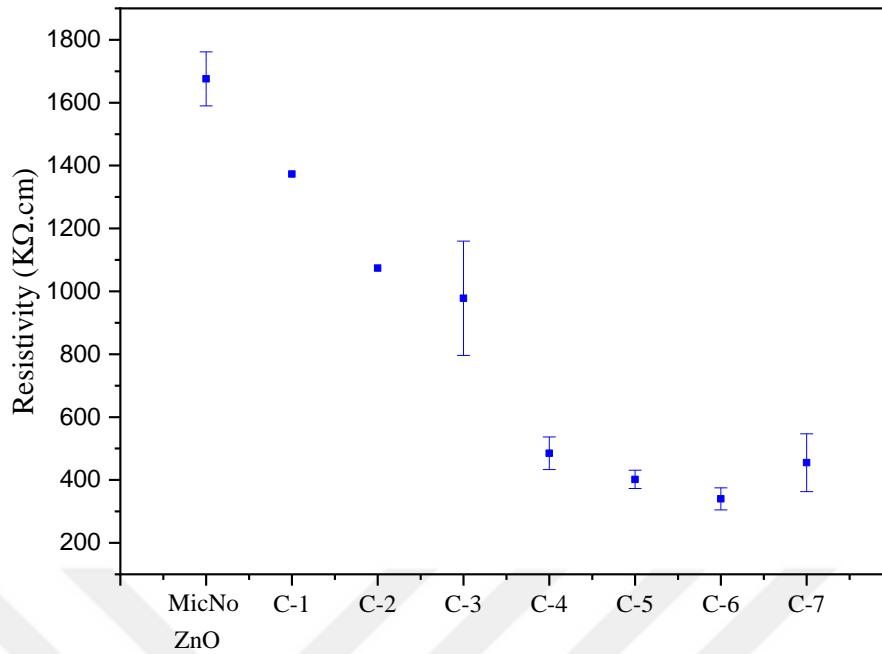
**Figure 4.30.** *Electrical resistivities of MicNo-ZnO and MicNo-GZO particles with different Ga doping amount*

## 4.3. Electrical Properties of MicNo-AZO or MicNo-GZO Added Conductive Polymer Composites

One of the other objectives of this study is determining the effect of Al and Ga doped MicNo-ZnO particles in the epoxy polymer matrix. This part of the study, Al and Ga doped MicNo-ZnO particles, which have appropriate resistivity, were used as conductive filler in polymer matrix. Sample B-6 was choosen from Al doped MicNo-ZnO particles and sample C-6 was choosen from Ga doped MicNo-ZnO particles. Doped MicNo-ZnO particles were added into polymer matrix different amounts such as 0, 2, 5 and 10 wt%.

First of all, surface resistivity measurements were completed $R_{S1}$ and $R_{S2}$ directions for B-6 added in polymer. Figure 4.31 a and b show that surface resistivity measurement of these samples. Surface resistivities were decreased to ~2 MΩ.cm at $R_{S1}$ direction and ~8 MΩ.cm at $R_{S2}$ direction. Sample C-6 added polymers have surface resistivities are ~1,5 MΩ.cm at $R_{S1}$ direction and ~8 MΩ.cm at $R_{S2}$ direction, Figure 4.32 a and b.

(a)



(b)
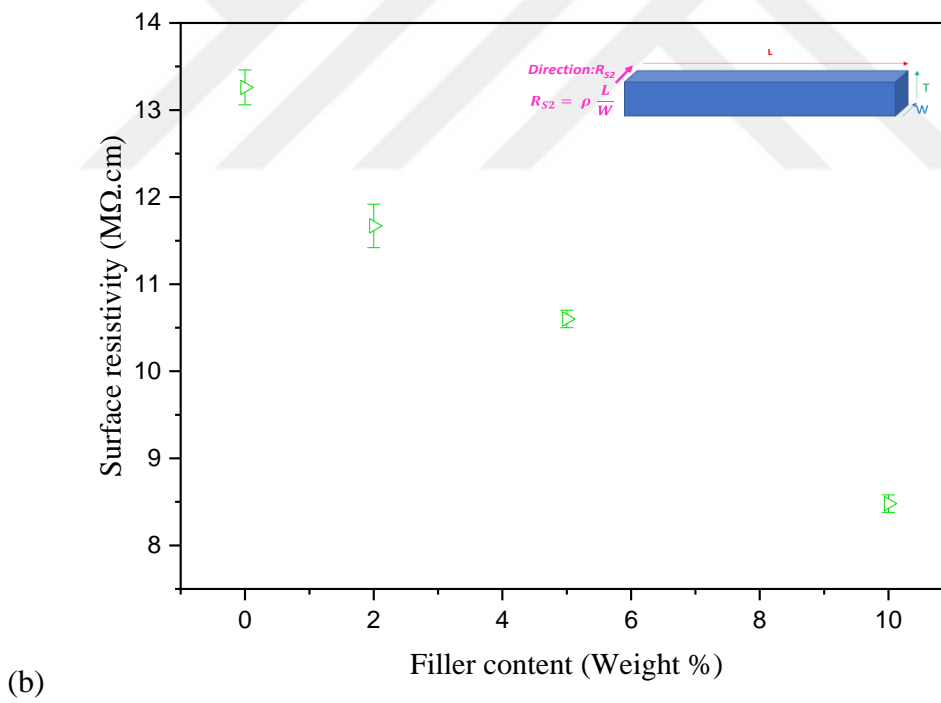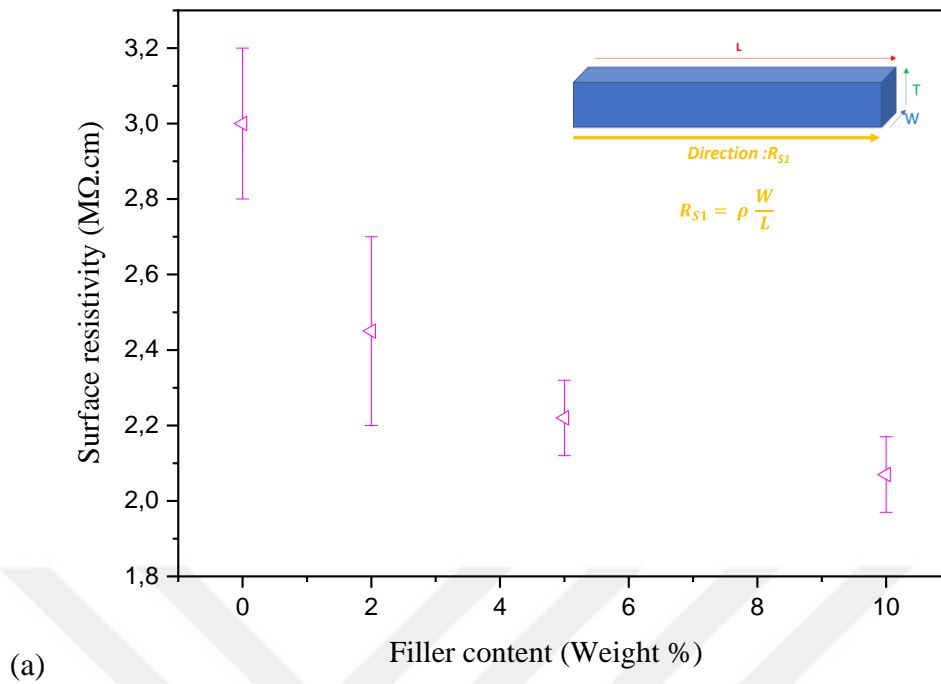
**Figure 4.31.** *Surface resistivities of Al doped MicNo-ZnO added polymers (a) $R_{S1}$ direction and (b) $R_{S2}$ direction*
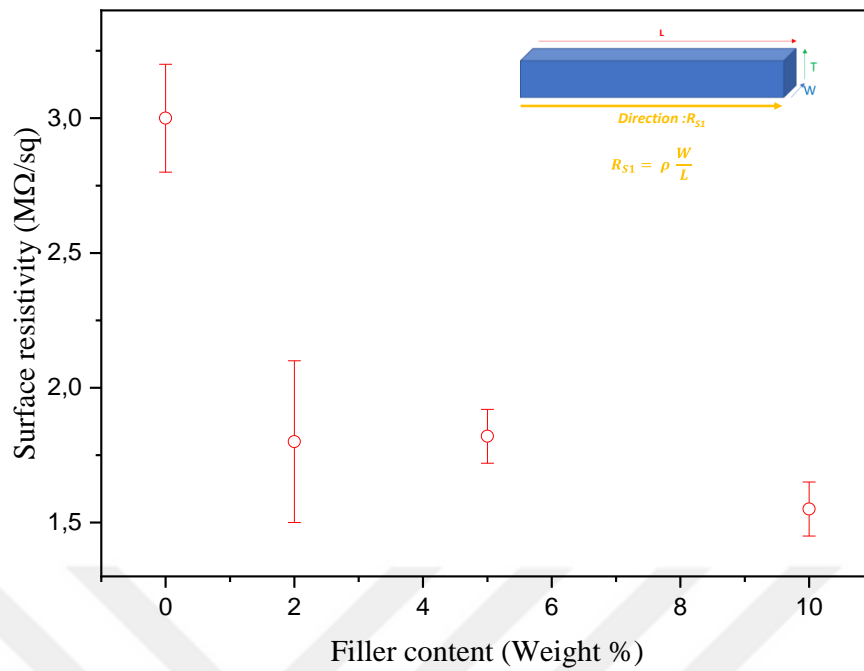
(a)
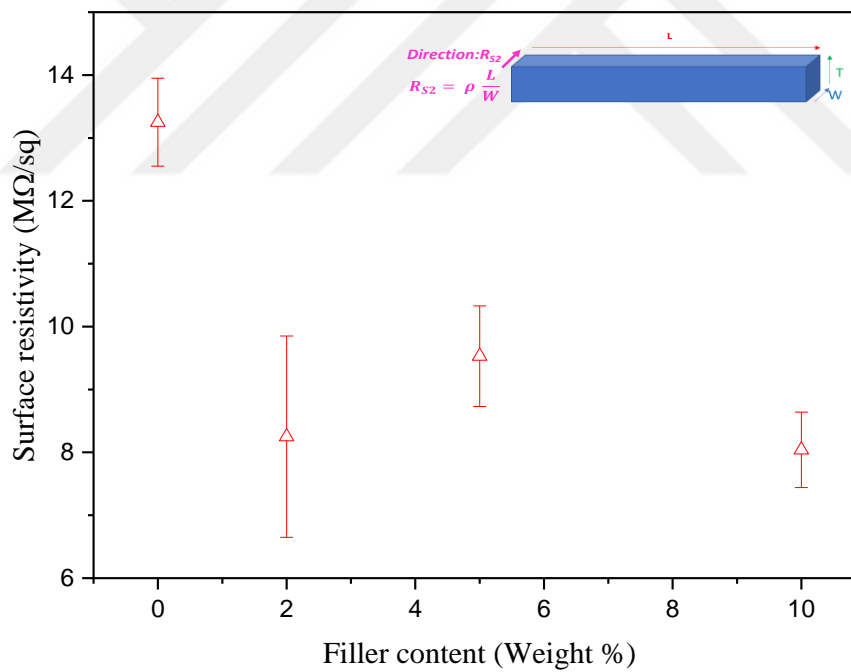


(b)

**Figure 4.32.** *Surface resistivities of Ga doped MicNo-ZnO added polymers (a) $R_{S1}$ direction and (b) $R_{S2}$ direction*

In the standards, surface resistivity measurement should be applied on the samples which have minimum 10x10 cm surface area. Therefore, to obtain more accurate electrical resistivities, we measured bulk resistivities of the polymer samples and compared, Figure 4.33. It was observed that Al doped MicNo-ZnO samples are more compatible for using as conductive filler materials. Because of these particles have lower electrical resistivities than Ga doped MicNo-ZnO particles. Polymer materials have 6 MΩ.cm resistivitiy without using filler materials. Ga doped MicNo-ZnO particles added polymers resistivities decrease to the range between 3-5 MΩ.cm. On the contrary, Al doped MicNo-ZnO added polymer sample resistivities decrease to 2 MΩ.cm.
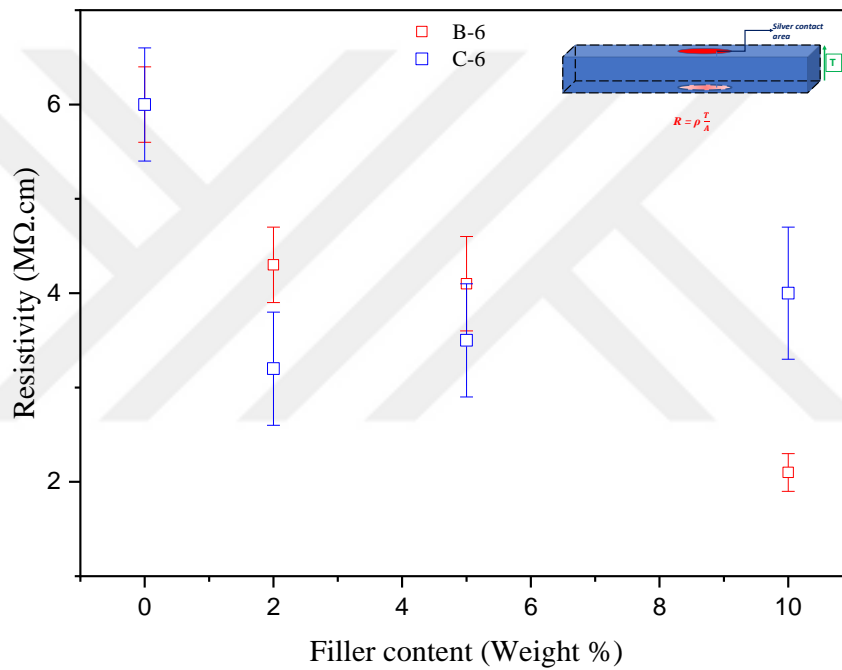


**Figure 4.33.** *Bulk resistivities of Al and Ga doped MicNo-ZnO added polymers*

# 5. DISCUSSION

In this section we will discuss Al and Ga doped MicNo-ZnO particles individually becuase dopant types have different effects on the MicNo-ZnO particles. Firstly, Al doped MicNo particles initially synthesized with using Material A for Al doping. After indicated that Material A is inappropriate for obtainig MicNo morphology, Material B used as Al dopant material. Doping amounts of Al and Ga doped particles were start from 0 to 15 mol% value. According to the ICP analyses, while Al doped particles' Al concentrations are range between 0 and 0.32 mol %, Ga doped particles' Ga concentrations are $0 - 2.3$ mol%. This difference can also be examined with x-ray diffraction techniques. Al and Ga doped particles basicly have same properties and particles show zinc oxide (ZnO) phase. However, 4 mol% Ga doped particles show $Ga_2O_3$ phase. Differently Al doped MicNo-ZnO particles do not show secondary phase formation. Therefore, secondary $Ga_2O_3$ phase lead to high Ga concentrations on ICP analyses.

Moreover, materials have solubility limit which is limit of how much solute will dissolve in a material. Solubilitiy limit may directly related to the synthesis conditions and the material properties. There is a study that reported by Serier et al. Al solubility limit in ZnO is 0.3 mol% for Pechini routes [58]. Zhang et al. reported that AZO particles have solubility limit less than 4 mol% for sol-gel method [59]. This situation is not different in Ga doping process. Ga doped MicNo particles results are also consistent with Jang et al., who reported that the maximum solubility limit of Ga in GZO ceramics is 0.5 mol % [54]. Additionally, Yoon et al. reported that GZO ceramics have maximum solubility limit is 0.5 mol% [55].

ZnO crystal structure, wurtzite type structure, $Zn^{2+}$ occupy half of the sites and the other half of the tehtrahedral and octahedral sites are empty. There are three possible dopant locations for tetrahedral sites which are $Zn^{2+}$ substitutional sites, interstitial sites for $Al^{3+}$ ions and empty tetrahedral sites [60]. As mentioned above lattice shirinkage occurs due to decreasing with interplanar distances of ZnO crystals. Therefore, XRD patterns of doped MicNo-ZnO particles are slightly shifted toward high 2Ө angles with respect to undoped ZnO particles. This lattice shrinkage mainly occurs because of incorporation of $Al^{3+}$ as a substitutional defect due to its smaller size compared to that of $Zn^{2+}$. If $Al^{3+}$ ions interstitially placed into ZnO structure caused shifting the diffraction

angles towards lower values [61,62]. Peak shifts on the XRD patterns of MicNo-AZO particles were not systematically change upon increasing Al doping concentrations. This strongly related to defect types in ZnO structure. $Al^{3+}$ ions are not only placed substantial sites also it can be placed interstitial sites. At this point effective dopant amounts are important parameter for interpreting peak shifts. Therefore, it is expected that Al substantial defects occurs at Al dopant amounts is less than solubiliy limit value. Ga doping should lead to same effect on the crystal structure and XRD patterns. Namely, it is expected that peak shifts toward to high 2Θ angles. When analyzed Ga doped MicNo-ZnO particles, there are no peak shifts at critical degree. This can be related to $Ga^{3+}$ ions are not placed substantially.

Raman analyses of these particles show that undoped MicNo-ZnO and doped MicNo-ZnO particles have distinct peaks at about 330 $cm^{-1}$ and 437 $cm^{-1}$. $E_2$ high mode at 437 $cm^{-1}$ is related to corresponded to vibration of oxygen atoms [51,52,63]. These two peaks are observed in both group of doped MicNo-ZnO which are Al and Ga doped ZnO, particles. Expected effect of doping on Raman spectrums decreasing $E_2$ high peak intensitiy with increasing dopant concentrations. We observed this Al and Ga doped MicNo-ZnO particles Raman spectrums. Ga doped ZnO particles Raman spectrums also showed additional Raman peaks that might be related to Ga doping. Ga doped particles Raman spectrums are consisting with XRD results as these particles have secondary $Ga_2O_3$ phase. There is also additional peak on FTIR spectrums of Ga doped MicNo-ZnO particles. Additionally, Al doped MicNo-ZnO particles FTIR spectrums have additional peaks at 600-800 $cm^{-1}$ which is related to Al-O bonding. These results help to prove Al and Ga doping into ZnO crystal structure. Otherwise the differences in Raman spectra and FTIR spectra of undoped MicNo-ZnO and doped MicNo-ZnO can be hard to distinguish since the effective dopant amount in powders are quite low.

Particle size of MicNo-ZnO and doped MicNo-ZnO platelets from light scattering (LS) analysis $d_{50}$ values are in the range between 8 to 10 μm. LS measurements give particle size information in a liquid medium from the platelet volume. Crystallite size from XRD analyses are within 22 – 30 nm for Al doped MicNo-ZnO particles. Ga doped MicNo-ZnO particles have 35 – 45 nm crystallite size. Both group of samples demonstrate that increase in particle size with doping of MicNo-ZnO particles. On the other hand, specific surface area measurement (S.S.A) used for calculating equivalent

spherical diameters. Both group of samples have similar S.S.A results and equivalent spherical diameter are in the same range which 35 – 45 nm in size. These values are larger than the values obtained from XRD results. This is related to the BET is a gas adsorption technique which are affected by particle surface morphology, porosity and degree of agglomeration. As we know that MicNo particles have not spherical morphology.

Optical characteristics of undoped MicNo-ZnO particles and doped MicNo-ZnO particles samples have highly transparent characteristics in the visible range (400-700 nm). Estimating band gap energies, Tauc plots were used. Thus, calculated band gap values are in the range between 3.05 – 3.13 eV for Al doped MicNo-ZnO particles; on the other hand, 3.1 – 3.2 eV for Ga doped MicNo-ZnO particles. In general, doping processes lead to changes in the electronic and optical characteristics of the materials. Sutanto et al. reported that band gap energies are increasing after a critical amount of Al dopant concentrations [64]. Burstein – Moss effect is explained by increasing in band gap energy (blue shift) and observed at high doping levels. Moreover, absorption peak shifts to the short wavelength values with increasing Ga doping concentrations [65]. According to the all these dopant amounts are low to distinguish these differences systematically, thus we can say that band gap values are in the specific range.

Electrical properties of the pellets which are prepared from undoped and doped MicNo-ZnO particles are inversely proportional to the dopant amounts. Namely, increasing dopant concentrations electrical resistivities are decreasing up to a critical doping concententration which is also called inflection point. After this concentration electron mobilities are decreasing due to carrier-carrier scattering [8,61,66]. Therefore, electrical resistivities are increasing after these concentrations. Especially Al doped MicNo-ZnO particles have much smaller electrical resistivities than Ga doped MicNo-ZnO particles. Theoretically 10 mol % Al doped sample, which is 0.3 mol% according to the ICP analyses, have 40 KΩ.cm electrical resistivity but 10 mol % Ga doped MicNo-ZnO particles, which is 1.2 mol% according to the ICP analyses, have 340 KΩ.cm.

Al doped ZnO particles which are commercially produced by Hakusui Tech. (Pazet CK and products of Hakusui Tech.) shows 10 KΩ.cm bulk resistivity [38]. When comparing these particles MicNo-AZO particles have optimum resistivity value for antistatic products. On the other hand, commercial 3 wt% Ga doped ZnO particles (Pazet GK and products of Hakusui Tech.) shows 30 Ω.cm bulk resistivity values. Ga doped

MicNo-ZnO particles have higher electrical resistivity than these commercial particles. Y.Q.Li et al reported that 4 mol% Ga doped ZnO nanoparticles exhibit 5 MΩ.cm electrical resistivity [67]. These studies are also show that electrical resistivites of MicNo-GZO particles are strongly affected by synthesis processes and Ga doping concentrations and critical Ga doping concentration is 0.4 mol% to formation $Ga_2O_3$ phase. Secondary phase formation caused to electron barrier between primary particles thus lowering electron mobility and conductivity.

The second objective of this study was to determine whether doped MicNo-ZnO particles used effectively in polymer matrix as conductive filler or not. Doped MicNo-ZnO particles added into epoxy resin and gives different resistivities according to the dopant type. Al doped MicNo-ZnO particles exhibit approximately 1.7 MΩ.cm at 10 wt % filler loading. Particularly, polymer part without doped MicNo-ZnO filler have 6 MΩ.cm and Al doped particles provide to decrease this value to 1.7 MΩ.cm. Polymer composites, which Ga doped particles added into polymer, do not achieved this resistivity values. Samples have approximately 4 MΩ.cm resistivity at different weight percent filler amounts. In this study, doped MicNo-ZnO particles using have advantages because of high transparent characteristics and lack of uncontrolled agglomeration. Therefore, specifically MicNo-AZO particles might be used as conductive fillers in CPCs for obtaining better percolation behavior due to their high aspect ratio and unique platelet morphology.

# 6. CONCLUSIONS

In this thesis, syntheses of Al and Ga doped MicNo-ZnO particles were achieved by MicNo process and characterizations of these particles were completed. In the first part of the study the effects of Al and Ga doping on the structural, morphological, electrical and optical properties of MicNo-ZnO particles were investigated. Then, effects of these particles in polymer matrix as a conductive filler. The most important results and effects are as follow:

- Al doped MicNo ZnO particles were synthesized by using Material B with designated morphology.

- Al dopant concentration were not affect particle morphology up to 15 mol % doping amounts.

- Ga doped MicNo ZnO particles were synthesized by using Material C and particle morphology were not affected by dopant concentration.

- MicNo-AZO and MicNo-GZO particles optical characteristics are similar with undoped MicNo-ZnO particles. They have highly transparent characteristics in the visible range (400-700 nm) also high absorption characteristic ın the UV range (240-400 nm).

- Al doped MicNo-ZnO particles have band gap energy is in the range between 3.05-3.13 eV; Ga doped MicNo-ZnO particles are in the range between 3.1-3.2 eV.

- MicNo-ZnO particles have ~2500 KΩ.cm electrical resistivity and bulk resistivities of the MicNo-AZO and MicNo-GZO particles are decreasing with increasing doping ratio. Al doped MicNo-ZnO particles show minimum electrical resistivity at the sample B-6 which is ~40 KΩ.cm. Ga doped MicNo-ZnO particles show minimum electrical resistivity at the sample C-6 which is ~340 KΩ.cm

- Al and Ga doped MicNo-ZnO added polymer samples show that Al doped MicNo-ZnO particles enhanced the resistivity better than Ga doped MicNo-ZnO particles. Samples bulk resistivities decrease to about 2 MΩ.cm.

# REFERENCES

[1] http-1, www.hsa.ie/eng/ Topics/Electricity/D angers_of_Electri city/Elec trical _Fata lity_Statistics – (05.02.2017).

[2] ESD Association, (2013) "Fundamentals of Electrostatic Discharge, Part One: An Introduction to ESD", ESD Association, Rome NY.

[3] Secker E.P., Taylor and David M., (1994), "Industrial electrostatics: Fundamentals and measurements", Research Studies Pre.

[4] Al-Saleh M.H., (2009), "Nanostructured conductive polymeric materials".

[5] Aylward P.T, Majumdar D., Yau H.L., Durkin W.J., Bigelow D.O., Slater D.A., and Robinson K.S., (2006), "Antistatic layer for electrically modulated display" In.: Google Patents.

[6] Anand A., Rani N., Saxena P., (2015), "Development of polyaniline/zinc oxide nanocomposite impregnated fabric as an electrostatic charge dissipative material", Polymer International, 64[9], 1096-103.

[7] Feng Y., Zou H., Tian M., (2012), "Relationship between dispersion and conductivity of polymer nanocomposites: a molecular dynamics study", The Journal of Physical Chemistry B., 116[43], 13081-88.

[8] Gornicka B., Mazur M., Sieradzka K., (2010), "Antistatic properties of nanofilled coatings", Acta Physica Polonica-Series A General Physics, 117[5], 869.

[9] Callister W.D, Rethwisch D.G., (2011), "Materials Science and Engineering", John Wiley & Sons NY, 5.

[10] Karadurmuş M., (2017), "Epoksi Reçine ile Hazırlanan Kompozit Malzemelerin Mekanik ve Tribolojik Özelliklerinin İncelenmesi", Yüksek Lisans Tezi, Samsun, Ondokuz Mayıs Üniversitesi, Fen Bilimleri Enstitüsü.

[11] Ahmad S., Jamal Y., (2009), "Machining of Polymer Composites", Springer.

[12] Radzuan N., Nabilah A.M., Sulong A.B., and Jaafar S., (2016). "A review of electrical conductivity models for conductive polymer composite", International Journal of Hydrogen Energy.

[13] Boyle M.A., Martin C.J., Neuner J.D., (2001), "Epoxy Resins", ASM Handbook Composites, 21, 78-89

[14] Zhang S., Deng H., Zhang Q., (2014), "Formation of conductive networks with both segregated and double-percolated characteristic in conductive polymer composites with balanced properties", ACS Applied Materials & Interfaces, 6[9], 6835-44

[15] Markarian J., (2008), "New developments in antistatic and conductive additives", Plastics, Additives and Compounding, 10[5], 22-25

[16] Pionteck J., Wypych G., (2007), "Handbook of antistatics", Chem. Tec. Publishing.

[17] Shang Q., Sue H., Weili W., Dongsheng F., Tianlong M., (2013), "Preparation and characterization of antistatic coatings with modified BaTiO3 powders as conductive fillers", Journal of Adhesion Science and Technology, 27, 2642-52.

[18] Sun L., O'Reilly J.Y., Tien C.W., (2008), "Preparation of Electrically Conductive Polystyrene/Carbon Nanofiber Nanocomposite Films", Journal of Chemical Education, 85[8], 1105.

[19] Liang J., Yang Q., (2007), "Aggregate structure and percolation behavior in polymer/carbon black conductive composites"., Journal of Applied Physics, 102[8], 083508.

[20] Shui X., Chung D.D.L., (2000), "Submicron diameter nickel filaments and their polymer-matrix composites", Journal of Materials Science, 3, 1773-85.

[21] Guo J., Zheng J., Xinzhao S., and Kun S., (2013), "Synthesis and conductive properties of Ga-doped ZnO nanosheets by the hydrothermal method", Materials Letters, 97, 34-36

[22] Altynbek M., (2012), "Complex oxides as novel transparent conductors".

[23] Moezzi A., Andrew M., Cortie M.B,. (2012), "Zinc oxide particles: Synthesis, properties and applications", Chemical Engineering Journal, 185, 1-22.

[24] Steiner T., (2004), "Nanostructures for Optoelectronic Applications", Artech House Inc., London.

[25] Özgür U., ALlivov Y., Liu C., Teke A., Reshchikov M. A., Doğan S., Avrutin V., Cho S. J., Morkoç, H., (2005) "A comprehensive review of ZnO materials and devices", Journal Of Applied Physcs, 98, 041301.

[26] Wang Z.L., (2004), "Zinc Oxide Nanostructures: Growth, Properties and Applictions", Journal of Physics: Condensed Matte, 16[25].

[27] Salam S., Islam M., Akram A., (2013) "Sol–gel synthesis of intrinsic and aluminum-doped zinc oxide thin films as transparent conducting oxides for thin film solar cells", Thin Solid Film, 529:242, 47.

[28] Robertson J., Falabretti B., (2011), "Electronic structure of transparent conducting oxides", Handbook of Transparent Conductors, Springer., 27-50

[29] Slassi A., Naji S., Benyoussef A., (2014), "On the transparent conducting oxide Al doped ZnO: first principles and Boltzmann equations study", Journal of Alloys and Compounds, 605, 118-23.

[30] Duenow J.N., Gessert T.A., Wood D.M., (2007), "Transparent conducting zinc oxide thin films doped with aluminum and molybdenum", Journal of Vacuum Science & Technology A: Vacuum, Surfaces, and Films, 25[4], 955-60.

[31] Henni A., Merrouche A., Telli L., (2016), "Studies on the structural, morphological, optical and electrical properties of Al-doped ZnO nanorods prepared by electrochemical deposition", Journal of Electroanalytical Chemistry, 763, 149-54

[32] Tsay C.Y., Lee W.C., (2013), "Effect of dopants on the structural, optical and electrical properties of sol–gel derived ZnO semiconductor thin films", Current Applied Physics, 13[1], 60-65.

[34] Si X., Liu Y., Wu X., (2015), "The interaction between oxygen vacancies and doping atoms in ZnO", Materials & Design, 87, 969-73.

[35] Takaki T., Keiko K., Hadi R., Sohei S., Noritaka S., Kenji K., Kunihiko N., Taisei H., (2010), "Electrolytic Synthesis of Al-Doped ZnO Nanopowders With Low Electrical Resistivity", Journal of the American Ceramic Society, 93, 3088-91.

[36] Zheng J., Shuang Z., Liang L., Xuejia L., Yangyang S., Ming S., (2015), "Homogeneous precipitation synthesis and conductive properties of Ga-doped ZnO nanopowders", Journal of Materials Science: Materials in Electronics, 26, 5433-39.

[37] Hartner S., Moazzam A., Christof S., Markus W., Hartmut W., (2009), "Electrical properties of aluminum-doped zinc oxide (AZO) nanoparticles synthesized by chemical vapor synthesis", Nanotechnology, 20, 445701.

[38] Izumi T., Izumi K., Kuroiwa N., Senjuh A., Fujimoto A., Adachi M., Yamamoto T., (2009), "Preparation of electrically conductive nano-powder of zinc oxide and application to transparent film coating", Journal of Alloys and Compounds, 480, 123-25.

[39] Khan R., Ubair A.S., Mohammad A.A., Boumaza M., Saeed M.A.Z., (2013), "Effect of ZnO Nano Powder on Mechanical Properties of Epoxy/Polyaminoamide Adduct Coatings", International Journal of Advances in Computer Science and Technology, 2[11], 25-28

[40] Oberdörster G., Oberdörster E., Oberdörster J., (2005), "Nanotoxicology: an emerging discipline evolving from studies of ultrafine particles", Environmental health perspectives, 113, 823.

[41] Sharma V., Ritesh K.S., Neha S., Devendra P., Mukul D., Dhawan A., (2009)., "DNA damaging potential of zinc oxide nanoparticles in human epidermal cells", Toxicology letters, 185, 211-18.

[42] Suvacı E., Yılmazoğlu G., "Mikron boyutlu çinko oksit (ZnO) plakaların üretim yöntemi" (TR200907209A1) Ulusal Patent (2012).

[43] Warren B.E., (1990), "X-Ray Diffraction, Courier Corporation"

[44] http-2, https://www.researchgate.net/post/Particle_size_calculation_based_on_BET_data3, (13.09.2018)

[45] O'Leary S.K., Lim P., (1997), "On determining the optical gap associated with an amorphous semiconductor: A generalization of the Tauc model", Solid State Communications, 104[1], 17-21.

[46] Tan S.T., Chen B., Sun X., (2005), "Blueshift of optical band gap in ZnO thin films grown by metal-organic chemical-vapor deposition", Journal of Applied Physics, 98[1], 013505.

[47] Hancock J.M., (2013), "Formation and analysis of zinc oxide nanoparticles and zinc oxide hexagonal prisms and optical analysis of cadmium selenide nanoparticles", Brigham Young University.

[48] McCluskey M., Jokela S., (2009), "Defects in ZnO", Journal of Applied Physics, 106[7], 10.

[49] Kumar R.S., Sathyamoorthy R., Sudhagar P., (2011), "Effect of aluminum doping on the structural and luminescent properties of ZnO nanoparticles synthesized by wet chemical method", Physica E: Low-dimensional Systems and Nanostructures. 43[6], 1166-70.

[50] Pal M., Bera S., Sarkar S., (2014), "Influence of Al doping on microstructural, optical and photocatalytic properties of sol–gel based nanostructured zinc oxide films on glass", RSC Advances.4[23], 11552-63.

[51] Jin Y., Cui Q., Wen G., (2009), "XPS and Raman scattering studies of room temperature ferromagnetic ZnO: Cu", Journal of Physics D: Applied Physics, 42[21], 215007.

[52] Azam A., Babkair S.S., (2014), "Low-temperature growth of well-aligned zinc oxide nanorod arrays on silicon substrate and their photocatalytic application", International Journal of Nanomedicine. 9, 2109.

[53] Temizer N.K., Nori S., Narayan J., (2014), "Ga and Al doped zinc oxide thin films for transparent conducting oxide applications: Structure-property correlations", Journal of Applied Physics, 115[2], 023705.

[54] Jang M., Ryu M., Yoon M., Lee S., Kim H., Onodera A., Kojima S., (2009), "A study on the Raman spectra of Al-doped and Ga-doped ZnO ceramics", Current Applied Physics, 9[3], 651-57.

[55] Yoon M., Lee S., Park H., Kim H., Jang M., (2002), "Solid solubility limits of Ga and Al in ZnO", Journal of Materials Science Letters, 21[21], 1703-04.

[56] Yang Y., Qi J., Liao Q., Zhang Y., Yan X., Huang Y., Tang L., (2009), "Fabrication, structural characterization, and photoluminescence of Ga-doped ZnO nanobelts" Applied Physics A, 94[4], 799-803.

[57] Jang M.S., Ryu M.K., Yoon M.H., Lee S.H., Kim H.K, Onodera A., Kojima S., (2009), "A Study on the Raman Spectra of Al-doped and Ga-doped ZnO ceramis", Current Applied Physics, 9, 651-657

[58] Serier H., Gaudon M., Ménétrier M., (2009), "Al-doped ZnO powdered materials: Al solubility limit and IR absorption properties", Solid State Sciences. 11[7], 1192-97

[59] Zhang Y., Yang Y., Zhao J., (2011), "Optical and electrical properties of aluminum-doped zinc oxide nanoparticles", Journal of Materials Science, 46[3], 774-80

[60] Kelchtermans A., Elen K., Schellens K., (2013), "Relation between synthesis conditions, dopant position and charge carriers in aluminium-doped ZnO nanoparticles", RSC Advances, 3[35], 15254-62.

[61] El-Manouni A., Manjón F., Mollar M., (2006), "Effect of aluminium doping on zinc oxide thin films grown by spray pyrolysis", Superlattices and Microstructures, 39[1-4], 185-92

[62] Saravanakumar K., Ravichandran K., (2012), "Synthesis of heavily doped nanocrystalline ZnO: Al powders using a simple soft chemical method", Journal of Materials Science: Materials in Electronics, 23[8], 1462-69

[63] Lara A.J., Oliveira A.G., Mariucci V.V.G., (2017), "Effects of $Al^{3+}$ concentration on the optical, structural, photocatalytic and cytotoxic properties of Al-doped ZnO", Journal of Alloys and Compounds, 729, 978-87.

[64] Sutanto B., Arifin Z., (2018), "Structural Characterisation and Optical Properties of Aluminum-Doped Zinc Oxide Nanofibers Synthesized By Electrospinning", Journal of Engineering Science and Technology, 13[3], 715-24.

[65] Zhou H., Wang H., Tian X., Zheng K., Xu F., Su Z., Tian K., Fang F., (2014), "Solvothermal synthesis of gallium-doped zinc oxide nanoparticles with tunable infrared absorption", Materials Research Express, 1[4], 045022.

[66] Lu Z., Zhou J., Wang A., (2011), "Synthesis of aluminium-doped ZnO nanocrystals with controllable morphology and enhanced electrical conductivity", Journal of Materials Chemistry, 21[12], 4161-67

[67] Li Y.-Q., Yong K., Xiao H.M., Ma W.J., Zhang G.L., Fu S.Y., (2010), "Preparation and electrical properties of Ga-doped ZnO nanoparticles by a polymer pyrolysis method", Materials Letters, 64[15], 1735-37.

# CIRRICULUM VITAE

**Pınar ŞENGÜN – Material Scientist & Engineer**

**Date and place of birth:** 19/09/1992 – Bursa/Turkey
**Phone:** +90 534 698 7302
**E-mail:** sengunpnar@gmail.com

Education:

| | | |
|---|---|---|
| **Master** | Anadolu University – Materials Science & Engineering (09/2015 - ) | ( - ) |
| **University** | Anadolu University – Material Science & Engineering (09/2010,06/2015) | (3,38/4,00) |
| **High School** | Fatih Anatolian High School – Eskişehir (09/2006,06/2010) | (80.07/100) |

Publications:

- Sengun P., Kesim M.T., Caglar M., Savaci U., Turan S., Sahin I., Suvaci E., Characterization of Designed, Transparent and Conductive Al Doped ZnO Particles and Their Utilization in Conductive Polymer Composites *(in preparation)*
- Sengun P., Suvaci E., Kesim M.T., Caglar M., Preparation of Electrically Conductive Ga-doped ZnO (MicNo-GZO) Particles with Designed Morphology for Antistatic Applications *(in preparation)*

Honors & Awards:

- The Third Best Poster Award – IV. International Ceramics, Glass, Porcelain, Enamel, Glaze and Pigment Congress October 10-12, 2018 Eskisehir Turkey
- Graduating from Anadolu University Materials Science & Engineering Department on 10/06/2015 as Honor Student
- Anadolu University, Materials Science & Engineering, Highest Ranked Student 2014-2015, July 2015
- Certificate of High Honor – Anadolu University 2014-2015 Spring Term
- The Best Poster Award – MLZ-441 Nanomaterials and Nanotechnology Course Anadolu University
- Certificate of Honor – Anadolu University 2014-2015 Fall Term

- Certificate of High Honor – Anadolu University 2013-2014 Spring Term
- Certificate of Honor – Anadolu University 2013-2014 Fall Term
- Certificate of High Honor – Anadolu University 2012-2013 Spring Term
- Certificate of High Honor – Anadolu University 2012-2013 Fall Term

Work Experience:

**11.2018 -**     **Research & Development Engineer**

Entekno Materials Corp., Eskisehir, Turkey

**06.2015 –**     **Research student**

Anadolu University (Eskişehir/Turkey) – Advanced Technical Ceramics Laboratory.

I expertised on the synthesis of inorganic powders by using different solution-based synthesis methods and studied on syntheses of undoped and/or doped zinc oxide (ZnO) powders with tailored morphologies and investigation of the effect of the dopant elements on electrical and optical properties of zinc oxide materials.

**06.2014 – 07.2014**     **Internship**

TÜBİTAK – Marmara Research Center (MAM) (Kocaeli/Turkey)

During the internship programme, I worked on research Project on investigation of ceramic slurry recipes for slip casting process.

**06.2013 – 07.2013**     **Internship**

DemirDöküm Industry (Bilecik/Turkey)

Worked at purchase department for purchasing production process materials.

Projects:

- Anadolu University Scientific Research Project – Master Thesis Project, "Synthesis and Characterization of Designed Shape Doped Zinc Oxide (ZnO) Particles", Project No:1703F082
- Anadolu University Scientific Research Project, "Synthesis and Characterization of Aluminum and Gallium Doped Zinc Oxide Particles and Investigation of Electrical and Optical Properties" Project No:1508F608

Technical Skills:

- Project writing and follow-up processes
- Inorganic powder synthesis
- Application of Scanning Electron Microscopy and sample preparation process
- X-Ray Diffraction (XRD) techniques and sample preparation processes and interpretation of results
- Specific surface area analysis (BET Techniques)
- Thermogravimetric Analysis – Analyses of TG-DTA and sample preparation process and interpretation of results
- Raman Spectrometer Analysis and sample preparation process
- Fourier Transform Infrared Spectrophotometer (FTIR) analysis and sample preparation process
- UV-VIS Spectrophotometer analysis and sample preparation process
- Particle size measurement analysis
- Using of laboratory type furnaces

Computer Skills:

- Competent with most Microsoft Office programmes
- XRD Database programmes – MDI JADE, EVA, TOPAS
- CES EDUPACK
- ORIGIN

Courses and Trainings Attended:

- 2017 Time Management Training
- 2016 TA Instruments Q600 Model Simultaneous DSC/TGA Instrument Operator Training
- 2016 5S Methodology Training
- 2015 TÜBİTAK 1601 Business Focused Entrepreneurship Certificate Program

Conference, Exhibition and Symposium:

- Poster Presentation - IV. International Ceramics, Glass, Porcelain, Enamel, Glaze and Pigment Congress October, Eskisehir Turkey (10-12 October 2018)
- Poster Presentation - 15th International Materials Research 2018 Conference, Paris-FRANCE (19-20 February 2018)
- Poster Presentation -18th International Metallurgy and Materials Congress-IMMC2016, İstanbul-TURKEY (29 Sept. – 01 Oct. 2016)
- Poster Presentation - The International Conference on Ceramic Processing Science-ICCPS-13, Nara-Japan (8-11 May 2016)
- SERES 2014, Eskişehir-TURKEY (15-17 October 2014)